UNIVERSITY OF BIRMINGHAM

Project A: Characterisation of novel PRMT1 interacting proteins

Project B: Hepatocyte-Lymphocyte cell-in-cell structures: Implications for the host cell

Mres Biomedial Research Thesis

by Scott Philip Davies

School of Immunity and Infection

Institute of Biomedical Research

College of Medical and Dental Sciences

University of Birmingham

Student Number: 957566

Project A Supervisor: Dr. Clare Davies

Project B Supervisor: Dr. Zania Stamataki

Word Count: 14971

MRC | Medical Research Council

UNIVERSITY OF BIRMINGHAM

Project A: Characterisation of novel PRMT1 interacting proteins

A MINI-PROJECT BY SCOTT PHILIP DAVIES

This project is submitted in partial fulfilment of the requirements for the award of the MRes

School of Cancer Sciences

College of Medical and Dental Sciences

University of Birmingham

May 2014

Project Supervisor: Dr. Clare Davies

Word Count: 7904

ABSTRACT

Protein arginine methylation has become of interest in recent years for its involvement in diverse cellular processes. This modification is catalysed by protein arginine methyltransferases (PRMTs). PRMT1 is the predominant methyltransferase in eukaryotes, performing 85% of all cellular arginine methylation. There are 7 known PRMT1 splice-variants which vary in cellular localisation and activity. Several physiological processes, including gene expression and cellular signalling, have been shown to involve PRMT1. Furthermore, PRMT1 is upregulated in several cancers and its direct involvement in progression of leukaemia and ERα-driven breast cancers is evident. Information regarding PRMT1 regulation is lacking. The Davies laboratory recently discovered potential interactions between PRMT1v1 and the deubiquitylases USP11 and USP7. However, it was unknown if these interactions were direct or indirect. To address this, we generated recombinant proteins of His-SUMO-PRMT1v2, GST-USP11 and GST-USP7 for use within pull-down protein-interaction assays. Both GST-USP11 and GST-USP7 were capable of direct interaction with His-SUMO-PRMT1v2. These interactions were not seen under non-physiological NaCl levels, suggesting that such events could occur *in vivo*. It is unconfirmed if such interactions are enzyme-substrate events or whether they regulate protein activity through direct binding. Once this is elucidated, intervention of these interactions could be of therapeutic and anti-tumourigenic importance.

ACKNOWLEDGEMENTS

Thanks are given to both the Medical Research Council and the University of Birmingham for funding this work. Many thanks to Mark Bedford, Goedele Maertens and Helen Walden for providing the plasmids which were necessary for the undertaking of this project. Many thanks to the Jo Parish and Jo Morris lab for making the floor a very enjoyable place to work. Special thanks are given to Dr. Kelly Cheung for all of your support and teaching throughout this project, and also to Tom Clarke for your help and always making sure we had a good laugh. Lastly, I would like to thank Dr. Clare Davies for all of your help, support, excellent teaching, perseverance and tolerance for my weirdness. I can honestly say I have become a much better scientist as a result of this project.

Contents

1 INTRODUCTION

1.1 The structure and regulation of PRMT1

PRMT1 is the major type I protein arginine methyltransferase in eukaryotes (1, 2); it conducts asymmetric dimethylation and shares conserved structural features of the other 8 enzymatically active PRMTs. Arginine methylation and PRMT family members are summarised in Figures 1 and 2. PRMT1 is present throughout embryonic and adult tissues and is thought to catalyse 85% of total arginine methylation, based on PRMT1 immunodepletion in rat liver preparations (1). The embryonic lethality of PRMT1 knockout mice suggests it has necessary functions in embryonic development (3). Furthermore, conditional knockout of PRMT1 in mouse embryonic fibroblasts (MEFs) results in the dysregulation of the cell cycle and genomic instability (2). These studies display the importance of PRMT1 in the regulation of normal cellular functioning. PRMT1 generally methylates arginines within glycine-rich sequences, the RGG/RG motifs, which allows potential substrates to be identified to some degree of confidence (4). However, there are exceptions to this observation; RING domain activator AP-1 coactivator-1 (RACO) is methylated by PRMT1 but does not possess this motif (5). Additionally, other residues, distal to the methylated arginine are thought to contribute to substrate recognition and direct methylation (6, 7).

The ubiquitous nature of PRMT1 suggests it must possess a complex regulatory system, although the details of such mechanisms are lacking. Studies have shown that its activity is controlled through the formation of complexes with regulatory proteins. PRMT1 interacts individually with B-cell translocation genes 1 and 2 (BTG1 and BTG2) (8). The addition of either protein was shown to increase the activity of exogenous PRMT1, as well as to activate latent endogenous PRMT1 in quiescent rat

fibroblasts, suggesting that each can act as positive regulators (9). Following this, another binding partner of BTG1, CCR4-associated factor 1 (hCAF1), was also found to influence the activity of nuclear PRMT1 (10). Using siRNA, it was shown that hCAF1 inhibits the methylation of Sam68 and histone H4R3 by PRMT1. PRMT1 activity is also regulated through PTM, as it has recently been shown to be phosphorylated at Tyr291, juxtaposed to the THW domain, resulting in an impairment of substrate binding and methylation (11). Further research has shown that PRMT1 methylation may also be regulated through crosstalk with other PTMs (12). For example, asymmetric methylation by PRMT1 of H4R3 promotes the acetylation of lysine 5 (H4K5ac). This leads to chromatin relaxation which promotes transcriptional activation (12, 13). Conversely, K5 acetylation promotes symmetric methylation of H4R3 by PRMT5, causing transcriptional repression (12). Thus, H4K5 acetylation acts as a mediator, providing a negative feedback mechanism between two PRMTs with distinct methyltransferase activity. As PRMT1 is involved in many important, interlinking processes, there are likely to be other mechanisms which regulate its activities.

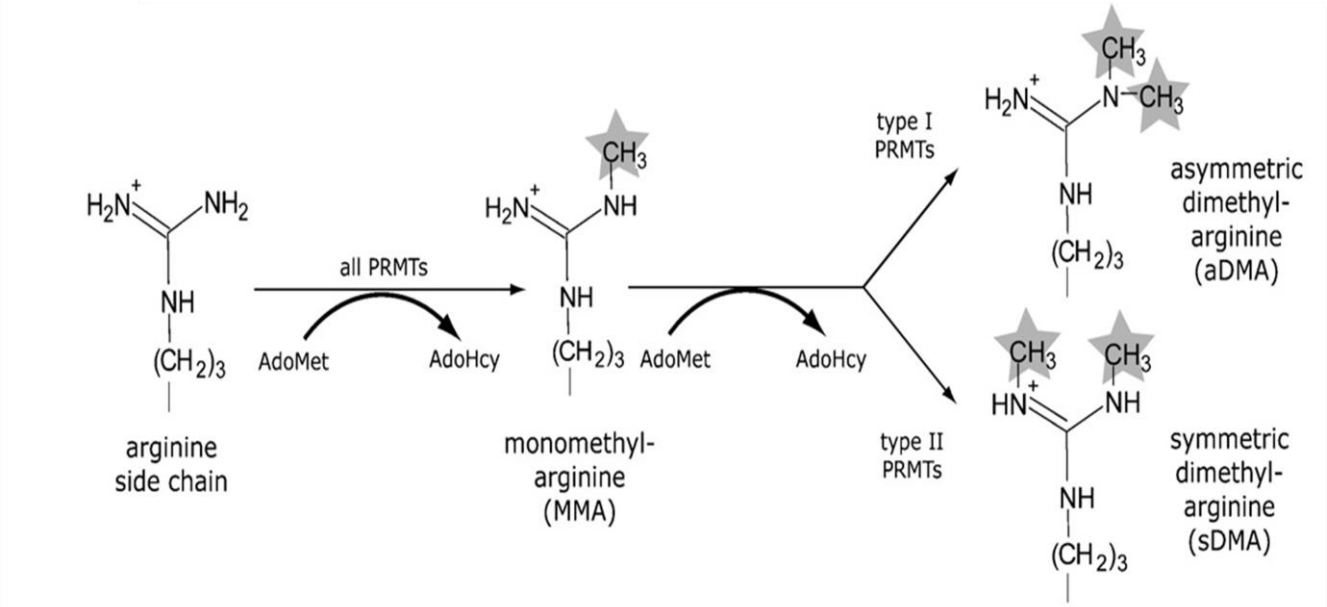

Figure 1 Process of Arginine Methylation by Protein arginine methyltransferases (PRMTs). All PRMTs initially conduct monomethylation at a single guanadino group of an arginine residue. Following this, a second methyl group can be added to same guanadino group by type 1 PRMTs, forming asymmetric dimethyl-arginine (ADMA). Alternatively, this second methyl group may be added to the next guanadino group by type II PRMTs, giving rise to symmetric dimethyl-arginine (SDMA). Each step requires S-Adenosylmethionine (AdoMet) as a methyl group donor, consequently yielding S-adenosyl-L-homocysteine (AdoHcy). Diagram from Pahlich *et al*, BiochimBiophys Acta (4).

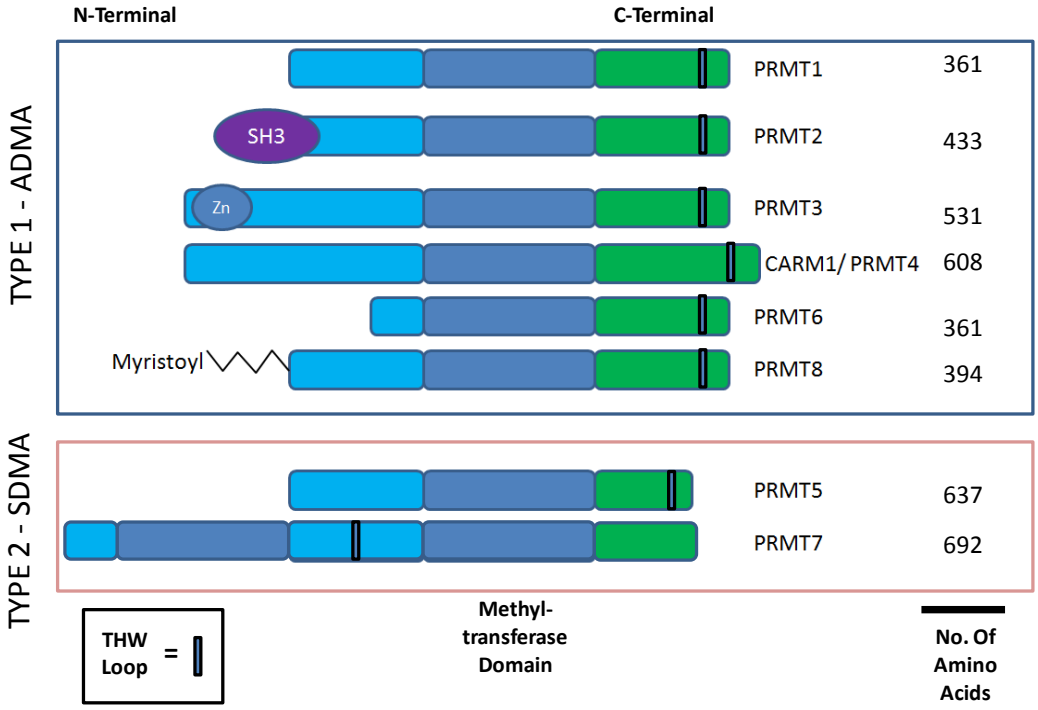

Figure 2: Members of the PRMT family with Methyltransferase activity: Type 1 enzymes give rise to asymmetric dimethyl-arginine (ADMA), whereas type 2 members yield symmetric dimethyl-arginine (SDMA). Each share a common methyltransferase domain, as well as a conserved THW loop, which defines them as a members of the PRMT family. PRMT7 contains two methyltransferase domains. Other members contain N-terminal alterations which affect their localisation and substrate specificity. For example, PRMT8 is largely associated at the plasma membrane due the myristoyl group, and the SH3 domain of PRMT2 allows for interactions with PRMT8.

1.1.1 PRMT1 is alternatively Spliced

The prmt1 gene comprises 12 exons, the first 5 of which undergo alternate splicing, giving rise to 7 known isoforms with distinct N-terminal protein sequences (9, 14). RT-PCR analysis of human tissues shows that each isoform possesses distinct expression profiles (Figure 3) (14). For example, isoform 4 (PRMT1v4) is uniquely expressed in heart tissue, whereas PRMT1v5 is predominantly expressed in the pancreas. The activity of such organ-exclusive isoforms may be tailored to the specific requirements of each tissue. The only two isoforms expressed in multiple tissues are PRMT1v1 and PRMT1v2 (14). These differ through the inclusion of exon 2 in PRMT1v2 (Figure 3). Amino acid sequence analysis and mutagenesis studies have demonstrated that exon 2 contains a CARM1-dependent nuclear export signal (15VATLANGMSL24), thereby explaining the observation that PRMT1v2 is generally cytoplasmic, whereas PRMT1v1 is nuclear (14). As such, the subcellular localisation of these isoforms dictates their individual substrate specificity and activity (15). The evidence for this is discussed in section 1.4. The structural differences and distribution of individual isoforms is likely to contribute to the widespread, diverse functionality of PRMT1.

1.2 PRMT1 regulates diverse cellular processes

1.2.1 Histone Methylation and gene expression

PRMT1 is a well-characterised coactivator of transcription via the methylation of H4R3. One mechanism by which increased gene activation occurs is through the recruitment and activation of the histone acetyltransferase p300, subsequently leading to H4K5 acetylation (12, 16). Acetylation-mediated chromatin relaxation allows for the recruitment of transcription factors and other co-activators. PRMT1 has been shown to interact with numerous nuclear receptors and is an important regulator of oestrogen receptor alpha (ERα) (16-18). This steroid receptor undergoes a conformational change upon binding oestradiol, which leads to the activation of exonuclear signal transduction, namely the phosphatidylinositol-3-kinase (PI3K) pathway, or activation of genes under the control of oestrogen response elements (ERE) (19, 20) . Both events result in breast epithelial cell proliferation. PRMT1 upregulates the transcriptional activity of ERα in response to oestradiol in breast cancer cells, through the recruitment of p300 to the pS2 promoter (17). This suggests that PRMT1 is a necessary mediator of ERα-induced gene expression.

A

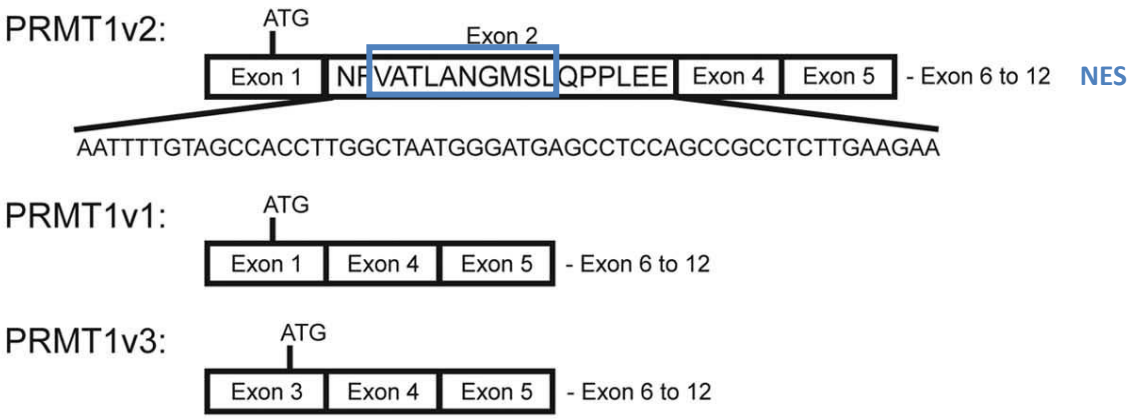

B

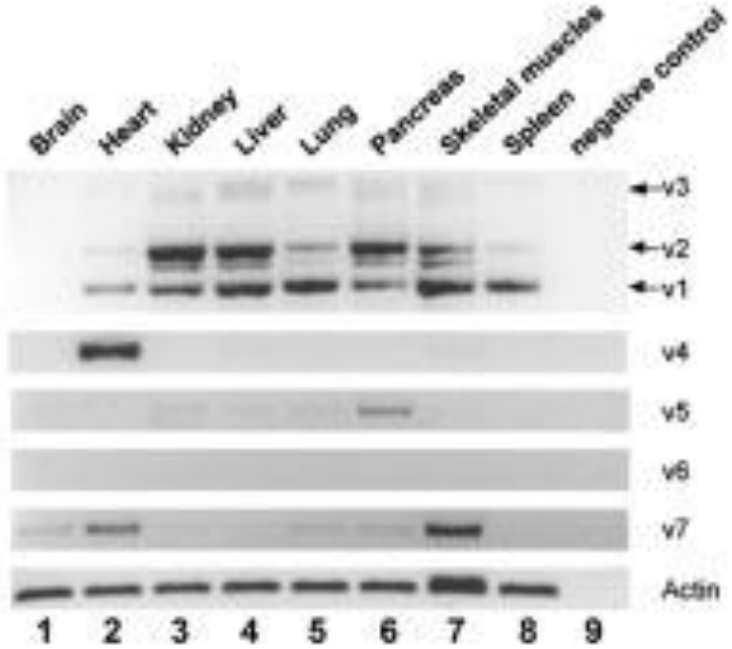

Figure 3: PRMT1 undergoes N-terminal alternate splicing yielding 7 different isoforms: A Schematic representing the N-terminal alterations between exons 1 and 5 of PRMT1 splice variants. Amino acid and DNA sequence are shown for exon 2 included for PRMT1v2. Nuclear export sequence is highlighted in blue. Taken from Baldwin *et al*, Cell Cycle, 2012 (23). **B** RT-PCR analysis of expression for PRMT1 splice variants in human tissues. Actin represents cDNA loading control. Taken from Goulet *et al*, J Biol Chem, 2007 (22).

Additionally, many studies have observed PRMT1-mediated transcriptional activation through interactions with co-activation proteins. For example, it was also found that PRMT1 methylates the transcriptional coactivator peroxisome proliferator-activated receptor γ coactivator-1α (PGC-1α) (21). PGC-1α associates with nuclear receptors and augments the expression of genes under its control. It was found that methylation of PGC-1α by PRMT1 leads to its increased activation and potentiating the activity of ERα, glucocorticoid receptor and thyroid receptor (21). This represents another level at which PRMT1 contributes to ERα-regulation and displays its necessity for nuclear receptor-mediated gene expression. More recently, PRMT1 was shown to form a regulatory complex with the AP-1/c-Jun transcription factor and a co-regulator protein RACO-1 (5). In this instance, RACO-1 is methylated twice by PRMT1 at R98 and R109. This leads to increased protein stability by the inhibition of autoubiquitylation and a conformational change, allowing RACO-1 to dimerise and then interact with c-Jun. Subsequently, the AP-1 transcriptional complex is activated, allowing for gene expression changes and cellular proliferation. Taken together, these studies show how PRMT1 is capable of widespread manipulation of gene expression through a diverse plethora of mechanisms.

1.2.2 Signalling and Survival

More recently, evidence has implicated PRMT1 in processes of cell signalling and survival. As well as acting as a coactivator of ERα mediated transcription, PRMT1 has also been implicated in oestrogen-dependent exonuclear signal transduction. Romancer *et al,* 2008 showed that ERα is methylated in the cytoplasm by PRMT1, resulting in the formation of a complex containing kinase Src and the p85 subunit of PI3K (18) . This leads to the activation of mitogen-activated protein kinase (MAPK) and Akt signalling and cellular proliferation. Methylation by PRMT1 was shown to be necessary for the formation of this complex. Therefore, it is evident that PRMT1 mediation of ERα is complex, regulating both gene transcription and exonuclear signalling.

The activity of PRMT1 plays an important role in Wnt signalling through interactions with β-catenin (22). This is an important signalling pathway involved in cell fate determination, cell proliferation and development. Under non-signalling conditions, β-catenin is phosphorylated by glycogen synthase kinase 3β (GSK3β) and casein kinase 1 (CK1) (23). This permits its ubiquitylation by β-TrCP, targeting the protein for proteasomal degradation. This phosphorylation is made possible through interactions with scaffolding proteins APC and Axin. Wnt-mediated activation of the Frizzled receptor results in the 'destruction complex' of Axin, APC and GSK3β becoming localised to the cytoplasmic tail of lipoprotein receptor-related protein 5,6 (LRP-5,6), enabling its phosphorylation to occur (23). Axin subsequently binds these phosphorylation sites and is sequestered at the cell membrane. This allows for cytoplasmic accumulation and subsequent nuclear localisation of β-catenin, leading to TCF-LEF-dependent transcriptional activation (23, 24). Cha *et al* showed that Axin interacts with PRMT1 and is methylated at R378 (22). This methylation event

increased the stability of Axin and promoted interactions with GSK3β. Hence, a reduction in PRMT1 by siRNA-mediated knockdown resulted in increased stability of β-catenin (22). Taken together, this suggested that PRMT1 acts a negative regulator of the Wnt signalling pathway, through stabilisation of Axin and the destruction complex.

1.3 PRMT1 and Cancer

PRMT1 is involved in several processes, including survival signalling, DNA repair and gene activation, which are commonly deregulated in cancer (25). This suggests a potential role of PRMT1 in tumourigenesis. Studies have shown elevated PRMT1 expression in leukaemia, as well as in breast, colorectal, prostate, bladder and lung cancers (18, 26-30). Importantly, siRNA knockdowns of PRMT1 in cancer cell lines, including breast, bladder, lung and leukaemia, were shown to reduce cancer cell proliferation and viability (15, 29-31). Recent studies have shown a direct involvement of this enzyme in malignant progression. Cheung *et al* demonstrated that PRMT1 was required for the transforming properties of the Multiple Lineage Leukaemia (MLL) fusion protein (31). Using chimeras of MLL fused with the PRMT1 interacting protein, SAM68, as well as PRMT1 directly, they were able to recapitulate the immortalisation conferred by the founding member of MLL-fusion proteins, MLL-EEN. Furthermore, PRMT1 siRINA-knockdowns abolished this activity, suggesting the necessary requirement of PRMT1 in tumourigenesis.

ERα methylation has also been implicated in breast cancer development (18). The activation of stimulatory signalling pathways by ERα is heavily implicated in breast cancer tumourigenesis, with approximately 70% of all breast tumours being positive for this receptor. Immunohistochemical analysis of breast tumours has shown that 50% show much higher levels of methylated ERα, compared to normal breast

tissues (18). Furthermore, increased levels of PRMT1 in breast cancers correlate to lower disease free survival and a poorer prognosis (32). In this case, the status of PRMT1 expression could be used as a diagnostic factor. The evidence presented indicates PRMT1 as a tumourigenic protein, although the processes through which it promotes cancer progression are poorly understood.

1.4 PRMT1v1 and PRMT1v2 display differential roles in pathogenesis

PRMT1v1 and PRMT1v2 have clearly defined roles in breast cancer (14, 15). RNAi-mediated silencing of PRMT1v2 expression caused a decrease in breast cancer cell viability and induced apoptosis in MCF7 breast cancer cell lines (15). Concurrent with this, overexpression of PRMT1v2 in the same cell line resulted in a more motile and invasive phenotype, that did not form tight colonies, suggesting a loss of cell-cell adhesions. Accordingly, cytoplasmic β-catenin levels were reduced. As well as being a major component of Wnt signalling, β-catenin also regulates cell adhesion through interactions with cadherins (23). In contrast, PRMT1v1 overexpression did not promote an invasive phenotype. All of these observations are in agreement with previous evidence; PRMT1 was thought to be a negative regulator of Wnt signalling through interactions with Axin (22). As Axin is a cytoplasmic protein, PRMT1v2 is likely the major regulator of this process. Overall, this study suggests that PRMT1v2 may have a more profound effect on breast cancer development than PRMT1v1.

It is notable, however, that PRMT1v1 overexpression, whilst not affecting invasion, increases the motility of breast cancer cells (15). As this was not associated with a depletion of β-catenin, it seems that PRMT1v1 is also tumourigenic, but acts through different mechanisms than PRMT1v2, perhaps due to their distinct cellular compartmentalisation. Consistent with this, a separate study found that lower

expression of PRMT1v1 was associated with a higher disease-free survival, where as PRMT1v2 expression did not correlate with disease progression. Taken together the results of such studies display a direct involvement of PRMT1 in cancer progression and that different isoforms contribute to tumourigenesis through separate mechanisms.

1.5 Previous work in the Davies lab shows that PRMT1 interacts with USP7 and USP11

Correlative and functional data linking PRMT1 to cancer is strong. However a mechanistic understanding into how aberrant arginine-methylation promotes tumourigenesis is lacking. To address this, the Davies lab uses affinity purification strategies, coupled with mass spectrometry analysis to identify novel binding partners of PRMT1, in the context of cancer. In particular, the lab employs Tandem Affinity Purification (TAP) assays for investigating such protein interactions. This stringent technique employs two consecutive rounds of affinity-purification, using a recombinant protein featuring a “bait” protein of interest attached to the “TAP-tag” (Figure 4A) (33). The tag used by the Davies lab comprises a *Staphylococcus aureus* protein A domain, which binds IgG sepharose beads for an initial purification step. A tobacco etch virus (TEV) protease cleavage site enables cleavage of the protein complexes isolated with the composite TAP-tag from IgG sepharose. The second tag, calmodulin binding protein (CBP), binds to calmodulin beads, enabling a second purification step. Stable human embryonic kidney 293T (HEK293T) cell lines were created expressing a tetracycline inducible TAP-vector. A methyltransferase-dead (MD) PRMT1v1 was used as bait in order to facilitate the trapping of PRMT1v1 substrates. Cells were stimulated with tetracycline for 48 hours, enabling expression of the TAP-tag PRMT1v1 MD protein before being harvested and lysed. Cell lysates

from induced and un-induced cells were subjected to affinity purification assays, protein complexes were resolved by sodium dodecyl sulphate-polyacrylamide gel electrophoresis (SDS-PAGE) and the identity of specific PRMT1v1 interacting proteins were determined by mass spectrometry (MS) (Figure 4B). The analysis identified heterogeneous nuclear ribonucleoprotein U (hnRNP-U) and Ubiquitin-specific protease 11 (USP11) as interacting proteins for PRMT1. The hnRNP family of proteins are involved in correct processing of mRNA. These proteins account for 65% of asymmetrically methylated proteins in the nucleus and have already been identified as substrates of PRMT1(34). As such, hnRNP-U acts as a positive control, showing that this assay can pull-out both novel and known PRMT1 interactors. USP11 however had not previously been identified as a substrate or interacting protein of PRMT1.

Upon further review of the literature, it was found that USP11 is known to directly interact with the related protein USP7 (or HAUSP) (Figure 4C) (35, 36). To validate the MS findings, ectopic immunoprecipitation assays were conducted using myc-tagged PRMT1 and haemagglutinin (HA)-tagged USP11 or USP7. PRMT1 immunoprecipitated both USP7 and USP11 suggesting that PRMT1 interacts with both proteins (Figure 4D).

A

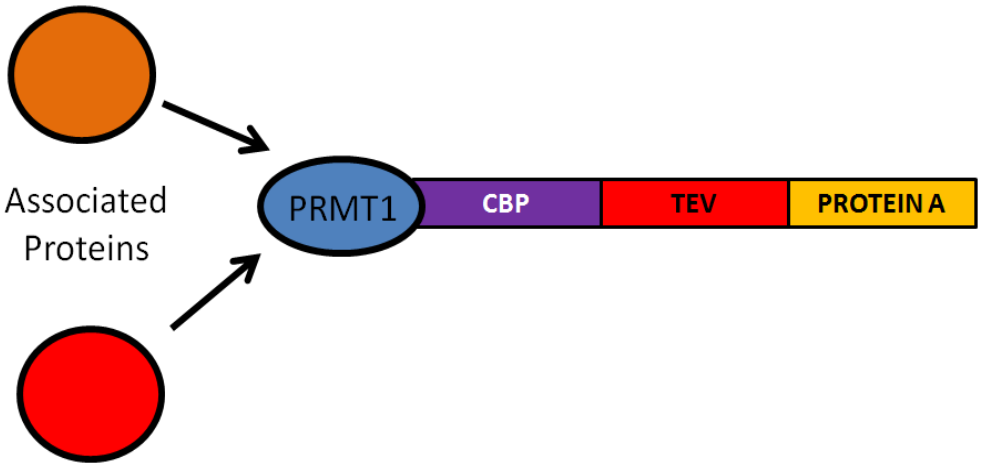

B

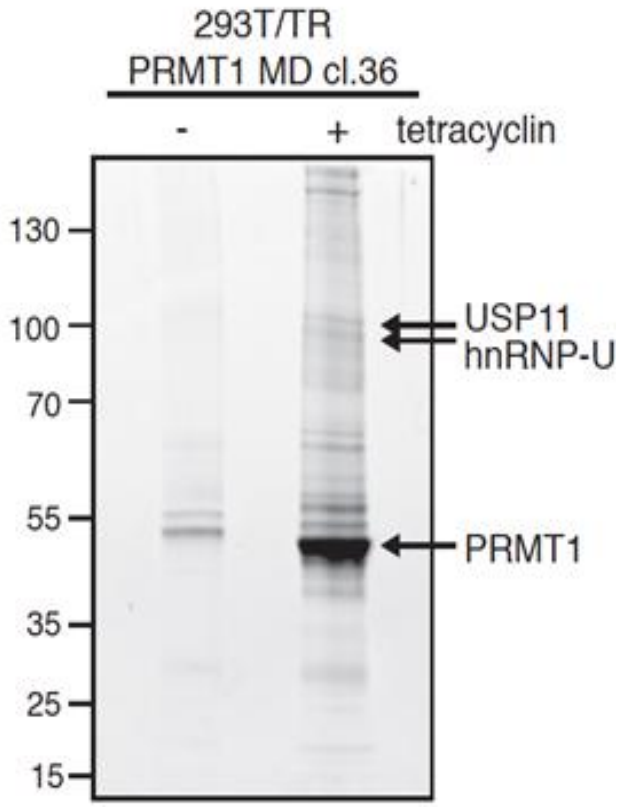

	no. pepties	coverage
PRMT1	33	86%
hnRNP-U	14	22%
USP11	16	18%

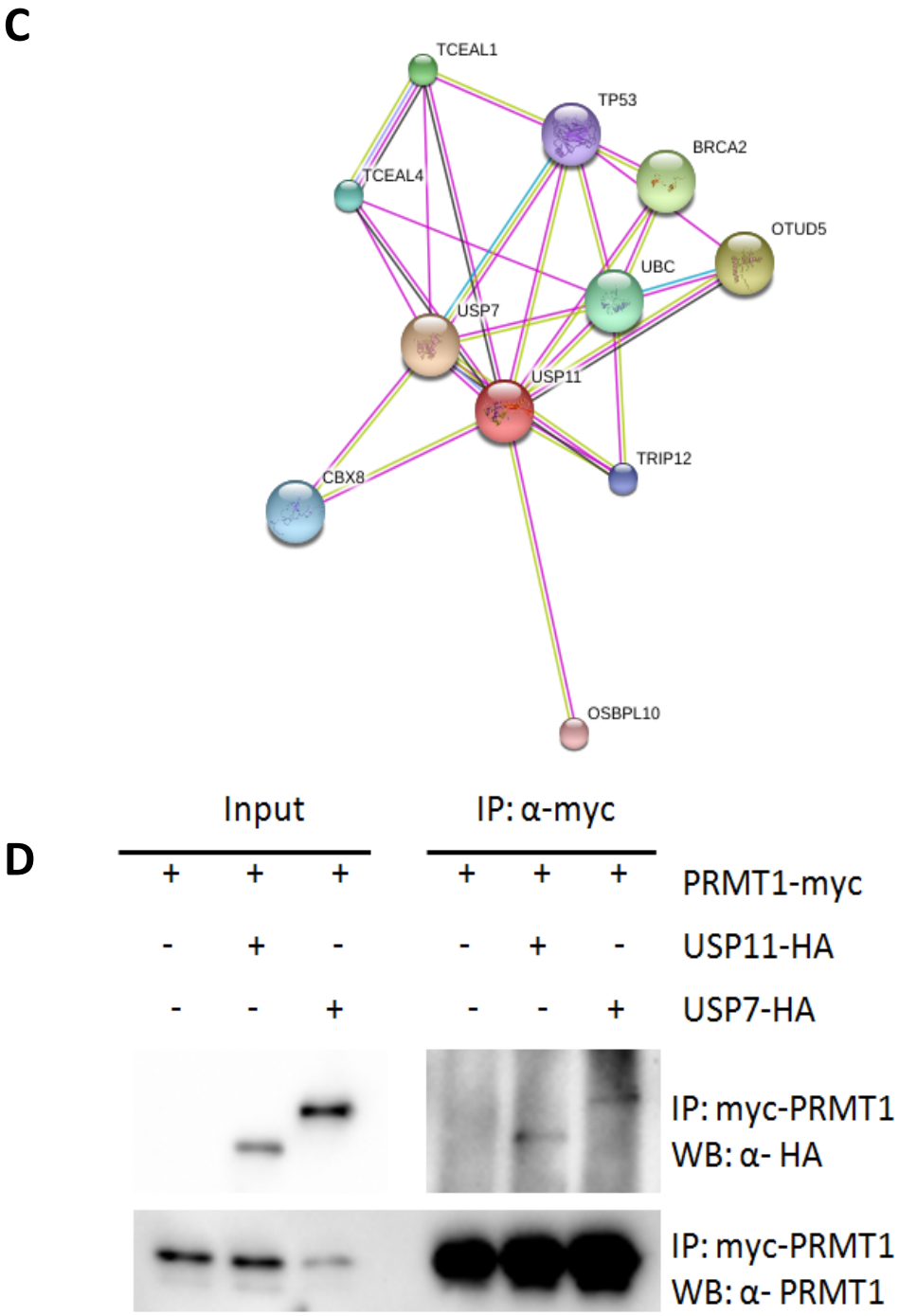

Figure 4: Previous work in the lab showing potential interactions between PRMT1, USP7 and USP11: A Schematic of TAP-tagged recombinant PRMT1v1. TEV; Tobacco etch virus cleavage site; CBP; Calmodulin binding protein. **B** Western blot and mass spectrometry data of PRMT1 TAP-tag assay. HEK293T cells were transfected for stable expression of tetracycline-inducible TAP-PRMT1v1 construct. The lysates from tetracycline treated and untreated cells were subjected to the TAP-tag purification assay. Extracted proteins were resolved through SDS-PAGE and western blotting. Protein bands exclusive to induced cells were cut out and analysed by mass spectrometry. Table represents the number of peptides used which match the identified protein and the percentage coverage of their protein sequences. **B** String diagram representing known interactions involving USP11. Source:www.string-db.org. **C** myc-PRMT1 Immunoprecipitation (IP) assay; HEK293T cells were transfected with myc-tagged PRMT1 together with haemagglutinin-tagged USP11 or USP7. Lysates were then incubated with anti-myc monocloncal antibody-conjugated sepharose beads. IPs were then resolved using sodium dodecyl sulphate-polyacrylamide gel electrophoresis (SDS-PAGE) and western blotting. Data courtesy of Kelly Cheung

1.6 USP7 and USP11 are important Deubiquitylases (DUBs)

Deubiquitylases (DUBs) catalyse the removal of ubiquitin chains from substrates. The removal of K48-linked chains generally leads to the stabilisation and accumulation of their substrates (37). Five families of DUB exist, each of which are separated based on their specific enzymatic activity. The ubiquitin-specific proteases (USPs) family of DUBs share a common catalytic process; a conserved triad of aspartate, histidine and cysteine in the catalytic domain carry out a nucleophilic attack on isopeptide bonds joining adjacent ubiquitin molecule (Figure 5) (37). USPs are the largest DUB family, with each member possessing accessory domains that dictate their activity and available substrates. However, each member does not discriminate between different ubiquitin chain linkages, with the exceptions of USPL1 and USP18, which removes Small Ubiquitin-like Modifier (SUMO) and ISG15 (38, 39). As such, the outcome of their activities is dictated by their substrate specificity. Many USPs have known roles in DNA damage repair and the aberrant expression of almost all of them have been linked to cancer progression (39).

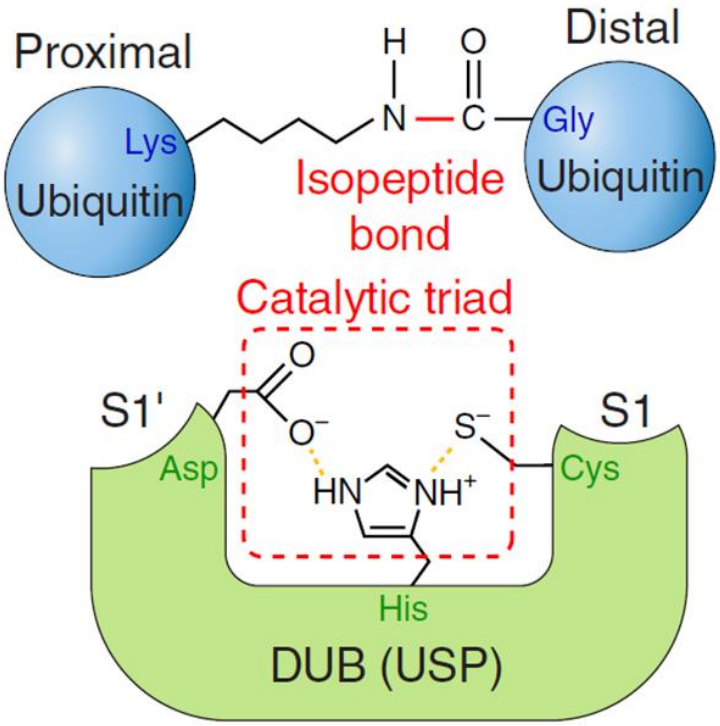

Figure 5: Schematic of ubiquitin-specific protease catalytic activity. Catalytic triad composed of aspartate, histidine and cysteine conducts a nucleophilic attack against isopeptide bonds linking two ubiquitin molecules. S1 and S1' represent binding sites for both proximal and distal ubiquitins. Taken from Clague *et al*, 2013 (44)

1.6.1 The functions of USP11

USP11 is predominantly found in the brain and varies in cellular localisation depending on the current state of cell division (40, 41). Studies have shown it to be a key mediator of DSB repair (42, 43). siRNA knockdown of USP11 elicited a greater rate of spontaneous DNA damage and malfunctioning homologous repair and a reduced recruitment of RAD50 and 53BP1 to foci of DSBs (43). Furthermore, it was found that USP11 also interacts with BRCA2, a necessary regulator of DNA repair (42). USP11 has also been heavily implicated in inflammatory signalling (44). Together with related proteins, it has also been show to function as part of tumour growth factor-beta signalling (TGFβ)(45). Upon TGFβ receptor activation, the expression of SMAD7 is increased. SMAD7 targets TGFβ receptors for ubiquitylation and proteasomal degradation. USP11 has been shown to directly interact with SMAD7, leading to the deubiquitylation and stabilisation of ALK5, a type 1 TGFβ receptor (45). In line with this, USP11 inhibition caused a reduction in TGFβ signalling and epithelial-mesenchymal transition (EMT). Since TGFβ signalling and EMT are important for malignant progression, these results imply that USP11 may function as an oncogene.

1.6.2 The functions of USP7/HAUSP

USP7 has gained a large amount of interest as a critical regulator of development; USP7 knockout mice are embryonic lethal, due to a deregulation of p53 (46). This well-known tumour suppressor is under tight control by the E3-ligase, MDM2. In response to DNA damage, MDM2 is destabilised, which frees p53 from proteasomal degradation. USP7 binds and destabilises MDM2, but also deubiquitylates p53 (46, 47). Both processes lead to p53 stabilisation and promote its activity. Interestingly, although reduced levels of USP7 lead to p53 destabilisation, its complete loss results in further stabilisation. This is likely in part due to the effect of the interaction

between USP7 and MDMX; a negative transcriptional regulator of p53, which is also stabilised by USP7 (47). Thus, USP7 is a vital regulator of p53, through multiple protein interactions.

1.6.3 USP11 and USP7 interact and conduct shared cellular processes

Although USP11 and USP7 have their own distinct set of interacting proteins, both of these enzymes are predominantly found in the nucleus and are capable of interacting with each other (36). Moreover, a recent study showed how USP11 and USP7 interact, subsequently regulating the activity of Polycomb group (PcG) proteins MEL18 and BMI1 (35). These proteins are responsible for the repression of the *INK4a/ARF* locus, which encodes tumour suppressors $p16^{INK4a}$ and $p14^{ARF}$. It was found that both USP11 and USP7 alter the ubiquitylation status of PcG proteins. Deubiquitylation results in a larger association at chromatin and further repression of the *INK4a/ARF* locus. Thus it is evident that, despite each protein possesing diverse substrate repertoires, both USPs are capable of cooperating to induce a specific phenotype.

1.7 Project Aims – Does PRMT1 directly interact with USP7 and USP11?

The Davies lab identified USP11, but not USP7, as a substrate of PRMT1 using TAP-tag affinity purification. However, in cells, it was shown that both USPs were capable of interacting with PRMT1. It is currently unknown as to whether the interactions between PRMT1 and these related proteins are direct or indirect. TAP-tag experiments suggest USP7 may indirectly interact with PRMT1 through USP11, whereas immunoprecipitation assays imply that a complex exists. In order to discover the nature of this interaction, plasmids expressing recombinant tagged constructs of PRMT1, USP11 and USP7 will be cloned into bacteria. Recombinant

protein will then be purified and used for pull-down assays in order to determine if USP11, USP7 or both directly interact with PRMT1.

2 MATERIALS AND METHODS

2.1 Antibodies

Antibody	Source	Purpose
Rabbit Anti-PRMT1	Cell Signalling Technology (F339)	Western Blot Primary (1:2000)
Polyclonal Swine Anti-Rabbit Immunoglobulins/HRP (Horseraddish peroxidise)	Dako (P0217)	Western Blot Secondary (1:5000)

Table 1: Details of the antibodies used throughout the investigation

2.2 Bacterial Strains

Bacterial Strain	Source	Purpose
Alpha-Select Gold Efficiency DH5α	Bioline (**BIO-85027)**	Cloning of His-SUMO-PRMT1v2 and extracting DNA
Rosetta™ BL21 DE3 Competent Cells	EMD Millipore (70954)	Expression and purification of His-SUMO-PRMT1v2 and GST- USP proteins

Table 2: Details of the bacterial strains used throughout the investigation

2.3 Plasmids

Plasmid	Source	Components	Purpose
GFP-PRMT1v2	Kind gift from Mark Bedford, University of Texas, Smithville, Texas, USA	PRMT1v2 is flanked by restriction sites; 5' BamH1 3' Not1	Cloning of His-SUMO-PRMT1v2; Donor
pET28-His-SUMO	Kind gift from Helen Walden (London Research Institute, UK)	Multiple cloning site, kanamycin Resisitance	Cloning of His-SUMO-PRMT1v2; Vector
pGM-GST-USP11	Kind gift from Goedele Maertens, Imperial College, London, UK	Ampicillin Resistance	Bacterial Transformation and purification of GST-USP11
pGM-GST-USP7	Kind gift from Goedele Maertens, Imperial College, London, UK	Ampicillin Resistance	Bacterial Transformation and purification of GST-USP7

Table 3: Details of the plasmids used throughout the investigation

2.4 Reagents

Reagent	Purpose	Components
TAE Buffer (Tris-acetate-EDTA)	Component of agarose gel and agarose electrophoresis	40mM Tris base
		5.71% (v/v) Glacial Acetic Acid
		1mM Ethylenediaminetetraacetic

		acid (EDTA)
Agarose Gel	Separation of DNA through electrophoresis	1% (w/v) Agarose (Sigma)
		0.01% (v/v) Ethidium Bromide
		100ml TAE
Agar plates with kanamycin	Growth of transformed bacteria	2% (w/v) LB broth (Sigma™; L3022)
		1.4% (w/v) LB Agar (Sigma™ L2897)
		50µg/ml kanamycin
Agar plates with ampicillin	Growth of transformed bacteria	2% (w/v) LB broth (Sigma™; L3022)
		1.4% (w/v) LB Agar (Sigma™ L2897)
		100µg/ml ampicillin
Ni^{+} NTA-Lysis Buffer	Purification of His-SUMO-PRMT1v2	300mM NaCl
		5% (v/v) Glycerol
		10mM β-Mercaptoethanol
		50mM sodium diphydrphosphate (NaH_2PO_4)
		50mM disodium hydrophosphate (Na_2HPO_4)
		10mM DTT
		10µg/ml Leupeptin
		10µg/ml Aprotinin

Ni^{+} NTA Wash buffer	Purification of His-SUMO-PRMT1v2	300mM NaCl
		5% (v/v) Glycerol
		10mM β-Mercaptoethanol
		50mM sodium diphydrophosphate (NaH_2PO_4)
		50mM disodium hydrophosphate (Na_2HPO_4)
		50mM Imidazole
Elution Buffer	Elution of His-SUMO PRMT1v2	300mM NaCl
		5% (v/v) Glycerol
		10mM β-Mercaptoethanol
		50mM sodium diphydrophosphate (NaH_2PO_4)
		50mM disodium hydrophosphate (Na_2HPO_4)
		300mM Imidazole
Glutathione Sepharose Lysis Buffer	Purification of GST-USP11 and GST-USP7	50mM Tris-HCL pH 7.4
		2mM EDTA
		0.25% (v/v) Triton-x-100
		1mM Phenylmethanesulfonylfluoride (PMSF)
		10mM Dithiotheitol (DTT)
		10µg/ml Aprotinin

		10µg/ml Leupeptin
Glutathione Sepharose Wash Buffer	Purification of GST-USP11 and GST-USP7	50mM Tris HCl pH 7.4
		2mM EDTA
		500mM NaCl
SDS-PAGE Running Buffer	SDS-PAGE	25mM Tris Base
		50mM Glycine
		0.01% (w/v) sodium dodecyl sulphate (SDS)
Fixing Solution	Coomassie Staining	10% (v/v) Glacial Acetic Acid
		50% (v/v) MeOH
Coomassie Blue Stain	Coomassie Staining	10% (v/v) Glacial Acetic Acid
		45% (v/v) MeOH
		3mM Coomassie Brilliant Blue
Destaining Solution	Coomassie Staining	10% (v/v) Glacial Acetic Acid
		45% (v/v) MeOH
5X Laemmli Sample Buffer	SDS-PAGE	2.5% (w/v) Bromophenol blue
		2.5M DTT
		25% SDS
		2.5M Tris-HCL pH6.8
Transfer Buffer (pH 8.3)	Western Blotting	25mM Tris
		192mM Glycine
		0.1% (w/v) SDS
		20% (v/v) MeOH
Tris Buffered Saline (TBS)	Western Blotting	20mM Tris Base

pH 7.6		137mM NaCl
TBS Tween (TBST)	Western Blotting	TBS 0.1% (v/v) Tween

Table 4: Details of chemical reagents used throughout the investigation

2.5 Cloning

2.5.1 Primers

Name	Purpose	Sequence
P1V2F	Forward primer: PCR amplification of PRMT1v2	5'- cca**ggatcc**gcggcagccgaggccgcga-3'
P1V2R	Reverse Primer: PCR amplification of PRMT1v2	5'- aat**gcggccgc**tcatcagcgcatccggtagtcggt-3'

Table 5: Details of primers used for cloning within this investigation

2. 5.2 PCR Amplification of PRMTv2

PRMT1v2 was amplified via polymerase chain reaction (PCR) using the procedures and reagents stated below. Forward primer contains BamH1 recognition site (**GGATCC**). Reverse primer contains Not1 recognition site (**GCGGCCGC**) and 2 stop codons (TCA). Both primers comprise an excess 5' codon providing a larger binding site for restriction enzymes. Accuzyme (Bioline; BIO-21051) DNA polymerase was used as it conducts proofreading. Dimethyl sulfoxide (DMSO) was added to lower the required annealing temperature of the reaction.

A

Reagent	**Concentration**
GFP-PRMT1v2 template	2ng/µl
Scott 1 Primer	500nM
Scott 2 Primer	500nM
DMSO	5% (v/v)
Accuzyme	2.5U
10X Accuzyme Reaction Buffer (Supplied with accuzyme)	10% (v/v)
Deoxynucleotide Triphosphates (dNTPs)	200µM

B

- Initialization step - 95°C – 3 min
- Denaturation step – 95°C 30 sec
- Annealing step - 60°C – 45 sec
- Extension step – 72°C – 1.4 min

35 Cycles

- Final extension - 72°C – 10 min
- Hold - 4°C

Figure 6: Details of polymerase chain reaction (PCR) procedures used for cloning within this investigation: **A** Components of PCR mixture. **B** Details of cycles used.

2.5.3 Cloning of PRMT1v2 into pET28-His-SUMO

PCR products were purified using agarose gel electrophoresis. Samples were run at 80V for 1 hour on a 1% agarose gel in TAE. Bands were excised and DNA was extracted using an E.Z.N.A Poly-Gel DNA Extraction Kit (OMEGA Biotek D2561) as per the manufacturer's instructions.

PRMT1v2 PCR products and 20 µl pET28-His-SUMO were digested overnight with both BamH1-HF (New England Biolabs [NEB]; R3136) and Not1-HF (NEB; N3189) overnight or for 2 hours at 37°C. Additional buffer and reagent requirements for each enzyme were fulfilled as per the manufacturers guidelines. pET28-His-SUMO then was treated with 10U calf-intestinal alkaline phosphatase (CIP; NEB M0290) for 20 min at 37°C to remove 5' phosphate groups and prevent re-ligation of the vector. DNA was then extracted from the enzymatic reaction using an E.Z.N.A Poly-Gel DNA Extraction Kit. The concentrations of both vector and insert were elucidated by NanoDrop.

Ligation was then conducted using a vector: insert ratio of 1:3. DNA was incubated with 40U T4 DNA Ligase (NEB M0202S) in 1X T4 ligase buffer (NEB; B0202S) for 3 hours at room temperature (RT). A separate ligation containing pre-digested pET28-His-SUMO alone was conducted as a control for ligation and enzymatic digest efficiency following bacterial transformation. Ligated pET28-His-SUMO-PRMT1v2 or pET28-His-SUMO control was used to transform DH5α competent bacteria. 10µl of ligation reaction was added to 50µl bacteria on ice. After 20min, bacteria were heat-shocked at 42°C for 30sec and then allowed to rest on ice for 2min. Bacteria were then incubated for 1 hour at 37°C, 200rpm with 9-times the original volume (450µl) of super optimal broth with catabolite repression (SOC) medium (Sigma; S1797). Cultures were then plated on agar plates containing kanamycin. In order to identify

positive clones, bacterial were picked and grown in 4ml LB broth with 50µg/ml kanamycin overnight at 37°C, 200rpm. DNA was extracted from cultures using a plasmid Minikit (OMEGA Biotek D6942) according to manufacturer's instructions. Plasmid preps were digested with Bam1-HF and Not1-HF and then separated by agarose electrophoresis as described earlier. The presence of a 1Kb insert indicated if bacteria were expressing the PRMT1v2 open-reading frame.

2.6 Purification of His-SUMO PRMT1v2 Protein from Rosetta Bacteria using Ni^+ NTA Agarose

To obtain recombinant His-SUMO PRMT1v2, pET28-His-SUMO-PRMT1v2 was used to transform Rosetta BL21 DE3 bacteria according the suppliers recommendations. Single colonies were picked and used to inoculate 50ml of LB broth. This starter culture was incubated overnight at 37°C, 200rpm. 10ml of this culture was used to inoculate 4x500ml LB broth, giving a 2L total. Each culture was propagated at 37°C, 200rpm to an optical density (OD) of 0.4-0.6. Plasmid expression was then stimulated in each culture with the additional of 400µM Isopropyl β-D-1-thiogalactopyranoside (IPTG). Cultures were grown for a further 4 hours under the same conditions, before centrifugation at 4000g, 10min at 4°C. Pellets were resuspended in Ni^+ NTA lysis buffer and sonicated twice on ice for 10s at 40% amplitude. Bacterial lysates were then incubated on ice with 1mg/ml lysozyme for 10mins and then centrifuged at 20,000g for 20min at 4°C. A 50µl sample of supernatent was maintained for later analysis of all soluble proteins; soluble fraction. The remaining supernatent was incubated with 250µl packed Ni^+ NTA agarose beads (Qiagen, 30210) per 10ml supernatent for 2 hours at 4°C on a rotator. Beads were prewashed 3 times Ni^+ NTA wash buffer prior to incubation. Following this, a 50µl sample of supernatent was taken to analysis the efficiency of

the affinity purification; depleted fraction. Beads were then washed 3 times with Ni^+ NTA wash buffer and made into a 1:1 slurry in Ni^+ NTA wash buffer for storage. Both extracts fragments and 20µl of 1:1 beads were denatured at 95°C for 5 minutes in 5X Laemmli Sample Buffer and resolved by SDS-PAGE as an assessment of the purification.

To elute protein from the beads, 100µl packed beads were incubated in 400µl elution buffer on ice for 1 min. Beads were then centrifuged at 200g, 3min at 4°C and the supernatent was retained. This was repeated and supernatents were pooled. The total volume of supernantent was made up to 5ml with Ni^+ NTA lysis buffer, lacking phosphatase and protease inhibitors, in order to dilute the imidazole. To concentrate the proteins and pass out the imidazole, the solution as then diafiltrated using an Amicon Ultra-4 Centrifugal Filter Unit with Ultracel-10kDa (Merck Millipore; UFC801096); the solution was added and then centrifuged at 3220g for 10min at RT. The volume of retained solution was again increased to 5ml and centrifuged and previously done. The retained protein solution was then mixed with 10% glycerol and alloquoted for storage at -80°C.

2.7 Purification GST-USP7 and GST-USP11 from Rosetta Bacteria using glutathione 4B Sepharose beads

In order to purify GST-USP7 and GST-USP11, previously mentioned plasmids were used in conjunction with an adapted protocol as stated by the author(35). Rosetta bacteria were transformed using pGM-GST-USP7 or pGM-GST-USP11 according the suppliers recommendations. Single colonies were used to inoculate 50ml of liquid broth. These starter cultures were incubated overnight at 37°C, 200rpm. 10ml of this culture was used to inoculate 4x500ml LB broth, per USP, giving a total of 2L each. Cultures were propagated at 37°C, 200rpm to an optical density (OD) of 0.4-

0.6. Plasmid expression was then stimulated in each culture with the additional of 1mM IPTG. Cultures were then incubated overnight at 18°C, 200rpm and then centrifuged at 4000g for 20min at 4°C. Bacterial pellets were resuspended in glutathione sepharose lysis and sonicated twice on ice for 10s at 40% amplitude. Lysates were then incubated on ice with 1mg/ml lysozyme for 10min and then centrifuged at 20,000g for 20min at 4°C. After this step, soluble and depleted fractions were maintained as previously done when purifying His-SUMO PRMT1v2. The resulting supernatent for each protein was then incubated with glutathione sepharose 4B beads (GE Healthcare 17-0756-01), at a ratio of 600µl packed beads to 10ml supernatent, for 2 hours at 4°C on a rotator. Beads were prewashed 3 times in glutathione sepharose lysis buffer prior to incubation. Following incubation, beads were washed 3 times with wash buffer and made into a 1:1 slurry, in wash buffer, for storage at 4°C. All removed fractions and 20µl of 1:1 beads were denatured at 95°C for 5 minutes 5X Laemmli sample buffer and resolved by SDS-PAGE as an assessment of the purification.

2.8 Pull-Down Assay

The following procedure was used to assess protein interactions between PRMT1v2 and USPs. 10µl packed USP-conjugated glutathione sepharose 4B beads were used for each separate experiment. 2µl of GST-conjugated beads, which were already available in the Davies lab, was used for controls. Beads were washed twice with their experimental incubation buffer then resuspended in 500µl of the same buffer containing 10µg/ml leupeptin and aprotinin. 4µg His-SUMO-PRMT1v2 was added to pull-down solutions where necessary. Pull-downs were then rotated at 4°C for 1 hour. Beads from each condition were centrifuged at 200g, 5min at 4°C and washed 4 times in incubation buffer. All residual buffer was removed using a fine-gauge

insulin syringe. Beads were denatured at 95°C for 5 minutes in 40µl Laemmli sample buffer. Each sample was dividing equally between a 10% and 12% acrylamide gel. For each gel, 200ng His-SUMO-PRMT1v2 was added to 13µl sterilised distilled water and denatured in 4µl Laemmli sample buffer and loaded as an input. All samples were resolved by SDS-PAGE. Bands from the 12% gel were then visualised using coomassie staining and those of the 10% gel were transfered to a Polyvinylidene fluoride (PVDF) membrane and subjected to western blotting.

2.9 SDS-PAGE

SDS-PAGE procedures were carried out using the BioRad Mini-PROTEAN Tetral Cell minigel electrophoresis system (165-8004). Acrylamide gel mixtures were made according to table 6, whilst withholding APS and TEMED. These reagents were added to mixtures immediately before pouring. 7.5-8ml of gel mixture was poured into the systems casting module. 1ml isopropanol was layered on top to exclude air bubbles and create a level surface. After polymerisation, the isoproanl layer was washed off with ddH_20, the stacking gel poured on top and combs inserted. Denatured samples were loaded into appropriate lanes. 2µl of Geneflow BLUeye Prestained protein ladder (S6-0024) was loaded separately as a marker. Gels were run at 125V for at least 90 min in 1X running buffer. For pull-down experiments, it was ensured that larger proteins GST-USP11 and GST-USP7 (110kDa and 130kDa respectively) migrate out of the stacking gel, whilst retaining the smaller GST in the resolving gel. Protein bands were then visualised using coomassie staining or protein transfer and western blotting.

Gel Category	Component	Concentration
Resolving	Tris	375mM
	Acrylamide	8, 10 or 12% (v/v)
	SDS	0.1% (w/v)
	Ammonium Persulphate (APS)	0.1% (w/v)
	Tetramethylethylenediamine (TEMED)	0.06% (v/v)
Stacking	Tris	125mM
	Acrylamide	5% (v/v)
	SDS	0.1% (w/v)
	APS	0.1% (w/v)
	TEMED	0.1% (v/v)

Table 6: Components of polyacrylamide gels. Percentage of acrylamide used was altered according to the molecular weights of the proteins visualised; smaller percentages were used when visualising larger proteins, e.g. GST-USP11 and GST-USP7, and vice versa.

2.10 Coomassie Staining

All staining procedures were conducted on a rocker at room temperature. Acrylamide gels were fixed for 10min in fixing solution, stained with coomassie blue solution for 5min and then destained for at least 2 hours in destaining solution before being imaged using a Peqlab FUSION FX7 Advance chemiluminescence imager.

2.11 Protein Transfer, Western Blotting and Enhanced Chemoluminescence

Hybond-P PVDF membranes (GE Healthcare Life Sciences, RPN303F) were used for protein transfer. Membranes were first activated in MeOH for 10sec, washed in distilled water for 2min and then equilibrated in transfer buffer for at least 5min prior to transfer. Acrylamide gels were also soaked in transfer before for at least 5min.

Protein bands were transferred using the Bio-Rad Trans-blot Turbo semi-dry transfer system at 25V for 25 min. Membranes were blocked in TBST with 5% (w/v) milk powder for at least one hour. After being briefly washed in TBST, membranes were incubated with rabbit anti-PRMT1 primary antibody in 5% BSA (w/v) overnight at 4°C. Membranes were then washed 3 times for at least 5 min each in TBST and then incubated in HRP-conjugated goat anti-rabbit secondary antibody in TBST 5% (w/v) milk powder, for 1 hour, RT. Blot was then washed in TBST as before and then treated with SuperSignal West Dura Enhanced chemiluminescence (ECL) HRP substrate(Thermo Scientific). Protein bands were then viewed using Amersham Hyperfilm ECL X-ray film (GE Healthcare Life Sciences 28-9068-36).

3 RESULTS

3.1 PRMT1v2 was cloned into pET28 His-SUMO background

In order to determine if PRMT1v2 interacts directly with USP11 or USP7, it was necessary to create tagged-recombinant proteins to be used for pull-down experiments. It was decided to clone PRMT1v2 as this isoform contains the addition 18 amino acids of exon 2. Furthermore, the prevalence of v2 in breast cancer tumourigenesis makes it a more relevant candidate for understanding its methods of regulation (15). The Davies lab had previously received plasmid constructs encoding GST-tagged, full-length versions of USP11 and USP7, as a kind gift from Goedele Maertens (35). As such, it was decided that His-tagged PRMT1 expression constructs would be generated. To this end, PRMT1v2 was PCR amplified, using GFP-PRMT1v2 as a template (see Materials and Methods) and cloned into pET28-His-SUMO, containing kanamycin resistance. The addition of an N-terminal SUMO tag is well known to increase the solubility and expression of eukaryotic proteins in *E. coli*(48). Cloning was conducted using the DH5α bacterial strain, which were then plated on kanamycin-containing agar plates. Colonies were then picked and used to inoculate starter cultures in liquid broth. Cultures were incubated overnight and DNA was extracted from cultures using the Omegabiotek Minikit according to the manufacturer's instructions.

To identify positive clones, where successful plasmid ligation had occurred, extracted DNA was subjected to restriction endonuclease digest, using BamH1 and Not1, followed by separation through agarose electrophoresis. 1% agarose gels were made with ethidium bromide in order to visualise DNA bands using ultraviolet light (Figure 7). DNA prepared from each of the 6 bacterial colonies each yielded two bands following resolution; a 0.8kb band, representing the PRMT1v2 insert, and a second, approximately 5.3kb, representing the pET28-His-SUMO vector. This shows that PRMT1v2 was correctly cloned into pET28-His-SUMO. Remaining DNA extracted from the bacteria was pooled, alloquoted and frozen at -80°C for storage.

3.2 Generation of Recombinant His-SUMO-PRMT1v2

Having generated the pET28-His-SUMO-PRMT1v2 expression plasmid, it was subsequently used to transform bacteria, from which to extract recombinant protein. To increase the resemblance of this exogenous protein to wild-type proteins generated in eukaryotes, Rosetta BL21 strain bacteria were used for transformations. This strain provided tRNAs for codons which are a rare in bacteria, thus enhancing the accuracy and expression of eukaryotic proteins. Bacteria were transformed with pET28-His-SUMO-PRMT1v2 and grown on kanamycin agar plates. A colony from these plates was picked and used to generate a 2L liquid culture with an OD of 0.6 (See materials and methods). Plasmid expression was induced with IPTG and cultures were then propagated further, as per materials and methods, before being harvested by centrifugation. Recombinant proteins were isolated from sonicated bacterial lysates by affinity purification using Ni^{+} NTA beads. Fractions were taken from lysates before and after incubation with beads, the soluble and depleted fractions respectively. Proteins were then eluted from the beads using a high concentration of imidazole. To concentrate the protein solution and dialyse

against the high molarity imidazole required for the solution, the protein-imidazole solution was diafiltrated twice using a filtration column which retains proteins larger than 10kDa. The presence of His-SUMO-PRMT1v2, both attached to beads and purified, was confirmed using SDS-PAGE and coomassie staining (Figure 8A). Fractions were run along-side as an assessment of recombinant protein solubility and the quality of the purification. Multiple proteins were seen attached to the beads, suggesting the purification is highly impure. These are likely proteins with exposed histidine residues or degraded recombinant proteins. However, the strongest band seen for both purified and bead-conjugated protein was in the region of 50kDA. PRMT1v2 has a molecular weight of approximately 42.5kDa, where as the SUMO tag is 8kDA. This suggests that this 50kDa band is His-SUMO-PRMT1v2 and that had successfully been purified. Furthermore, corresponding bands of similar intensities are seen for both eluted and conjugated proteins, suggesting that the elution process was highly efficient. Disappointingly, the recombinant protein band is of a similar strength to proteins within both fragments, implying weak expression of the plasmid. Concurrent with this, the corresponding 50kDa band seen in both fractions is faint suggesting that His-SUMO-PRMT1v2 may have low solubility. Nevertheless, as His-SUMO-PRMT1v2 is the predominant eluted protein, this solution can be confidently used for subsequent pull-down assays.

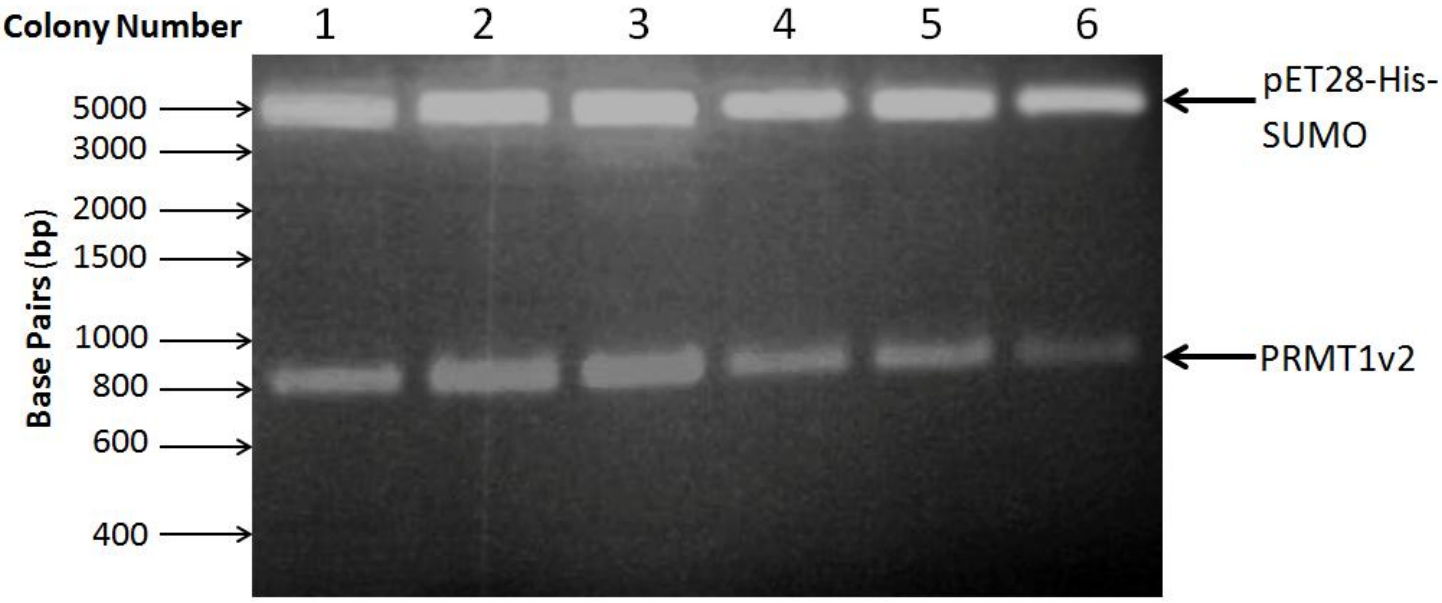

Figure 7: Agarose electrophoresis of DNA digests extracted from bacterial clones transformed with pET28-His-SUMO PRMTv1:PRMT1v2 was cloned into pET28 His-SUMO vector. This plasmid was used to transform super-competent DH5α Rosetta™ bacteria (Bioline), which were then plated on kanamyocin containing agar. DNA was purified from successfully transformed colonies, using a miniprep kit (Omega Biotek). DNA was then digested using BamH1-HF and Not1-HF restriction endonucleases. The resulting DNA was resolved using electrophoresis. Each lane represents an individual bacterial colony from which DNA was extracted using the miniprep kit.

3.3 Generation of GST-USP11 and GST-USP7 conjugated to glutathione Sepharose 4B Beads

Purification of recombinant GST-USP11 and GST-USP7 was achieved by adapting a protocol previously established by Goedele Maertens *et al*, 2010(35).To aid this, plasmids coding for GST-tagged versions of both enzymes had been generously donated by the same author. These were used to transform to Rosetta bacteria as previously done with His-SUMO-PRMT1v2. Transformed bacteria were grown on ampicillin agar plates. Single colonies for each transformation were picked and used to develop 2L liquid agar cultures. Plasmid expression was induced in these cultures with IPTG once they had reached an OD of 0.6. Cultures were then propagated, centrifuged and lysed as per materials and methods. Recombinant proteins, containing GST, were isolated from lysates with glutathione sepharose 4B beads. Soluble and depleted fractions were taken from lysates as previously done when isolating His-SUMO-PRMT1v2. The beads were then washed and refrigerated at 4°C for storage as 1:1 slurry in wash buffer. Fractions and samples of beads for each protein were then resolved using SDS-PAGE. Gels were then coomassie stained to assess the quality of purification (Figure 8B).

Protein yields for GST-USP11 and GST-USP11 were small, however the shear sizes of these proteins (136kDa and 156kDa respectively) make bacterial expression difficult. Consequently, several proteins are seen attached to both sets of beads, which are likely degradation products of recombinant proteins. Furthermore, the GST-USP11 yielded 2 particularly strong non-specific bands at approximately 55kDa and 85kDa, which could decrease the authenticity of any interactions observed from later experiments (Figure 8B). However, relatively strong bands corresponding to the sizes of GST-USP11 and GST-USP7 were observed from their respective

purifications, suggesting the preparation was successful. These preparations were subsequently used to assess the interactions between these enzymes and PRMT1v2.

3.4 Pull-down assays suggest that PRMT1v2 interacts directly with both USP11 and USP7 *in vitro*

Pull-down assays were performed to assess whether PRMT1v2 could interact directly with USP11, USP7 or both. Glutathione sepharose 4B-bound forms of GST-USP11 or GST-USP7 were incubated with or without purified His-SUMO-PRMT1v2 for 1 hour at 4°C. As the stringency of these interactions was unknown, each pull-down was performed in phosphate buffered saline (PBS) or in buffer physiological levels of NaCl (150mM). Beads were washed and denatured for resolution by SDS-PAGE. Each sample was divided between 2 gels. One was visualised by coomassie stain and the other was subjected to protein transfer to a PVDF membrane, followed by anti-PRMT1 western blotting (Figure 9A). An input of His-SUMO-PRMT1v2 alone was run on the gel subjected to western blotting, as a positive control for the antibody. Band patterns resembling those seen for the purification of GST-USPs were visible on the Coomassie stained gel. This showed that both GST-USP11 and GST-USP7 were present throughout the pull-down and that they were not lost as a consequence of technical error. Moreover, PRMT1 bands were not seen for pull-downs where His-SUMO-PRMT1 was not added, which shows the specificity of the antibody used.

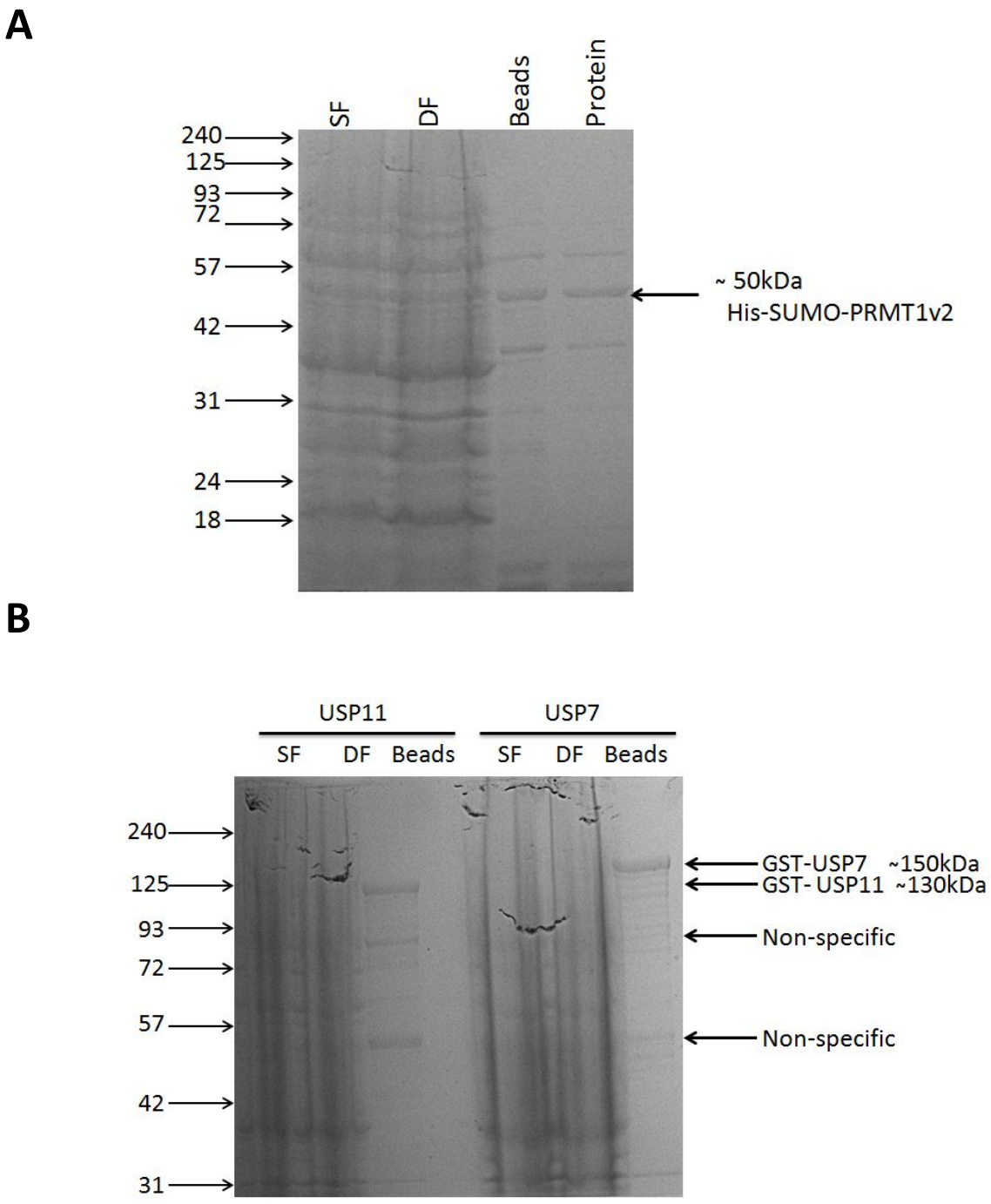

Figure 8: Coomassie blue stains showing stages of protein purification for His-SUMO-PRMT1v2, GST-USP11 and GST-USP7: Rosetta™ super-competent DH5α bacteria were transformed with plasmids expressing the required protein. Two litre liquid cultures for each protein were cultured to an OD of 0.6. Protein synthesis was induced with IPTG and cultures were allowed to grow for a set specific for each protein. Cells were lysed and each protein was extracted from supernatents. Samples were taken from supernatents before (Soluble Fraction; SF) and after (Depleted fraction; DF) incubation with beads to ensure the presence of proteins in the supernatent and to observe the effect of the beads. **A: Purification of His-SUMO-PRMTv2**. Cultures were incubated for a further 5 hours at 37°C before harvesting. Bacterial lysates were incubated with Ni^{+} NTA beads for 2 hours. Beads were then washed and a sample was taken for SDS-PAGE. Half of the beads were incubated with buffer containing a high concentration of imidazole in order to elute protein from the beads. The buffer was passed through a filtration column in order to concentrate the protein. A sample from this protein solution was subjected to SDS-PAGE. **B Purification of GST-USP11 and GST-USP7.** Cultures were incubated overnight at 18°C before harvesting. Bacterial lysates were incubated with glutathione 4B sepharose beads for 2 hours. Beads were then washed and a sample was taken for SDS-PAGE.

However, with the addition of His-SUMO-PRMT1v2 to GST-USP11 and GST-USP7, a clear 50 kDa band, consistent with the size of this His-SUMO-PRMT1v2 PRMT1, was apparent suggesting that PRMT1v2 interacts directly with USP11 and USP7 (Figure 9A). This band was present in pull-downs conducted in both and 150mM NaCl buffers; however PRMT1v2 binding to USP11/7 was substantially reduced in 150mM NaCl, reflecting the more stringent conditions of this buffer. This shows that potentially both enzymes are capable of directly interacting with PRMT1v2. Further anti-His or anti-SUMO immunoblotting using the samples could have been used to confirm the identity of this 50kDa band,

To further confirm the occurrence of these interactions and investigate the specificity of these interactions, each pull down was repeated at different concentrations of NaCl (150, 250 or 400mM). A third pull-down using beads conjugated to GST alone was included as a negative control (purified protein already available in the Davies lab) (Figure 9B). A large 26kDa band was seen on the coomassie stained gel which denotes the high concentration of GST used in the reaction. However, despite the substantial proportion of GST utilised, a negligible signal for His-SUMO-PRMT1v2 is seen for the pull-down conducted at 150mM NaCl. Furthermore, the interactions previously seen at 150mM for GST-USP11 and GST-US7 have repeated. Together this shows that the observed interactions are highly specific for these USPs. As expected, bands representing PRMT1v2 are not seen at salt concentrations above the physiological level. This suggests that the observed reactions are physiologically relevant and may occur *in vivo*. In conclusion, these results provide evidence that both USP11 and USP7 are capable of direct interaction with PRMT1v2.

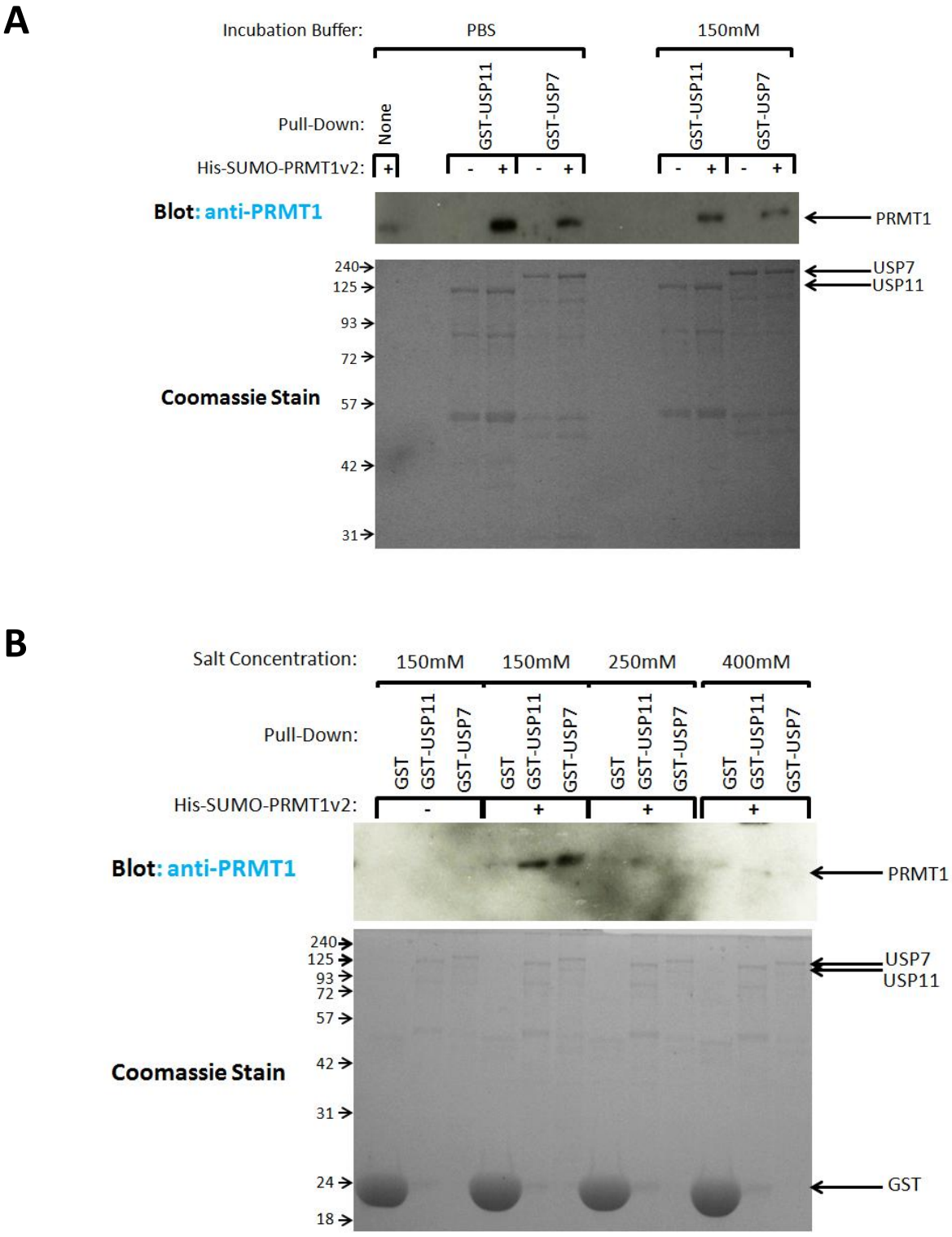

Figure 9: Western blot and Coomassie stain analysis of pull-down assays assessing interactions of PRMT1v2 with USP11 and USP7 at different salt concentrations: Glutathione sepharose 4B beads conjugated to GST-USP11 or GST-USP7 were was incubated with or without His-SUMO-PRMT1v2 for 1 hour at 4°C. Beads were then washed and denatured for SDS-PAGE. Each sample was divided between 2 acrylamide gels. One gel underwent coomasie staining, whereas the other was subjected to western blot analysis using an anti-PRMT1 antibody**. A: Pull-down assays conducted in PBS and physiological levels of NaCl (150mM):** An input comprising His-SUMO-PRMT1 alone was added to the first lane as a positive control for the primary antibody. **B Pull-down down assays conducted at 150, 250 or 400mM NaCl**. A third pull-down was introduced using GST-conjugated beads as a negative control. n=3

4. DISCUSSION

4.1 Summary of Results

- PRMT1 variant 2 is capable of direct interaction with both USP11 and USP7.
- Interactions between PRMT1v2 and USP11/7 are lost at non-physiological salt levels, suggesting this reaction can occur *in vivo.*

4.2 The physiological role of the direct interaction

4.2.1 Does PRMT1 methylate USP11 and USP7?

Probably the most immediate question raised in response to these findings is as to whether USP11 and USP7 are methylated by PRMT1. PRMT1 is thought to target proteins containing RGG/RG repeats for methylation (4). Such motifs are present in the primary sequence of USP7, but not in USP11 (Figure 10). However, this is not to say that PRMT1 cannot methylate USP11, as many validated PRMT1 substrates are methylated independently of an RGG/RG motif (5). Furthermore, the TAP-tag assay previously used to discover USP11 as an interactor for PRMT1 used a methyltransferase dead PRMT1v1 as a bait protein. Not only does this suggest that the inclusion of exon 2 is not required for this interaction, but it is supports the notion that USP11 may be a methylated substrate of PRMT1. It is surprising that this initial investigation did not show USP7 as an interactor, as it possesses an RGG/RG motif with mice and humans. Furthermore, this RG motif is found within the catalytic domain (UniProt database), which implies that arginine-methylation of this motif could influence its deubiquitylase activity. However, the TAP-tag assay is a stringent investigation tool, due to the two rounds of affinity purification. As such, weak or transient interactions are sometimes lost throughout its proceedings, which may

explain why USP7 was not originally discovered. In total, it can be said that USP11 and USP7 could be potential substrates of PRMT1.

USP11

MAVAPRLFGGLCFRFRDQNPEVAVEGRLPISHSCVGCRRERTAMATVAANPAAAAAAVAAAAAVTEDR
EPQHEELPGLDSQWRQIENGESGRERPLRAGESWFLVEKHWYKQWEAYVQGGDQDSSTFPGCINNA
TLFQDEINWRLKEGLVEGEDYVLLPAAAWHYLVSWYGLEHGQPPIERKVIELPNIQKVEVYPVELLLVRH
NDLGKSHTVQFSHTDSIGLVLRTARERFLVEPQEDTRLWAKNSEGSLDRLYDTHITVLDAALETGQLIIME
TRKKDGTWPSAQLHVMNNNMSEEDEDFKGQPGICGLTNLGNTCFMNSALQCLSNVPQLTEYFLNNC
YLEELNFRNPLGMKGEIAEAYADLVKQAWSGHHRSIVPHVFKNKVGHFASQFLGYQQHDSQELLSFLLD
GLHEDLNRVKKKEYVELCDAAGRPDQEVAQEAWQNHKRRNDSVIVDTFHGLFKSTLVCPDCGNVSVT
FDPFCYLSVPLPISHKRVLEVFFIPMDPRRKPEQHRLVVPKKGKISDLCVALSKHTGISPERMMVADVFSH
RFYKLYQLEEPLSSILDRDDIFVYEVSGRIEAIEGSREDIVVPVYLRERTPARDYNNSYYGLMLFGHPLLVSV
PRDRFTWEGLYNVLMYRLSRYVTKPNSDDEDDGDEKEDDEEDKDDVPGPSTGGSLRDPEPEQAGPSS
GVTNRCPFLLDNCLGTSQWPPRRRRKQLFTLQTVNSNGTSDRTTSPEEVHAQPYIAIDWEPEMKKRYY
DEVEAEGYVKHDCVGYVMKKAPVRLQECIELFTTVETLEKENPWYCPSCKQHQLATKKLDLWMLPEILII
HLKRFSYTKFSREKLDTLVEFPIRDLDFSEFVIQPQNESNPELYKYDLIAVSNHYGGMRDGHYTTFACNKD
SGQWHYFDDNSVSPVNENQIESKAAYVLFYQRQDVARRLLSPAGSSGAPASPACSSPPSSEFMDVN

USP7

MNHQQQQQQQKAGEQQLSEPEDMEMEAGDTDDPPRITQNPVINGNVALSDGHNTAEEDMEDDTS
WRSEATFQFTVERFSRLSESVLSPPCFVRNLPWKIMVMPRFYPDRPHQKSVGFFLQCNAESDSTSWSC
HAQAVLKIINYRDDEKSFSRRISHLFFHKENDWGFSNFMAWSEVTDPEKGFIDDDKVTFEVFVQADAP
HGVAWDSKKHTGYVGLKNQGATCYMNSLLQTLFFTNQLRKAVYMMPTEGDDSSKSVPLALQRVFYEL
QHSDKPVGTKKLTKSFGWETLDSFMQHDVQELCRVLLDNVENKMKGTCVEGTIPKLFRGKMVSYIQCK
EVDYRSDRREDYYDIQLSIKGKKNIFESFVDYVAVEQLDGDNKYDAGEHGLQEAEKGVKFLTLPPVLHLQ
LMRFMYDPQTDQNIKINDRFEFPEQLPLDEFLQKTDPKDPANYILHAVLVHSGDNHGGHYVVYLNPKG
DGKWCKFDDDVVSRCTKEEAIEHNYGGHDDDLSVRHCTNAYMLVYIRESKLSEVLQAVTDHDIPQQLV
ERLQEEKRIEAQKRKERQEAHLYMQVQIVAEDQFCGHQGNDMYDEEKVKYTVFKVLKNSSLAEFVQSL
SQTMGFPQDQIRLWPMQARSNGTKRPAMLDNEADGNKTMIELSDNENPWTIFLETVDPELAASGAT
LPKFDKDHDVMLFLKMYDPKTRSLNYCGHIYTPISCKIRDLLPVMCDRAGFIQDTSLILYEEVKPNLTERIQ
DYDVSLDKALDELMDGDIIVFQKDDPENDNSELPTAKEYFRDLYHRVDVIFCDKTIPNDPGFVVTLSNR
MNYFQVAKTVAQRLNTDPMLLQFFKSQGYRDGPGNPLRHNYEGTLRDLLQFFKPRQPKKLYYQQLKM
KITDFENRRSFKCIWLNSQFREEEITLYPDKHGCVRDLLEECKKAVELGEKASGKLRLLEIVSYKIIGVHQED
ELLECLSPATSRTFRIEEIPLDQVDIDKENEMLVTVAHFHKEVFGTFGIPFLLRIHQGEHFREVMKRIQSLL
DIQEKEFEKFKFAIVMMGRHQYINEDEYEVNLKDFEPQPGNMSHPRPWLGLDHFNKAPKRSRYTYLEK
AIKIHN

Figure 10: Amino acid sequences of *Homo sapien* USP7 and USP11. RGG/RG of USP7 is highlighted in red. Source: www.pubmed.gov

Further investigation is necessary to elucidate as to whether USP7 and USP11 are methylated by PRMT1. Employing both *in vitro* and *in vivo* methylation assays will be of great benefit. *In vitro* assays employ the use of radioactively labelled SAM ([^{3}H]-SAM) as a catalyst for methylation by PRMT1 (49). As such, recombinant PRMT1 is incubated with potential recombinant substrates and [^{3}H]-SAM. True substrates will become radioactively labelled, which can be visualised by SDS-PAGE and fluorography. The purified versions of His-SUMO-PRMT1v2, GST-USP11 and GST-USP7 could be used within this assay to assess their methylation status. To determine if methylation occurs within cells, *in vitro* findings should be confirmed with *in vivo* methylation assays. Cell lines can be first treated with adenosine dialdehyde (AdOx) to expose potential methylation sites and cycloheximine to block de novo protein synthesis, and then cultured in media containing [^{3}H] methylmethionine (50). Through the methionine metabolic pathway, tritium becomes encorporated into endogenous SAM and methylated proteins labelled. Specific methylation of the protein of interest is achieved through immunoprecipitation, separation via SDS-PAGE and fluorography. Importantly, through the inhibition of de novo protein synthesis, radiolabelled methyl groups can only be encorporated as a PTM, hence the radiolabelling is a reflection on methyltransferase activity rather than the incorporation of radiolabelled methionine into translated proteins. Repeating these procedures in the presence of siPRMT1 will confirm that PRMT1 is responsible for this methylation. Functional assays for USP activity would be required following this to determine the functional significance of arginine methylation. For example, USP7 or USP11 could be incubated with known substrates, such as p53 and ALK5 respectively (45, 46). Substrate stability could be determined through SDS-PAGE and western blotting under conditions where PRMT1 is present or absent.

4.2.2 Do USP11 and USP7 regulate the activity and stability of PRMT1?

Although the TAP-tag assay previously used in the Davies lab was initially optimised to identify novel methylated substrates of PRMT1, it is a possibility that interactions between USP11 and USP7 may be concerned with regulating the activity of PRMT1. One clear mechanism in which this may occur is through deubitiquitylation. Information as to if PRMT1 is ubiquitylated is lacking. Deubiquitylation of K48-linked chains however could lead to the stabilisation of PRMT1. At the end of this investigation, the half-life of PRMT1 was assessed using separate treatments of HEK293T cells with cycloheximide or MG132 to inhibit protein synthesis and proteasomal degradation, respectively (data not shown). Subsequent anti-PRMT1 western blot analysis of cell lysates showed persisting PRMT1 bands for up to 10 hours following these treatments, suggesting that PRMT1 is a highly stable protein and that half-life experiments would need to be conducted using ^{35}S-labelled methionine. Furthermore, after the completion of this project, the Davies lab has now shown that overexpression of USP11 and USP7 increases protein levels of PRMT1. Future work will be needed as to determine if these observations are caused by altering the stability of PRMT1 or via an increase in mRNA expression.

USP11/7 may regulate the activity of PRMT1, or vice versa, through none-enzymatic association and protein complex formation. Although this investigation has shown that both USP11 and USP7 interact directly with PRMT1, it is not known if each protein interacts separately with PRMT1, or if the three proteins form a tertiary complex (Figure 11). This would largely depend on the spatiotemporal qualities of each DUB. USP7 was not identified as a substrate of PRMT1 through TAP-tag affinity purification. Evidence which explains this finding supports a non-enzymatic regulation between these two proteins. For example, it suggests that USP7 is not methylated but can still interact with PRMT1. In support of this, a study has outlined a consensus amino acid sequence for the recognition of interactors by USP7 (47). Multiple sequences of P/AXXS were found to be important for USP7 recognition of p53 and MDM2 (47). Such a sequence is found in PRMT1v1 and PRMT1v2 (Figure 12), which represents a prime candidate for the interaction site between USP7 and PRMT1. Interestingly, the best described positive regulator of PRMT1, BTG1, also possesses two P/AXXS motifs (Figure 12). USP7 may therefore regulate the activity of PRMT1 through direct interactions but also through the control of BTG1. As such, USP7 may be targeted to PRMT1 by BTG1 or vice versa. Site-directed mutagenesis of these residues will confirm their importance in USP7-PRMT1 association and the functionality of each protein.

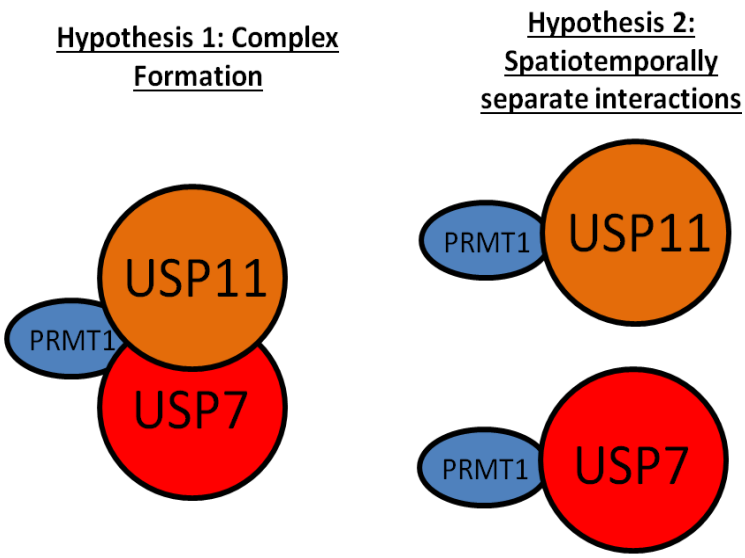

Figure 11: Schematic displaying potential models of PRMT1 interactions with USP11 and USP7.

PRMT1

MEVSCGQAESSEKPNAEDMTSKDYYFDSYAHFGIH
EEMLKDEVRTLTYRNSMFHNRHLFKDKVVLDVGSG
TGILCMFAAKAGARKVIGIECSSISDYAVKIVKANKLD
HVVTIIKGKVEEVELPVEKVDIIISEWMGYCLFYESM
LNTVLYARDKWLAPDGLIFPDRATLYVTAIEDRQYKD
YKIHWWENVYGFDMSCIKDVAIKEPLVDVVDPKQL
VTNACLIKEVDIYTVKVEDLTFTSPFCLQVKRNDYVH
ALVAYFNIEFTRCHKRTGFSTSPESPYTHWKQTVFY
MEDYLTVKTGEEIFGTIGMRPNAKNNRDLDFTIDLD
FKGQLCELSCSTDYRMR

BTG1

MHPFYTRAATMIGEIAAAVSFISKFLRTKGLTSER
QLQTFSQSLQELLAEHYKHHWFPEKPCKGSGYR
CIRINHKMDPLIGQAAQRIGLSSQELFRLLPSELT
LWVDPYEVSYRIGEDGSICVLYEASPAGGSTQNS
TNVQMVDSRISCKEELLLGRTSPSKNYNMMTV
SG

Figure 12: Amino acid sequences of *Homo sapien* PRMT1v1 and BTG1. Potential USP7-recognition motifs are highlighted in red. Source: www.pubmed.gov

4.3 Do PRMT1 splice variants interact differently with USP11 and USP7?

Functional differences in the activity between PRMT1v1 and PRMT1v2 are evident, both in normal physiology and tumourigenesis (15). This is mostly likely due to their specific localisations. These differences may give some insight as to the spatiotemporal organisation of USP11 and USP7. Both enzymes are predominantly nuclear and 50% of USP7 is chromatin bound (35). PRMT1 is commonly chromatin-bound in order to co-activate nuclear receptor-induced gene transcription though histone H4R3 methylation (12, 13, 16). It is possible that USP7 or USP11 interaction may be necessary for PRMT1 control of gene expression. More specifically, these proteins may predominantly associate with PRMT1v1 due its nuclear localisation. This is not to say that they cannot interact with other isoforms. USP11 is also found in the cytoplasm, which is necessary for deubiquitylation of ALK5 and promoting TGFβ signalling (45). In this instance, USP11 may interact solely with the cytoplasmic PRMT1v2. In support of this, it has been shown that PRMT1 methylates Smad6, which causes its relocalisation to BMP-receptors (51). PRMT1v2 was also shown to associate at type II BMP-receptors. Both USP11 and PRMT1v2 have been separately shown to associate at these receptors and promote TGFβ signalling(45, 51). PRMT1 may also interact simultaneously with both USPs under certain circumstances. For example, PRMT1 interaction may regulate the repression of *Ink4a* by chromatin-bound USP11 and USP7 (35). In conclusion it is likely that USP11 and USP7 individually interact with PRMT1 in response to specific signals. The specific isoform with which each interacts will likely depend on the spatiotemporal properties of the specific signals and downstream consequences.

4.4 Protocol Optimisation and Further Investigation

4.4.1 Optimisation of protein purification protocols

One of the most difficult challenges when conducting this investigation was the purification of GST-USP11 and GST-USP7. Both proteins are over 100kDa, thus ensuring accurate and stable exogenous expression was a challenge. As such, although full-length proteins were acquired, several products of degradation from these proteins were present on glutathione sepharose 4B beads. These impurities could have masked the true nature of the observed interactions, or perhaps created false-positive results through multiple, non-specific interaction with PRMT1. Technical challenges were even present upon completion of the purification. Following affinity purification, the beads became incredibly adhesive. This is likely due to, again, the number of impurities in each set of beads, or potentially the large size of the proteins giving rise to multiple non-specific reactions with free amino acid side chains. GST-USP11-conjugated beads were particularly adherent, potentially due to the strong 55kDA and 85kDa bands seen in the preparation. This made the beads difficult to handle and most likely caused protein to be lost as beads were washed. Furthermore, this may have restricted the movement of the beads during the pull-down incubation.

Smaller proteins are much easier to purify and are often expressed at higher proportions in the soluble fraction. For that reason, it would be beneficial to repeat these proceedings using plasmids that encode fragments of USP11 and USP7. Using smaller proteins would increase protein solubility, bacterial expression and reduce the impurity of each preparation. In addition, repeating these processes using sequential, overlapping peptides of each USP's sequence, important motifs and residues could be identified and the binding site could be mapped. The findings from

this could then be elucidated further using x-ray crystallography and site-directed mutagenesis. This technique may also be used in tandem with *in vitro* and *in vivo* methylation assays, in order to identify and map methylated arginine residues. Such actions would improve the quality of this investigation and increase our molecular understanding of these interactions.

4.5 Targeting the interaction between USP11 and USP7 for the treatment of breast cancer

Although the nature and purpose of the direct interactions of PRMT1 with both USP11 and USP7 have yet to be elucidated, it is conceivable that the invention of such events could be of therapeutic importance. One possibility is that PRMT1 is deubiquitylated and stabilised by USP11 and USP7. Alternatively, the association of PRMT1 with these proteases, either for methylation or direct regulation, may contribute to the tumourigenic actions of either protein. In either case, the inhibition of these interactions could be employed for an anti-cancer therapy. PRMT1 is thought to contribute to the progression of ERα-dependent breast cancer, and has is also found upregulated in other tumours (19, 25). As such several studies have been devoted to the discovery of PRMT1-specific inhibitors (52, 53). Of importance, it is not certain how PRMT1 inhibition would affect patients. Due to the diverse activities of PRMT1, its inhibition could yield many side-effects, although a reduction to normal expression levels could be of benefit for cancer patients. In addition, achieving PRMT1-specificity is challenging due to the similarities in activity between PRMT family members. Targeting USP11 and USP7 for inhibition presents similar problems. Evidence suggests that a decrease in USP7 activity would induce p53 destabilisation and a complete removal would cause p53-induced senescence (46).

A loss of USP11 may also promote further tumourigenesis through increased frequency of DSB and increased NFκB activity (42-44).

Exclusive intervention of PRMT-USP interactions, possibly through use of by small interfering molecules or peptides could be of therapeutic value. Specific inhibition of the interactions described in this investigation could reduce the activities of PRMT1, either through a reduction in protein stability or regulation by interactors. As we have shown that PRMT1 is highly stable, coupled to the likely presence of other regulatory processes, interrupting these reactions would probably preserve its baseline function in cellular homeostasis. Importantly, the necessary activities of both USP11 and USP7 would also be preserved, which would limit the overall side-effects of this treatment. Although further insight into the mechanics and consequences of the interactions between PRMT1, USP11 and USP7 will be required before such procedures can come into fruition, this investigation has uncovered a potentially important relationship involving PRMT1 which could be exploited for treatment of several forms of cancer.

5 REFERENCES

1. Tang J, Frankel A, Cook RJ, Kim S, Paik WK, Williams KR, et al. PRMT1 is the predominant type I protein arginine methyltransferase in mammalian cells. J Biol Chem. 2000;275(11):7723-30.
2. Yu Z, Chen T, Hebert J, Li E, Richard S. A mouse PRMT1 null allele defines an essential role for arginine methylation in genome maintenance and cell proliferation. Mol Cell Biol. 2009;29(11):2982-96.
3. Pawlak MR, Scherer CA, Chen J, Roshon MJ, Ruley HE. Arginine N-methyltransferase 1 is required for early postimplantation mouse development, but cells deficient in the enzyme are viable. Mol Cell Biol. 2000;20(13):4859-69.
4. Gary JD, Clarke S. RNA and protein interactions modulated by protein arginine methylation. Progress in nucleic acid research and molecular biology. 1998;61:65-131.
5. Davies CC, Chakraborty A, Diefenbacher ME, Skehel M, Behrens A. Arginine methylation of the c-Jun coactivator RACO-1 is required for c-Jun/AP-1 activation. Embo j. 2013;32(11):1556-67.
6. Osborne TC, Obianyo O, Zhang X, Cheng X, Thompson PR. Protein arginine methyltransferase 1: positively charged residues in substrate peptides distal to the site of methylation are important for substrate binding and catalysis. Biochemistry. 2007;46(46):13370-81.
7. Wooderchak WL, Zang T, Zhou ZS, Acuna M, Tahara SM, Hevel JM. Substrate profiling of PRMT1 reveals amino acid sequences that extend beyond the "RGG" paradigm. Biochemistry. 2008;47(36):9456-66.
8. Hata K, Nishijima K, Mizuguchi J. Role for Btg1 and Btg2 in growth arrest of WEHI-231 cells through arginine methylation following membrane immunoglobulin engagement. Experimental cell research. 2007;313(11):2356-66.
9. Lin WJ, Gary JD, Yang MC, Clarke S, Herschman HR. The mammalian immediate-early TIS21 protein and the leukemia-associated BTG1 protein interact with a protein-arginine N-methyltransferase. J Biol Chem. 1996;271(25):15034-44.
10. Robin-Lespinasse Y, Sentis S, Kolytcheff C, Rostan MC, Corbo L, Le Romancer M. hCAF1, a new regulator of PRMT1-dependent arginine methylation. Journal of cell science. 2007;120(Pt 4):638-47.
11. Rust HL, Subramanian V, West GM, Young DD, Schultz PG, Thompson PR. Using unnatural amino acid mutagenesis to probe the regulation of PRMT1. ACS chemical biology. 2014;9(3):649-55.
12. Feng Y, Wang J, Asher S, Hoang L, Guardiani C, Ivanov I, et al. Histone H4 acetylation differentially modulates arginine methylation by an in Cis mechanism. J Biol Chem. 2011;286(23):20323-34.
13. Huang S, Litt M, Felsenfeld G. Methylation of histone H4 by arginine methyltransferase PRMT1 is essential in vivo for many subsequent histone modifications. Genes & development. 2005;19(16):1885-93.
14. Goulet I, Gauvin G, Boisvenue S, Côté J. Alternative splicing yields protein arginine methyltransferase 1 isoforms with distinct activity, substrate specificity, and subcellular localization. J Biol Chem. 2007;282(45):33009-21.
15. Baldwin RM, Morettin A, Paris G, Goulet I, Côté J. Alternatively spliced protein arginine methyltransferase 1 isoform PRMT1v2 promotes the survival and invasiveness of breast cancer cells. Cell Cycle. 2012;11(24):4597-612.
16. Wang H, Huang ZQ, Xia L, Feng Q, Erdjument-Bromage H, Strahl BD, et al. Methylation of histone H4 at arginine 3 facilitating transcriptional activation by nuclear hormone receptor. Science (New York, NY). 2001;293(5531):853-7.
17. Koh SS, Chen D, Lee YH, Stallcup MR. Synergistic enhancement of nuclear receptor function by p160 coactivators and two coactivators with protein methyltransferase activities. J Biol Chem. 2001;276(2):1089-98.

18. Le Romancer M, Treilleux I, Leconte N, Robin-Lespinasse Y, Sentis S, Bouchekioua-Bouzaghou K, et al. Regulation of estrogen rapid signaling through arginine methylation by PRMT1. Molecular Cell. 2008;31(2):212-21.
19. Le Romancer M, Treilleux I, Bouchekioua-Bouzaghou K, Sentis S, Corbo L. Methylation, a key step for nongenomic estrogen signaling in breast tumors. Steroids. 2010;75(8-9):560-4.
20. Manavathi B, Acconcia F, Rayala SK, Kumar R. An inherent role of microtubule network in the action of nuclear receptor. Proceedings of the National Academy of Sciences of the United States of America. 2006;103(43):15981-6.
21. Teyssier C, Ma H, Emter R, Kralli A, Stallcup MR. Activation of nuclear receptor coactivator PGC-1alpha by arginine methylation. Genes & development. 2005;19(12):1466-73.
22. Cha B, Kim W, Kim YK, Hwang BN, Park SY, Yoon JW, et al. Methylation by protein arginine methyltransferase 1 increases stability of Axin, a negative regulator of Wnt signaling. Oncogene. 2011;30(20):2379-89.
23. Rao TP, Kuhl M. An updated overview on Wnt signaling pathways: a prelude for more. Circulation research. 2010;106(12):1798-806.
24. Nusse R. Wnt signaling in disease and in development. Cell research. 2005;15(1):28-32.
25. Yang Y, Bedford MT. Protein arginine methyltransferases and cancer. Nature reviews Cancer. 2013;13(1):37-50.
26. Zou L, Zhang H, Du C, Liu X, Zhu S, Zhang W, et al. Correlation of SRSF1 and PRMT1 expression with clinical status of pediatric acute lymphoblastic leukemia. Journal of hematology & oncology. 2012;5:42.
27. Mathioudaki K, Papadokostopoulou A, Scorilas A, Xynopoulos D, Agnanti N, Talieri M. The PRMT1 gene expression pattern in colon cancer. British journal of cancer. 2008;99(12):2094-9.
28. Seligson DB, Horvath S, Shi T, Yu H, Tze S, Grunstein M, et al. Global histone modification patterns predict risk of prostate cancer recurrence. Nature. 2005;435(7046):1262-6.
29. Yoshimatsu M, Toyokawa G, Hayami S, Unoki M, Tsunoda T, Field HI, et al. Dysregulation of PRMT1 and PRMT6, Type I arginine methyltransferases, is involved in various types of human cancers. International journal of cancer Journal international du cancer. 2011;128(3):562-73.
30. Elakoum R, Gauchotte G, Oussalah A, Wissler MP, Clement-Duchene C, Vignaud JM, et al. CARM1 and PRMT1 are dysregulated in lung cancer without hierarchical features. Biochimie. 2014;97:210-8.
31. Cheung N, Chan LC, Thompson A, Cleary ML, So CW. Protein arginine-methyltransferase-dependent oncogenesis. Nat Cell Biol. 2007;9(10):1208-15.
32. Mathioudaki K, Scorilas A, Ardavanis A, Lymberi P, Tsiambas E, Devetzi M, et al. Clinical evaluation of PRMT1 gene expression in breast cancer. Tumour biology : the journal of the International Society for Oncodevelopmental Biology and Medicine. 2011;32(3):575-82.
33. Puig O, Caspary F, Rigaut G, Rutz B, Bouveret E, Bragado-Nilsson E, et al. The tandem affinity purification (TAP) method: a general procedure of protein complex purification. Methods (San Diego, Calif). 2001;24(3):218-29.
34. Boffa LC, Karn J, Vidali G, Allfrey VG. Distribution of NG, NG,-dimethylarginine in nuclear protein fractions. Biochemical and biophysical research communications. 1977;74(3):969-76.
35. Maertens GN, El Messaoudi-Aubert S, Elderkin S, Hiom K, Peters G. Ubiquitin-specific proteases 7 and 11 modulate Polycomb regulation of the INK4a tumour suppressor. EMBO J. 2010;29(15):2553-65.
36. Sowa ME, Bennett EJ, Gygi SP, Harper JW. Defining the human deubiquitinating enzyme interaction landscape. Cell. 2009;138(2):389-403.
37. Clague MJ, Barsukov I, Coulson JM, Liu H, Rigden DJ, Urbé S. Deubiquitylases from genes to organism. Physiol Rev. 2013;93(3):1289-315.
38. Schulz S, Chachami G, Kozaczkiewicz L, Winter U, Stankovic-Valentin N, Haas P, et al. Ubiquitin-specific protease-like 1 (USPL1) is a SUMO isopeptidase with essential, non-catalytic functions. EMBO reports. 2012;13(10):930-8.

39. Faesen AC, Luna-Vargas MP, Geurink PP, Clerici M, Merkx R, van Dijk WJ, et al. The differential modulation of USP activity by internal regulatory domains, interactors and eight ubiquitin chain types. Chemistry & biology. 2011;18(12):1550-61.
40. Kapushesky M, Emam I, Holloway E, Kurnosov P, Zorin A, Malone J, et al. Gene expression atlas at the European bioinformatics institute. Nucleic acids research. 2010;38(Database issue):D690-8.
41. Ideguchi H, Ueda A, Tanaka M, Yang J, Tsuji T, Ohno S, et al. Structural and functional characterization of the USP11 deubiquitinating enzyme, which interacts with the RanGTP-associated protein RanBPM. The Biochemical journal. 2002;367(Pt 1):87-95.
42. Schoenfeld AR, Apgar S, Dolios G, Wang R, Aaronson SA. BRCA2 is ubiquitinated in vivo and interacts with USP11, a deubiquitinating enzyme that exhibits prosurvival function in the cellular response to DNA damage. Mol Cell Biol. 2004;24(17):7444-55.
43. Wiltshire TD, Lovejoy CA, Wang T, Xia F, O'Connor MJ, Cortez D. Sensitivity to poly(ADP-ribose) polymerase (PARP) inhibition identifies ubiquitin-specific peptidase 11 (USP11) as a regulator of DNA double-strand break repair. J Biol Chem. 2010;285(19):14565-71.
44. Sun W, Tan X, Shi Y, Xu G, Mao R, Gu X, et al. USP11 negatively regulates TNFalpha-induced NF-kappaB activation by targeting on IkappaBalpha. Cellular signalling. 2010;22(3):386-94.
45. Al-Salihi MA, Herhaus L, Macartney T, Sapkota GP. USP11 augments TGFbeta signalling by deubiquitylating ALK5. Open Biol. 2012;2(6):120063.
46. Kon N, Kobayashi Y, Li M, Brooks CL, Ludwig T, Gu W. Inactivation of HAUSP in vivo modulates p53 function. Oncogene. 2010;29(9):1270-9.
47. Sheng Y, Saridakis V, Sarkari F, Duan S, Wu T, Arrowsmith C, et al. Molecular recognition of p53 and MDM2 by USP7/HAUSP. Nature Structural & Molecular Biology. 2006;13(3):285-91.
48. Malakhov MP, Mattern MR, Malakhova OA, Drinker M, Weeks SD, Butt TR. SUMO fusions and SUMO-specific protease for efficient expression and purification of proteins. Journal of structural and functional genomics. 2004;5(1-2):75-86.
49. Pahlich S, Zakaryan RP, Gehring H. Protein arginine methylation: Cellular functions and methods of analysis. Biochimica et biophysica acta. 2006;1764(12):1890-903.
50. Najbauer J, Aswad DW. Diversity of methyl acceptor proteins in rat pheochromocytoma (PC12) cells revealed after treatment with adenosine dialdehyde. J Biol Chem. 1990;265(21):12717-21.
51. Xu J, Wang AH, Oses-Prieto J, Makhijani K, Katsuno Y, Pei M, et al. Arginine Methylation Initiates BMP-Induced Smad Signaling. Mol Cell. 2013;51(1):5-19.
52. Cheng D, Yadav N, King RW, Swanson MS, Weinstein EJ, Bedford MT. Small molecule regulators of protein arginine methyltransferases. J Biol Chem. 2004;279(23):23892-9.
53. Spannhoff A, Heinke R, Bauer I, Trojer P, Metzger E, Gust R, et al. Target-based approach to inhibitors of histone arginine methyltransferases. Journal of medicinal chemistry. 2007;50(10):2319-25.

APPENDIX: LIST OF ABBREVIATIONS

Abbreviation	Meaning
53BP1	p53 Binding Protein 1
ADMA	Asymmetric Dimethylated Arginine
ALK	Anaplastic lymphoma kinase
AP-1	Activator Protein-1
APC	Adenomatosis Polyposis Coli
APS	Ammonium Persulphate
BMI-1	B cell-specific Moloney murine leukemia virus integration site 1
BTG1	B-cell translocation genes 1
BTG2	B-cell translocation genes 2
CBP	Calmodulin Binding Protein
CK1	Casein Kinase 1
CRM1	Exportin-1
DNA	Deoxyribonucleic acid
DSB	Double Strand Breaks
DTT	Dithiotheitol
DUB	Deubiquitylase
ECL	Enhanced chemiluminescence
EDTA	Ethylenediaminetetraacetic acid
EMT	Epithelial-Mesenchymal Transition
ERE	Oestrogen Response Elements
ERα	Oestrogen Receptorα
GFP	Green Fluorescent Protein
GSK3β	Glycogen Synthase Kinase 3β

GST	Glutathione S-Transferase
H4R3	Histone 4 Arginine 3
H5K5	Histone 4 Lysine 5
HA	Haemagglutinin
HAUSP	Herpes-virus-associated Ubiquitin-Specific Protease
hCAF1	CCR4-associated factor
HEK293T	Human Embryonic Kidney 293 with T antigen
His	6 Histidine Tag
hnRNP	Heterogeneous Nuclear Ribonucleoprotein
HRP	Horseraddish peroxidise
IgG	Immunoglobulin G
INK4a/ARF	Inhibitor of cyclin-dependent Kinase type 4/Alternate Reading Frame
IP	Immunoprecipitation
IPTG	Isopropyl β-D-1-thiogalactopyranoside
ISG15	Interferon-induced 17 kDa protein
LB	Liquid Broth
LRP-5,6	Lipoprotein Receptor-related Protein 5,6
MAPK	Mitogen-activated Protein Kinase
MCF7 Cells	Michigan Cancer Foundation-7 Cells
MCM-BP	Minichromosome Maintenance Binding-Protein
MD	Methyltransferase-dead
MDM2	Mouse double minute 2 homolog
MDMX	Mouse double minute X homolog
MEF	Mouse Embryonic Fibroblast
MLL	Multilineage Leukaemia

MMA	Monomethylated arginine
MS	Mass Spectrometry
NTA	Nitrilotriacetic Acid
PBS	Phosphate buffer solution
PcG	Polycomb Group
PCR	Polymerase Chain Reaction
PGC-1α	Peroxisome Proliferator-activated Receptor γ coactivator-1α
PI3K	Phosphatidylinositol-3-kinase
PMSF	Phenylmethanesulfonylfluoride
PRMT	Protein Arginine Methyltransferase
PTM	Post-Translational Modification
PVDF	Polyvinylidene Fluoride
RACO-1	RING domain activator AP-1 coactivator-1
RGG/RG	Arginine-glycine-glycine/Arginine-glycine
RING	Really Interesting New Gene
RNAi	Ribonucleic Acid interference
RT	Room Temperature
SAM	S-Adenosylmethionine
SAM68	Src-Associated substrate in Mitosis of 68 kDa
SDMA	Symmetric Dimethylated Arginine
SDS-PAGE	Sodium Dodecyl Sulphate-Polyacrylamide Gel Electrophoresis
siRNA	Small Interfering Ribonucleic Acid
SOC	Super Optimal broth with Catabolite repression
STAT	Signal transducer and activator of transcription
SUMO	Small Ubiquitin-Like Modifier

TAE	Tris-acetate-EDTA
TAP	Tandem Affinity Purification
TBS	Tris Buffered Saline
TBST	Tris Buffered Saline Tween
TCF-LEF	T-cell factor/lymphoid enhancer factor
TEMED	Tetramethylethylenediamine
TEV	Tobacco Etch Virus
TGF	Transforming growth factor
THW	Threonine-Histidine-Trytophan
tRNA	Transfer Ribonucleic Acid
USP	Ubiquitin Specific Protease
Wnt	Wingless-Int
β-TrCP	Beta-Transducin Repeat Containing Protein

UNIVERSITY OF BIRMINGHAM

Project B: Lymphocyte-hepatocyte cell-in-cell structures: implications for the hepatocyte host.

A MINIPROJECT BY SCOTT PHILIP DAVIES

This project is submitted in partial fulfilment of the requirements for the award of the MRes

Centre for Liver Research

School of Immunity and Infection

Institute of Biomedical Research

College of Medical and Dental Sciences

University of Birmingham

Project Supervisor: Dr. Zania Stamataki

Word Count: 7067

Abstract

Several investigations show how tumour cells can engulf live cells through entosis, generating cell-in-cell structures. This generates large intracellular vesicles which obstruct cytokinesis, resulting in binucleate, tetraploid cells. Polyploidisation is often associated with tumourigenesis, yet this is not known in the liver. However polyploidy, aneuploidy and multinucleation have been observed in hepatocytes. The origin and functional significance of this is not clear. Hepatocytes are also known to conduct phagocytosis. Evidence exists which implicates phagocytosis in the generation of polyploid cells. To investigate if hepatocyte phagocytosis affects ploidy, we used Huh-7 hepatoma cells as a model of hepatocytes and induced differentiation following consecutive rounds of phagocytosis of heat-killed lymphomas and hepatomas. Significant increases in multinucleation were observed following three rounds of phagocytosis. Surprisingly, prolonged phagocytosis generated differentiated, non-dividing Huh-7 subsets. In addition, it was confirmed that primary human hepatocytes are capable of phagocytosing heat-killed lymphomas. Finally, we developed a de novo double-staining technique for simultaneous identification of apoptosis and lymphocytes in diseased liver sections. This paves the way for new investigations to enhance our understanding of the mechanisms and consequences of hepatocyte phagocytosis and polyploidisation.

Acknowledgements

Thanks are given to the University of Birmingham and the Medical Research Council for funding this work. I would like to thank Sudha Purswani, Nick Weight, Abigail Jones, Becca Smith and Shivanee Nakum for all of your help, support and for making our lab a truly great place to work. I would also like to thank every in the centre for liver research for making me feel so welcome and comfortable. Special thanks is given to Dr. Elizabeth Humphries for providing primary human hepatocytes, for providing guidance with ISEL and for being so hilarious. I would also like to thank Gary Reynolds to all your help and contributions to immunohistochemistry and ISEL. Finally, I need to thank Dr. Zania Stamataki for so many things. Thank you for all of your support, your teaching, your advice and for all the times you made sure I had something to eat. But most of all, thank you for inspiring. You always make me believe that I can actually do science and I hope that never changes.

Contents

1 Introduction

1.1 Cell-in cell structures and ploidy

In recent years several lines of evidence have come to light which depict the generation of polyploidy cells due to the creation of the so-called ‘cell-in-cell’ structures (1). This describes the creation of large intracellular vacuoles, which contain live cells which have been ingested whole. This process of live-cell engulfment, known as entosis, has been studied in depth by the Overholtzer lab (2, 3). This group originally observed that metastatic breast cancer cell-lines were capable of engulfing members of the same cell line (2). Additionally, it appeared that live cells invaded others through an active process which was dependent on Rho GTPase signalling. As 70% of these internalised cells died as a result of this internalisation, entosis was defined as a method of cell death. However, other cells were shown to exit the cell and continue normal cellular processes, showing that entosis merely described the internalisation of live cells. The same study had also revealed the presence of entosis in primary human breast cancers, showing that this was a physiologically relevant process (2). Subsequent research by the same group revealed that the presence of this entotic vesicle could give rise to the formation of polyploid cells (Figure 1A) (3). Analysis of tumour cells possessing cell-in-cell structures revealed that 60% of such cells possess more than one nucleus. Further investigation utilising ectopic expression of fluorescently-tagged cytoskeletal proteins demonstrated that cell-in-cell structures could impose a physical block on the cytokinetic cleavage furrow (Figure 1B). This would lead to asymmetric cell division, generating binucleate, tetraploid daughter cells. Such cells would often experience subsequent dysregulation of cell divisions, resulting in cells with an incorrect number of chromosomes, known as aneuploid cells. The evidence displayed here suggested

that tumours could obtain polyploidy and further genomic instability through internalisation of their neighbours. This was dependent on cells becoming anchorage independent, a common feature of progressed tumours (2, 3). As such, the generation of cell-in-cell structures represented a remarkable new mechanism which elicits profound effects on the host cell and can often lead to the generation of polyploid cells.

A

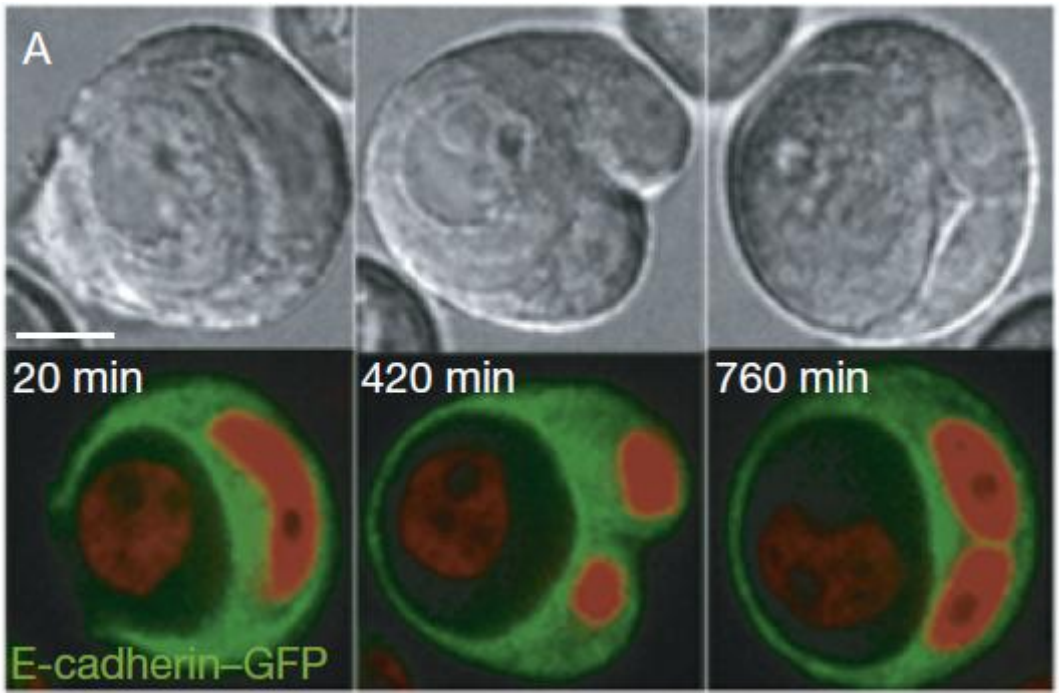

B

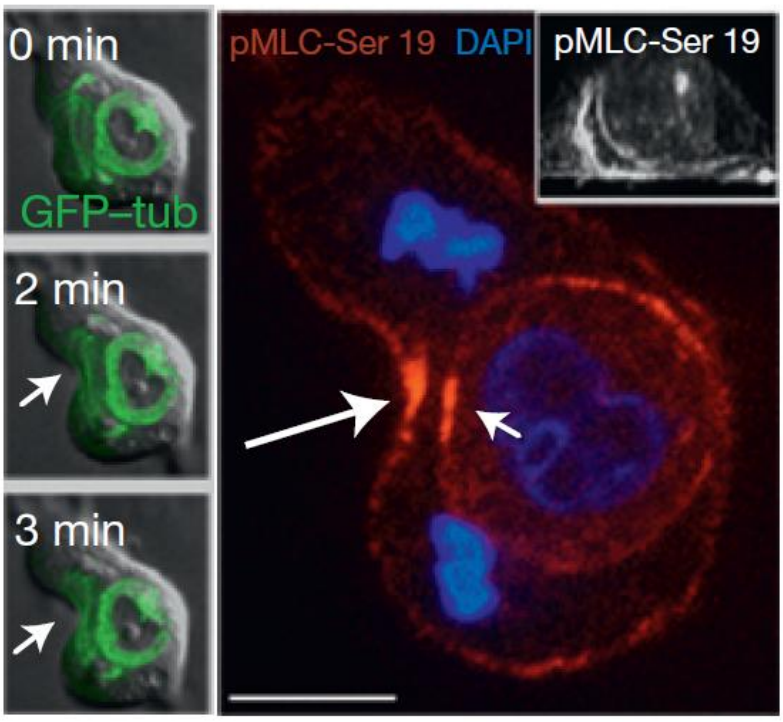

<u>Figure 1: Entosis of breast cancer cells by their neighbours resulting in asymmetric division, failure of cytokinesis and multinucleation.</u> A: Time-lapse differential interference contrast and fluorescent micrographs of dividing MCF10A breast cancer cells containing a cell-in-cell structure. MCF10A cells expressing E-cadherin-GFP and histone H2B-mCherry were propagated in soft agar, 3-D cultures. Cells were imaged from the beginning of entosis to the end of attempted cell division. **B Time-lapsed images of MCF10A cells displaying how cell-in-cell structures inhibit cytokinetic furrowing.** MCF10A cells expressing GFP-tubulin were immunostained for myosin light chain in order to visualise the contractile ring associated with cytokinesis . White arrows highlight the cytoplasmic furrowing and contractile ring. Taken from Krajcovic *et al*¸ 2011 (3)

1.2 The creation and consequences of polyploidy

1.2.1 Creation of polyploid cells

All normal somatic cells have a specific number of chromosomes within their nuclei which contain the required amount of genetic information for the development and functionality of the entire organism. The majority of eukaryotes obtain 2 sets of chromosomes from either parent, which results in all cells in body, excluding gametes, being diploid (2n). However, certain processes have been known to change the number of chromosomal sets within cells. Polyploidisation is well known to occur through heritable genetic abnormalities, derived from incorrect mitotic or meiotic divisions of gametes. As such, the subsequent fusion of these gametes gives rise to daughter cells with an incorrect higher number of chromosomes (4). Increases in ploidy can also occur through cellular fusion, such as in the case of myofibril formation (5), or through the generation of multiple nuclei through failed cytokinesis.

1.2.2 Consequences of polyploidy

It is evident that an increase in the total number of chromosomes within cells is a natural, dynamic process, where cells can shift between different states of ploidy to achieve a state of highest fitness(6). Whole genome duplications can therefore contribute towards Darwinian selection as with any other genetic alternation. Increases in ploidy can therefore be advantageous for some cell times. Experiments conducted in yeast, for example, display how higher ploidy levels improve the ability of these cells to recover from DNA damage and degenerative mutation (7). This is the result of increased redundancy between genes due to increased copy numbers of each allele. Furthermore, possessing more than 2 copies of each allele can lead to the masking of harmful, recessive mutations and also presents opportunities for

phenotypic diversification. However, the disadvantages of polyploidy have been commonly outlined in tumourigenesis. Polyploidisation is common in cancer; an increased risk of genomic instability is often advantageous for the developments of cancer cells (8). Tetraploid cells are commonly eliminated through p53-dependent apoptosis to prevent the survival unstable cells (9, 10). However, this is not due to an endogenous tetraploidy detection system (11, 12). Furthermore, p53-mutations are common in cancerous cells making them prone to polyploidisation. Cancerous cells can benefit from the increased ploidy through increased copy numbers of mutant alleles which drive or propagate tumourigenesis. Furthermore, increased ploidy could increase the tolerance of cancerous cells to deleterious mutations, granting more time for the acquisition of oncogenes. Taken together, polyploidy can be advantageous to specific cell types, but may also enhance the risk of tumour progression.

1.2.3 Failure of cytokinesis promotes polyploidy in cancers

Failed cytokinesis is often implicated in tumourigenic polyploidy, often caused by dysregulated microtube organisation and failures at mitotic checkpoints. For example, Sotillo *et al*, showed how prolonged overexpression of Mad2 promoted aneuploidy and polyploidy in mouse embryonic fibroblasts (13). Mad2 is a key regulator of the spindle assembly checkpoint, which negatively regulates the cdc20-anaphase promoting complex, ensuring that the cell cycle is continued without unattached chromosomal kinetochores. Its overexpression is common amongst human cancers, including liver cancer, and results in failed cytokinesis (13, 14). The frequency of polyploidy in human cancers as a result of failed cytokinesis is of particular interest to the investigation of cell-in-cell structures. Most cancers overcome the requirement of anchorage to the extracellular matrix (ECM) for

survival, propagation and migration, often through mimicking processes of the epithelial-mesenchymal transition (EMT). Furthermore, it was observed by Overholtzer *et al*, that breast cancer cells detach from the ECM prior to internalisation, which ultimately resulted in non-genetic cytokinetic failure (2). Taken together, it is plausible that polyploidisation is encouraged in tumour cells through the creation of cell-in-cell structures following detachment from the ECM.

1.3 Hepatocytes are naturally polyploid

1.3.1 The creation of polyploid hepatocytes

The generation of polyploid cells through failed cytokinesis and multinucleation can occur within cancer cells and promote irregular cellular divisions. However, certain cells can naturally tolerate increases in chromosome number. Hepatocytes have commonly been observed possessing more than 2 sets of chromosomes (15). Hepatocytes are regenerative cells which comprise ~85% of total cells within the liver and conduct the majority of the organs primary functions, including the secretion of bile, metabolism and detoxification (16). Variations in the DNA content and the number of nuclei are a frequent occurrence amongst hepatocytes. Cells commonly exist as mononucleates or binucleates, with rare cases of larger hepatocytes possessing 3-4 nuclei (17). Increases in hepatocyte ploidy have been observed in an age dependent manner (18). This suggests that mechanisms for changes in ploidy occur accumulatively over time. It was shown that failure of cytokinesis occurs post-natally in mouse livers, in a manner dependant on the Phosphatidylinotiside-3 kinase/Akt (PI3K/Akt) signalling pathway (19). This suggests a mechanism of gradual increases in ploidy, whereby consecutive failed cytokinesis events generate binucleate, tetraploid cells. Such cells then undergo successful division, yielding

mononucleate, tetraploid daughter cells. These cells eventually fail cytokinesis a second time to generate octoploid cells and so on (Figure 2A).

1.3.2 Functional significance of hepatocyte polyploidy

It is not certain as to the purpose of multinucleate cells within the liver. One theory suggests that polyploid cells provide the regenerative capacity of the liver. In support of this, polyploid hepatocytes have been shown to be highly proliferative and provide the regenerative capacity following hepatectomy (20). Another theory is that, similarly to processes that can occur in cancer cells, increases in ploidy enhance the functionality of these cells due to increased gene copy numbers and resistance to harmful mutations. Although it has been shown that polyploid hepatocytes display deviation from diploid counterparts in gene expression, genomic resilience would be of benefit to hepatocytes as processes of detoxification requires frequent exposure to mutagens, such as alcohol and certain carcinogenic catabolytes (21, 22). Interestingly, as with other cases of polyploidy, hepatocytes also undergo reductions in ploidy (23, 24). This gives the rise of the idea, coined by Duncan *et al*, 2010, of the ploidy conveyor model, whereby hepatocytes cycle through different stages of ploidy (Figure 2B) (23). Overall, changes in ploidy may act as a form of adaptation within the liver, in response to liver damage, in similar manner as how polyploidisation is a process under the influence of Darwinian selection. Taken together, it seems that hepatocytes are highly adaptable cells and utilise polyploidisation as a method of withstanding the harsh conditions of the liver. Of interest, although hepatocyte polyploidisation bares resemblance to that of cancer cells, they do not share similar phenotypes. Furthermore, sporadic hepatocellular carcinoma occurs in less than 4% of mice, suggesting that polyploidisation is unlikely to be a driver of this process (25).

A

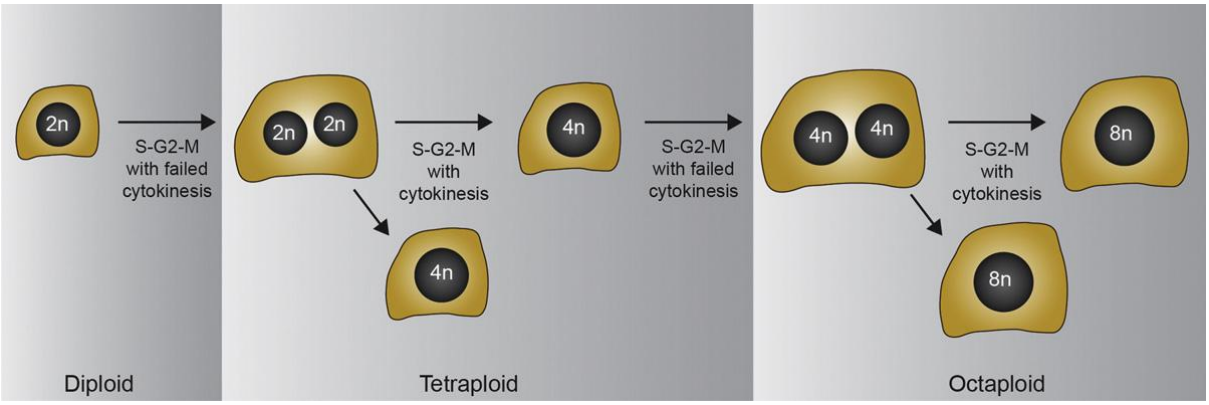

B

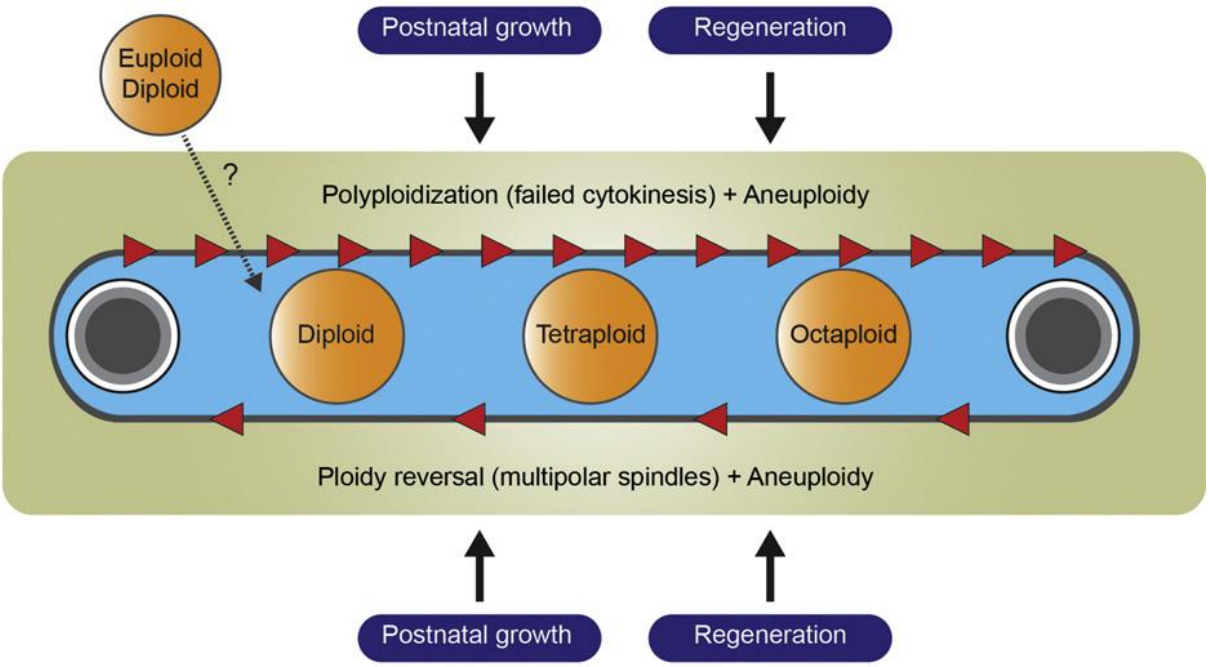

Figure 2: The dynamics of ploidy alterations in hepatocytes.

A: Schematic depicting the changes in nucleation and multinucleation in liver cells as a result of alternating cycles of success and failure of cytokinesis.

B: The ploidy conveyor model depicting the balance between changes in ploidy in hepatocytes. The large number of red arrows for polyploidisation and aneuploidy represents their dominance in the hepatocytes compared with ploidy reversal. Both processes are influence by regenerative and growth signals, although the origin of initial diploid cells within the cycle is not known. Taken from Duncan, 2013 (24)

1.4 Phagocytosis can also create large intracellular vacuoles and interrupt cytokinesis

It has been shown that internalisation of live cells can lead to the generation of a large intracellular vacuole which prevents correct segregation of dividing cells through cytokinesis (2, 3). However, other examples of asymmetric cell division have been described as a consequence of phagocytosis (26). Phagocytosis of invading pathogens and apoptotic cells has been well described in other renowned phagocytes (27). The contents of such phagosomes are often trafficked through the endosomal pathway, where they are degraded and in some cases presented to lymphocytes in the context of MHC molecules to establish innate immunity (27). However, under certain circumstances, phagocytosis is also thought to result in a persistent vacuole which can disrupt cytokinesis. It has been observed that multinucleated fibroblastic cells arise in rats in part due to phagocytosis of collagen (28). Furthermore, certain bacteria species can reside in phagosomes and disrupt normal cellular processes. For example, multinucleation in endocervical epithelium has been historically observed following infection with *Tuberculosis* (29). More recently, asymmetric cell division was been observed as a consequence of *Chlamydia* infection (26). *Chlamydia trachomatis*, an obligate intracellular parasite of humans, persists in host cells in large inclusion bodies. These can occupy up to 20% of host cell volume thus create a physical obstacle. As such, it was shown that *C. trachomatis* infections can inhibit furrowing during cytokinesis in a similar manner to cell-in-cell structures and generate binucleate cells (Figure 3) (26). In total, this shows that entosis is not the only means towards non-genetic polyploidy and the phagocytosis can be linked to multinucleation through cytokinesis failure.

1.5 What are the consequences of phagocytosis for hepatocytes?

It is of wide regard that hepatocytes are capable of phagocytosis. They have been historically shown to phagocytose erythrocytes (30). Additionally, they are capable of clearing their apoptotic neighbours, displaying another role of these cells in liver homeostasis(31). Finally, previous research conducted in the Stamataki lab has demonstrated the capability of both primary hepatocytes and hepatomas to phagocytose dead lymphocytes (32). However, unlike the phagocytic processes conducted by dedicated phagocytes, such as macrophages, the mechanisms by which hepatocytes take up cargo are poorly understood. Of interest, Bertolino and colleagues demonstrated that autoreactive CD8+ T-cells could be become activated in the liver and actively bore into hepatocytes through entosis, where they were eliminated through lysosomal degradation (33). Although such observations were not a consequence of phagocytosis, these studies demonstrated the existence a complex relationship between liver and immune cells, which may ultimately regulate the inflammatory response within the liver. Furthermore, this internalisation of autoreactive CD8+ T-cells supports the Overholtzer entosis theory of polyploidy (34). The consequences of both entosis and phagocytosis of lymphocytes and apoptotic cells by hepatocytes are under investigation (33). However, little attention has been given to the impact of cell-in-cell structures on the hepatocytes themselves. Studies suggest that multinucleation and polyploidy can arise from failed cytokinesis, as a result of a physical obstruction in cell cleavage (3, 24, 26). As hepatocytes are both phagocytic and exhibit polyploidy, there is likelihood that both processes are linked. This investigation will endeavour to establish the consequences of phagocytosis for the hepatocytes and analyse its effects on multinucleation, as a representation of polyploidy. These observations will be confirmed using immunohistochemical

staining of liver sections and experiments conducted with *ex vivo* primary hepatocytes.

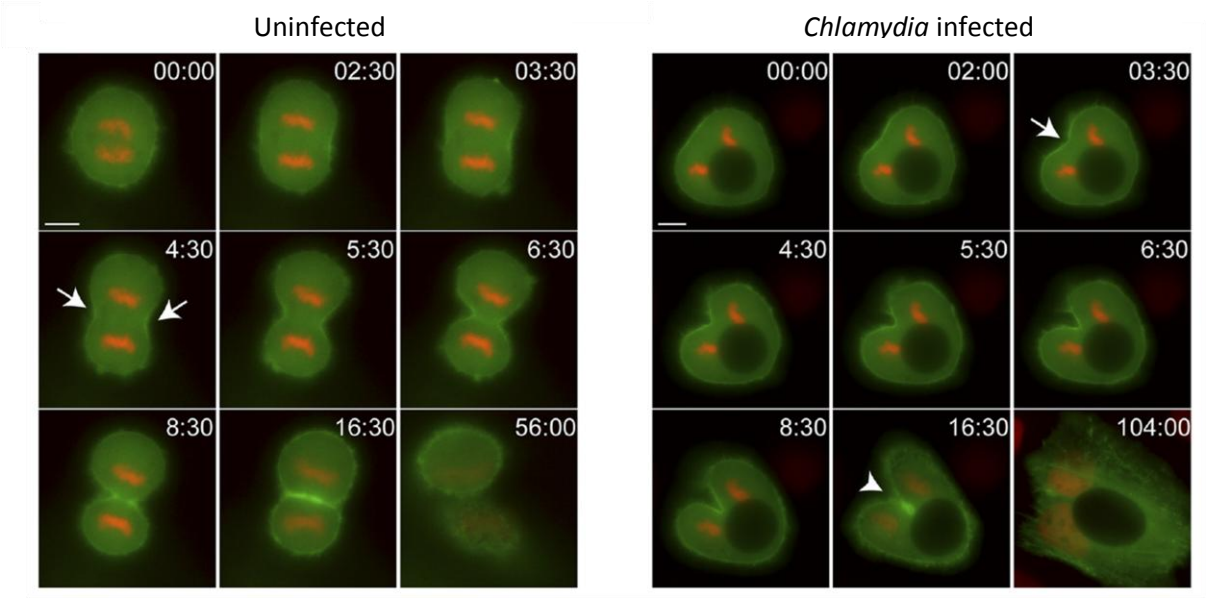

Figure 3: Time-lapse, epifluorescent images of showing asymmetric cleavage furrows in HeLa cells infected with *Chlamydia*. HeLa cells expressing histone H2B-mCherry and transiently expressing Cerulean-LifeAct (F-actin; green) were observed with or without a *Chlamydia* inclusion. Taken from Sun *et al*, 2011 (26).

1.6 Aims and Objectives

We hypothesise that phagocytosis of dead cells has consequences for hepatocyte ploidy. This investigation aims to identify the outcomes of hepatocyte phagocytosis and elucidate its effect on multinucleation. Such experiments will be conducting using Huh-7 hepatoma cell lines as a representative model for convenience. However, these cells are less differentiated and polarised than primary hepatocytes. As such, findings from these initial experiments will be supported with data obtained from primary hepatocyte experiments and with *in vivo* analysis of liver segments. We designed objectives to answer the following questions:

- Does phagocytosis of heat-killed cells affect cell division and multinucleation in hepatomas?
- Can primary hepatocytes phagocytose heat-killed cells?
- Can entosis or phagocytosis be observed and distinguished in liver sections from patients with chronic inflammation.

2 MATERIALS AND METHODS

2.1 Antibodies

Table 1: List of antibodies used throughout this investigation including their source and purpose

Antibody	Source	Purpose	Concentration
Mouse anti-CD3	abcam® (ab699)	Immunohistochemistry	1:50, 1:100 or 1:200
Mouse anti-CD4 monoclonal	Vector® (VP-C320)	Immunohistochemistry	1:10, 1:20 or 1:40
K9218 Mouse-anti HNF4	abcam® (ab41898)	Immunohistochemistry	1:100

2.2 Reagents

Table 2: List of reagents and chemicals used throughout this investigation including their source and purpose

Reagent	Source	Purpose
Dulbeccos modified eagles medium (DMEM), high glucose, high pyruvate	GIBCO/ Life Technologies™ (11995065)	Cell culture – Huh-7 growth medium
Iscove's Modified Dulbecco's Medium, + HEPES, no phenol red (IMDM)	GIBCO/ Life Technologies™ (21056-023)	Cell culture – Huh-7 growth medium following phagocytosis

Roswell Park Memorial Institute Medium 1640, high glutamine (RPMI 1640)	GIBCO/ Life Technologies™ (11875-085)	Cell culture – Jurkat growth medium
0.05% Trypsin-EDTA	GIBCO/ Life Technologies™ (H3570)	Cell culture – detachment of cells from culture flask
Fetal Bovine Serum	GIBCO/ Life Technologies™ (16000-044)	Cell culture – Media supplement
100X MEM Non-essential Amino acids (NEAA)	GIBCO/ Life Technologies™ (11140-035)	Cell culture – Media supplement
Penicillin-Streptomycin (Pen/Strep)	GIBCO/ Life Technologies™ (15140122)	Cell culture – Media supplement
Human serum	Life Technologies™ (34005-100)	Cell culture – Media supplement
Williams E Medium	GIBCO/Invitrogen™ (32551-020)	Cell culture – Primary human hepatocyte growth media
Primary Hepatocyte Maintenance Supplements	GIBCO/Invitrogen™ (CM4000)	Cell culture – Primary hepatocyte growth media supplement
CellMask™ Orange	Molecular Probes, Life Technologies™ (C10045)	Assessing multinucleation – cell membrane staining

Hoechst 33342 trihydrochloride trihydrate	Molecular Probes, Life Technologies™ (H3570)	Assessing multinucleation - nuclear Staining
Opti-MEM®	Life Technologies™ (11058021)	Reduced serum media for incubation with transfection reagents
Lipfectamine® 2000	Life Technologies™ (11668027)	Transfection of Huh-7 with exogenous fluorescent cytoskeletal elements
CellTracker™ red CMTPX	Molecular Probes, Life Technologies™ (C10613)	Fluorescent labelling of heat-killed Jurkat cells
CellTracker™ green CMFDA (5-Chloromethylfluorescein Diacetate)	Molecular Probes, Life Technologies™ (C2925)	Fluorescent labelling of Huh-7 cells
Paraformaldehyde (PFA)	Sigma-Aldrich (P6148-500G)	Fixing of phagocytosis primary cells
Tumour Necrosis Factorα (TNFα)	PeproTech™ (300-01A)	Analysing the effects of cytokines for PHH phagocytosis
Interferon-γ (IFNγ)	PeproTech™ (AF-315-05)	Analysing the effects of cytokines for PHH phagocytosis
Unmasking solution – High pH	Vector® (H3300)	ISEL/Immunohistochemisty

Unmasking solution – Low pH	Vector® (H3301)	ISEL/Immunohistochemisty
Peroxidase-Blocking Solution	Dako™ REAL (S2023)	Immunohistochemisty – Endogenous peroxidase block
10X Casein Solution	Vector® (SP-5020)	Immunohistochemisty
Xylene (sulphur free)	Pioneer Research Chemicals LTD (PRC/R/201)	ISEL/Immunohistochemisty – tissue rehydration and dehydration
Industrial Denatured Alcohol (IDA) 99%	Pioneer Research Chemicals LTD (PRC/R/101)	ISEL/Immunohistochemisty – tissue rehydration and dehydration
EnVision FLEX wash buffer (Tris-buffered saline Tween - TBST)	Dako (K8007)	Immunohistochemistry – tissue washes
Mayer's Haematoxylin	Pioneer Research Chemicals LTD (PRC/R/42)	Immunohistochemisty - counterstain
DPX Mounting Media & Section Adhesive	Leica (3808600ED)	Immunohistochemisty-mountant
ImmPRESS Universal Antibody Polymer Detection Kit	Vector® (MP7500)	Immunohistochemisty– secondary antibody
ImmPACT Diaminobenzidene (DAB)	Vector® (SK-4100)	Immunohistochemisty – Peroxidase

peroxidase substrate kit		substrate/detection
Sheep anti-digoxigenin alkaline phosphatase conjugated F'ab fragment	Roche (1093274)	ISEL
StayRed/AP substrate (alkaline phosphatase)	abcam® (ab103741)	ISEL detection
NovaRed™ peroxidase substrate	Vector® (SK4800)	Immunohistochemisty – Peroxidase substrate/detection
StayGreen/AP substrate	abcam® (ab156428)	ISEL detection
100% Ethanol (EtOh)	Sigma-Aldrich™ (E7023-500ML)	Sterilisation and tissue dehydration for ISEL/IHC double stain
Clearene Solvent	Leica (3803600 3803620)	Tissue dehydration for ISEL/IHC double stain
VectaMount AQ Aqueous Mounting Medium	Vector ® (H-5501)	Immunohistochemisty-mountant
Phosphate Buffered Saline (PBS)	GIBCO/Life Technologies™ (20012019)	Cell culture wash and PFA diluent

2.3 Cell Culture

All cell culture procedures were conducted within Laminar class II flow cabinets (Thermo Scientific Holten, Safe MS). Cabinets were sterilised before and after use by treatment with 10% Trigene solution, followed by 70% EtOh. All cells were cultured in 5% $C0_2$, at 37°C.

2.4 Cell Lines

2.4.1 Huh-7 Hepatoma cells

Huh-7 cells were cultured in T75cm^2 culture flasks in DMEM containing 10% Foetal Bovine Serum (FBS), 1% NEAA, 1% Pen/Strep, 1% L-glutamine. Cells were allowed to grow until reaching 100% confluence, which was assessed through light microscopy. At this stage, media was removed and cells were washed with 10 Phosphate Buffer Solution (PBS). 2.5ml 0.05% trypsin-EDTA was added to cultures, ensuring an even coverage, and flasks were incubated at for 4min 37°C, 5% $C0_2$ to allow trypsin to take effect. Cultures were agitated and then analysed by light microscopy to ensure that all cells had detached. Trypsing-EDTA was then quenched with the addition of 2.5ml DMEM. Media-Trypsin-solution was drawn up with an electronic pipette and released down the culture plane of the flask to ensure that all cells were collected in a pool at the bottom of the flask. 1ml was removed from these cultures and added to a new flask with 9ml DMEM with all supplements. Remaining cells were seeded elsewhere, heat-killed for phagocytosis experiments or discarded. Huh-7s were propagated twice per week in this fashion to ensure that cells remained healthy and did not overgrow.

2.4.2 Jurkat T-cell lymphoma cells

Jurkat cells were cultured in 20ml RPMI containing glutamine, supplemented with 10% FBS, 1% NEAA and 1% Pen/Strep. Cells were allowed to grow until solutions appeared cloudy and lost their phenol red colour. At this point, to ensure that cells remained healthy, 12ml of Jurkat suspension was removed with an electronic and discarded. Suspensions were then topped-up back to 20ml with supplemented RPMI. Jurkat cells were propagated twice per week in this fashion, unless they were used for experiments.

2.4.3 Primary Human Hepatocytes (PHHs)

Liver tissue was obtained from surgical procedures carried out at the Queen Elizabeth Hospital, Birmingham, UK. Ethical approval for the study was granted by the Local Research Ethics Committee (LREC) (reference number 06/Q702/61). Primary hepatocytes were isolated by Dr Elizabeth Humphreys. Liver tissue was obtained from fully informed and consented patients undergoing transplantation for a variety of end stage liver diseases or from normal donor tissue that was surplus to surgical requirements.

Hepatocyte isolations were carried out using a modified ‘two-stage’ collagenase procedure developed by Berry and Friend and further modified by Bhogal et al 2011 (35, 36). The cells were seeded at 80% confluence ($1.04x10^5$ cells) on a rat tail collagen-coated 48-well plate in arginine-free Williams E media supplemented with 10% fetal calf serum, hydrocortisone (2ug/ml), insulin (0.124U/ml) and L-ornithine (0.4mmol/L). Cells were cultured for 2 hours under normal conditions to ensure that the cells adhered to the bottom of the wells and were then switched to serum-free

Williams E media with supplements for 24 hours. The cells were then subjected to phagocytosis assays and were not propagated further.

2.5 Heat-killing

Phagocytosis assays were carried out using cell lines which had been killed with heat. Heat-killing was conducted with Huh-7s from a confluent flask and with Jurkat suspensions that had been allowed to grow for 3 days after being passaged. Prior to heat killing, Huh-7s underwent normal detachment procedures and transferred to a centrifugable tube. Jurkat cells were also transferred to a centrifugable tube. Cells were centrifuged for 3min, 1500rpm at room temperature. Supernatents were discarded and cell pellets were resuspended in 1ml of their respective culture media and transferred to a 1.5ml tube. Cells were then killed at 60°C on a heating-block for 30mins. Cells were given time to cool before they were added to live cell cultures.

2.6 Creation of *de novo* Huh-7 cell lines by phagocytosis

In order to assess in the effect of phagocytosis on Huh-7 multinucleation, novel Huh-7 cell lines were created by inducing phagocytosis. Huh-7s were detached through normal procedures and in new T25cm^2 culture flasks at 50% confluence (1.5x10^6) and allowed >8hours to adhere in 5ml media. Heat-killed Huh-7 cells or Jurkats were then added to cultures and were incubated under normal conditions. A control culture was also set which did not receive dead-cells but underwent the same treatments as phagocytosing cells. Phase contrast images of cultures at 20x magnification were taken throughout and proceeding phagocytosis using a Nikon Eclipse TE2000-S inverted microscope. The media was changed for each culture after 3 days,or if the culture media appeared a bright yellow colour, to remove non-phagocytosed cells remove harmful products released by heat-killed cells. Cells were allowed to continue phagocytosis until cultures became confluent or finished

phagocytosis. Cells were then detached by normal trypsin treatment. In this case, trypsin was quenched with IMDM containing 10% human serum, 1% NEAA and 1% Pen/Strep. Cells were then seeded in T75cm^2 flasks and cultured in IMDM until normal cell division patterns were restored. Cultures were then returned to normal DMEM conditions and from here on treated as in individual cell line, based on the cells they had phagocytosed and how many events of phagocytosis they had undergone (Huh-7/Jurkat feed 1, feed 2 etc). All events were then repeated with "feed 1 cells" and then again with "feed 2" giving a total of three feeding events.

2.7 Multinucleation Assays

All fluorescence imaging for this assay was conducted using the Nikon Eclipse TE2000-S inverted microscope. In order to assess multinucleation in new phagocytosis-derived Huh-7 cell lines, cells for each feed (including unfed controls) were seeded in 24-well-plates at 50% confluence (0.12x10^6 per well) and allowed to adhere for >8hours in 1ml supplemented DMEM. Nuclei were stained with 0.2µg/ml Hoechst dye in 1ml normal DMEM for 30min, at 37°C. The stain was removed and cells were briefly washed in 1ml PBS PBS before normal DMEM was replaced. Cells were briefly imaged to ensure that blue nuclei were visable. To distinguish individual cells in culture, cell membranes were stained with 5µg/ml CellMask Orange in 1ml DMEM for 5min, 37°C. Wells were then washed briefly in 1ml PBS and 1ml DMEM was added to each well before imaging. 10 fields of view at 20x magnification were analysed for each cell line. For each field of view, the total number of cells and the total number of multinucleate cells were counted. From this data, the average percentage of multinucleate cells was determined for each cell line. All data was plotted in Microsoft Excel and the highest and lowest percentages of multinucleation for each cell line were used for error bars.

2.8 Assessment of phagocytosis in primary human hepatocytes

All fluorescence imaging for this assay was conducted using the Nikon Eclipse TE2000-S inverted microscope. Once PHHs had adhered to collagen-coated wells, they were assessed for their ability to conduct phagocytosis. The original media was removed and PHHs were stained green with 5µM CellTracker CMFDA in 300µl DMEM, containing normal culture supplements, for 1 hour, 37°C in the dark. Wells were then washed in 500µl PBS and replenished with 500µl normal DMEM. PHHs were briefly analysed to ensure that the green stain was successful. 4 wells received media contained 100ng/ml TNFα, IFNγ or both. All cells were incubated for 1hour, 37°C, $C0_2$ before receiving heat-killed cells. Jurkat cells were stained with CMTPX and heat-killed as previously done (section 2.7). 100µl red, heat-killed Jurkats were added to each well and PHHs were allowed to conduct phagocytosis for 2 hours at 37°C, 5% $C0_2$. Following this, cells were fixed with 1% PFA in PBS for 5min, 37°C. The fixative was removed and 300µl PBS was added to ensure cells did not become dehydrated. Images of green PHHs, red Jurkats and merged were taken of 10 fields of view for each cytokine treatment, including untreated. These images were then analysed to assess the percentage of phagocytosing PHHs and the average number of Jurkats internalised per Huh-7. Jurkats were identified as internalised if their position correlated with the presence of a vacuole within Huh-7s. Tallies were made for cells possessing up to 6 internalised Jurkats. Data representing the mean percentage of phagocytic cells were analysed and plotted with Microsoft Excel. Data representing the mean number of internalised Jurkat cells were analysed and plotted with Prism (GraphPad) software.

2.9 Statistics

All data for Huh-7 multinucleation and primary human hepatocytes were statistically analysed using paired t-tests using Prism (GraphPad) software. Statistical significance in multinucleation changes was determined between unfed and feed 3 cell lines. Statistical significance was also assessed for increases in the percentage of phagocytosing PHHs due to cytokine treatments.

2.10 Immunohistochemistry (IHC)

2.10.1 Paraffin liver Sections from diseased livers

All sections were cut from liver tissue, obtained from surgical procedures carried out at the Queen Elizabeth Hospital, Birmingham, UK. Ethical approval for the study was granted by the Local Research Ethics Committee (LREC) (reference number 06/Q702/61). All tissues were fixed in formulin and embedded in paraffin wax. 3µm deep sections were then cut using a rotary microtome sections and then floated within a water bath to remove undesired tissue folding. Tissue sections were then mounted onto charged glass slides. Sections were then loaded into a metal rack and set by incubated at 60°C. Tissue sections came from patients suffering with chronic rejection, alcoholic liver disease, primary biliary cirrhosis and primary sclerosing cholangitis.

2.10.2 Anti-CD4 and CD3 staining

All IHC procedures were conducted at room temperature. All washes and were conducted in glass staining dishes or Coplin jars. Paraffin tissue sections were placed in a metal rack and rehydrated at room temperature within a fume hood, using the following treatment series: 3 x 2 min incubations in xylene, 2 x 2 min incubations in IDA and left in ddH_20 in order to wash off excess alcohol and keep

tissue sections hydrated. 1L, 0.1% high-pH unmasking solution (2X overall) was prepared and preheated in a microwave oven for 10 mins. Rehydrated tissue sections were submerged in pre-warmed unmasking solution and microwaved on the highest setting for a further 20min. Sections were allowed to cool for 10min following microwave proteolysis. Plastic staining trays were lined with damp paper towels, to ensure the atmosphere remains moist, and broken glass stripettes were placed parallel inside. Excess unmasking fluid was removed from tissues sections and they were washed in EnVision FLEX wash buffer (TBST from here on) for 5min and they were placed level on stripettes within the staining tray. The lid was replaced on the tray during all incubations. 100µl peroxidase-blocking solution was added to each section for 10min and then washed with 2x5 min washes in TBST. A working casein blocking solution was made by dilution 1ml 10X stock in 4ml TBST. 100µl of working casein block was added to each section for 10min. Tissues were then incubated with 100µl of anti-CD4 or anti-CD3 primary antibody in TBST at concentrations depicted by Table 1, for 1 hour at room temperature. Sections were then washed 2x5mins in TBST and then incubated with Vector ImmPRESS universal antibody polymer detection kit for 30min, according to the manufacturers guidelines. Sections were then washed 3 times in TBST and then suspended on staining rack over a sink. Sections were stained with Vector immPACT DAB peroxidase substrate using a Pasteur pipette for 5min, according to the manufacturer's guidelines. DAB was removed by drowning slides in distilled water. Mayers haemotoxylin was filtered twice using filter paper and a funnel prior to use. Tissues were counterstained for 30sec and the stain was developed by running slides under hot water. Tissue sections were then dehydrated by the following treatment series: 2 x 2 min incubations in IDA, followed by 2x2 min incubation in xylene. Tissue sections were

then mounted by adding one drop of DPX mounting media to a coverslip and carefully pressing the section on to the coverslip to ensure that no bubbles form. Slides were then imaged once the mountant had dried.

2.10.3Anti-HNF4α

HNF4α IHC staining was conducted following procedures outlined by Tanaka *et al*, 2006 (37). However, antigen unmasking procedures were not outlined by the author. As such, 3 methods of unmasking were conducted: high-pH, low-pH and no unmasking prior to initial washing in TBST. Following casein blocking, tissue segments were incubated with 100µl K9218 anti-HNF4 primary antibody (1:100) in 1% BSA/PBS (final concentration 10µg/ml) overnight at 4°C in the dark. All other procedures were identical to those of section 2.9.2.

2.11 In Situ End Labelling (ISEL)

ISEL staining was conducted for both paraffin embedded sections and frozen Jurkat cytospins which were already available in the lab. Jurkats had been cultured in normal RPMI or RPMI containing FasL. These cells were used as a control for the detection of apoptosis by ISEL. Paraffin sections underwent rehydration and epitope unmasking, as described in section 2.9.2. To optimise epitope unmasking and minimise non-specific staining, paraffin sections were microwaved for 20, 30 or 40min. During this time, frozen sections were re-fixed in acetone for 2min and allowed to air-dry. Plastic staining trays were lined with damp paper towels, to ensure the atmosphere remains moist, and broken glass stripettes were placed parallel inside. Finally, the ISEL mixture was prepared according on ice to table 4. Once frozen sections had dried and paraffin sections had cooled, wax was applied around each tissue section or cytospin to ensure that the mixture was retained. Sections were incubated with 100µl ISEL mixture, or negative control mixture where

the Klenow fragment was withheld, under glass coverslips for 1 hour, 37°C. Following this, coverslips were removed and slides were washed 3x 5 minutes in ddH_20, followed by then 5 minutes in TBS pH 7.2. Both cytospins and tissue sections were then incubated in 100µl, 3.75U/ml sheep anti-digoxigenin alkaline phosphatase conjugated F'ab fragment, diluted in TBS pH 7.2 for 1 hour at room temperature within the staining tray. Slides were then washed in TBS pH7.2 for 5min and then visualised by incubating with abcam StayRed/AP substrate for 15min. Slides were then washed in ddH_20 and counterstain with haematoxylin as previously stated (Section 2.9.2). Cytospins were mounted in VectaMOUNT aqueous mountant. Paraffin sections were dehydrated and mounted in DPX mountant as described (Section 2.9.2).

Component	**Concentration**	**Source**
$MgCl_2$	0.005M	Sigma Aldrich™, (M8266)
B-mercaptoethanol	0.001M	Sigma Aldrich™, (3148)
Bovine Serum Albumin (BSA)	5mg/ml	Sigma Aldrich™, (A7906)
dATP	0.001M	Amersham™, (27-2035-01)
dCTP	0.001M	Amersham™, (27-2035-01)
dGTP	0.001M	Amersham™, (27-2035-01)
Dig-11-dUTP	0.001M	Roche™, Basel Switzerland, (1093088)

DNA polymerase, Klenow Fragment	20U	Bioline™, Taunton MA USA, (BIO-27029)
TBS pH 7.2	1ml; Powder diluted in 500ml ddH_20	Thermo Scientific™ (28376)

Table 3: Components of the *in situ* end-labelling mixture

2.12 ISEL and Anti-CD3+ IHC double stain

The processes of both anti-CD3 staining and ISEL treatment of paraffin sections were combined in the following sequence. All washes and were conducted in glass staining dishes or Coplin jars. Paraffin sections underwent rehydration, epitope unmasking and 20min microwaving, as described in section 2.9.2. Following this, sections were washed in TBST for 5min and then incubate with peroxidase-blocking solution for 10min at room temperature. Slides were washed in TBST for 5min and then again in TBS for another 5min. Following this all ISEL procedures were conducted as describe in section 2.11, starting from the incubation with the ISEL mixture. For this technique, ISEL visualise was conducted using StayGreen/AP substrate. As this is light sensitive, sections were incubated with StayGreen/AP substrate for 30min in the dark at room temperature. Slides were washed in ddH_20 for 5min and then again in TBST for another 5min. IHC procedures detailed in section 2.9.2 were the conducted, beginning with casein block. Anti-CD3 was used at 1:100 dilution in TBST. IHC staining was visualised using Vector imPACT Novared peroxidase substrate according to the manufacturer's guidelines. This reaction was stopped by drowning slides in distilled water. Sections were counterstained with haematoxylin and then dehydrated using the following series, conducted in Coplin jars: 2x30sec in 100% ethanol, >30 sec in clearine. This series was done to ensure

that the Novared substrate did not leach. Slides were mounted using one drop of vectaMOUNT agueous mountant.

2.13 Tissue Section Microscopy

All stained tissue sections were imaged at 20x magnification using a Zeiss Axioskop 40 microscope. Representative images were taken for each slide and scale bars were added to all images indicating 100µm.

3 Results

3.1 Phagocytosis alters cell division and promotes multinucleation in human hepatomas

The generation of cell-in-cell structures through processes such as phagocytosis or entosis can have profound effects on cellular ploidy (1). Previous investigations in the Stamataki lab had shown that Huh-7 hepatoma cell lines are capable of phagocytosing heat-killed lymphocytes and cell lines, as well as their own kind. Interestingly, these cells do not undergo cell division whilst conducting phagocytosis. We endeavoured to characterise the consequences of this extended period of phagocytosis for the hepatocyte. Huh-7 cells were “fed” heat-killed Huh-7 or Jurkat lymphoma cell lines. Dead Huh-7 are larger than lymphomas and therefore large phagosomes may cause more mechanical disruption to cell division, yet dead lymphocytes are smaller and multiple cells can be phagocytosed at the same time. A control unfed culture of Huh-7 was set up for comparison. Unfed cultures divided as normal and were passaged as required. Phagocytosing cultures underwent minimal cycles of cell division throughout this period (1 week approximately). Figure 1A shows differences in Huh-7 morphology acquired after phagocytosis of heat-killed lymphomas or hepatomas.

To quantify the effects of sequential phagocytosis in hepatoma cell division, cultures were fed more cells or propagated. Cell lines were generated for up to three consecutive cycles of phagocytosis were generated of both Huh-7 and lymphoma phagocytosis Of great surprise and interest, Huh7s that underwent a third round of lymphoma phagocytosis appeared to undergo processes of differentiation (Figure 1B). Such cultures did not reach confluency even after one month after the completion of phagocytosis, and only required media changes. These cells

conducted 10-times fewer divisions than normal unfed cells (Figure 1C). Additionally, the culture appeared to become heterogeneous (Figure 1B);smaller box-like cells were present which resembled polarised primary hepatocytes and formed tight layers with each cells (differentiated cell type I), as well as larger cells, some of which were multinucleate (differentiated cell type II). Such a difference in phenotype may be the result of asymmetric cell division giving rise to 2 distinct cell lines. Our findings raise questions as to how phagocytosis of dead cells can lead to potential differentiation events.

In order to assess changes in multinucleation during phagocytosis, the percentage of multinucleate cells in 5 fields of view at x20 magnification was estimated for each cell line. Nuclei and cell membranes were stained with Hoechst dye and CellMask membrane dye, respectively, to assist the identification of single cells (Figure 1D). Multinucleation gradually increased in unfed culture propagated over 3 weeks. This is likely due to background phagocytosis of none-adherent cells within the culture. However, phagocytosis of both Huh-7 and lymphoma cells caused significant increase in multinucleation (Figure 1D). In particular, phagocytosis of lymphomas caused a 4% increase between the 1^{st} and 2^{nd} feeds and an even larger increase of 10% between the 2^{nd} and 3^{rd}. This suggests that the ability of these cells to phagocytose lymphomas is cumulative. Phagocytosis of dead Huh-7 cells also caused a 5% in multinucleation, compared to unfed cells. However, the increase been feeds 1 and 2 was minimal. This may be in part due to the larger size of Huh-7s compared to lymphomas or be due to molecular challenges. As such, the data for feed 3 was not obtained as the cells failed to adhere to the flask at passaging. Overall, these data show that prolonged phagocytosis has profound effects on cell division and leads to increases in multinucleation in Huh-7 cells.

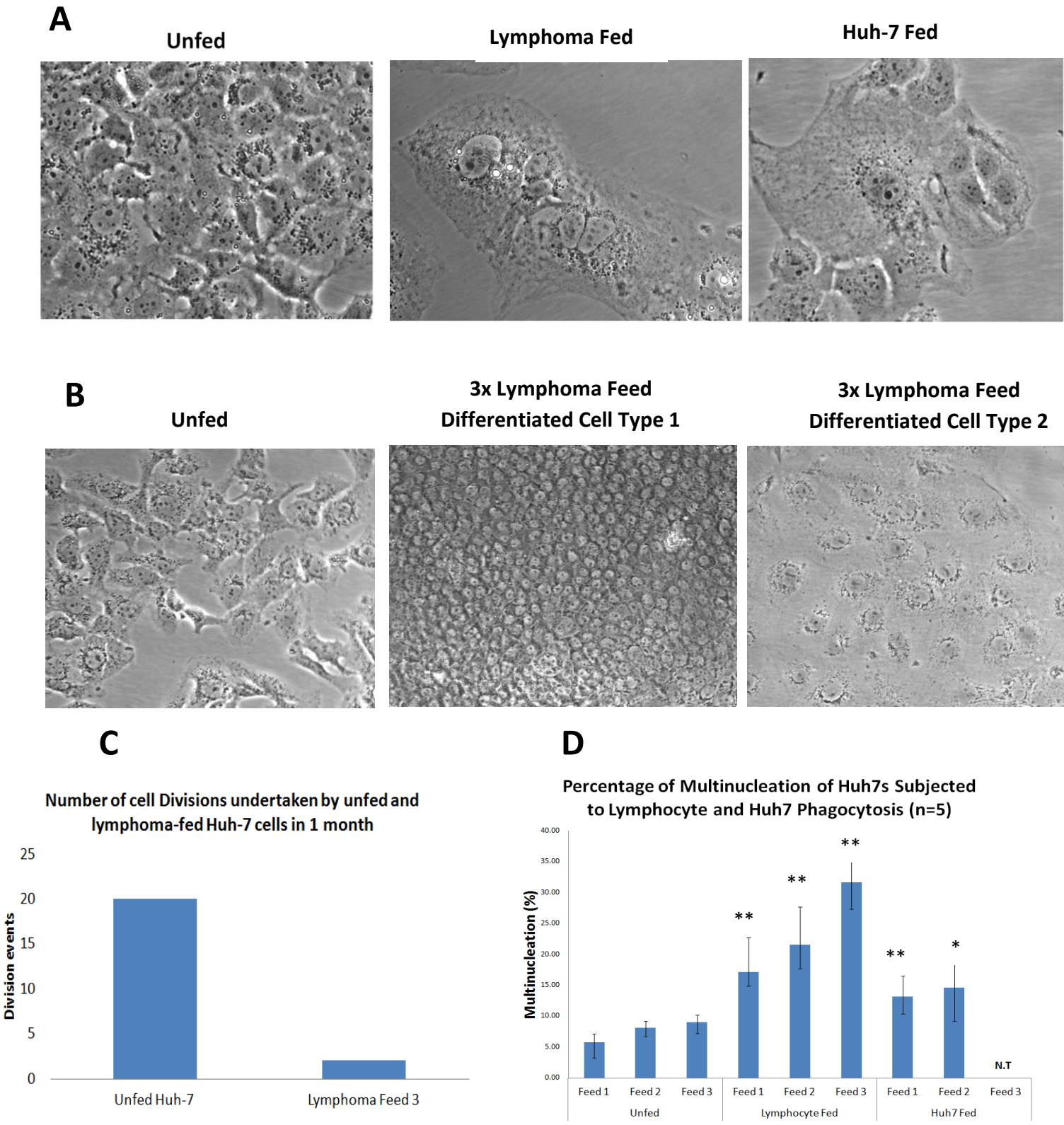

<u>Figure 4: Phagocytosis of heat-killed Huh-7 and lymphomas has profound effects on Huh-7 ploidy.</u> A: Light micrographs of phagocytosing Huh-7 cultures. Cultures were incubated heat-killed Huh-7s or lymphoma cell lines until cells ceased to phagocytose or until cultures became confluent. Media was changed once all cells were phagocytosis minimalise toixins released from heat-killed cells. **B: Light micrographs of normal Huh-7s and the heterogeneous culture generated following 3 round of lymphoma phagocytosis**. **C: The number of cell divisions undertaken by normal, unfed Huh-7 cells and lymphoma –fed Huh-7s undertaking their third round of phagocytosis. D: Bar chart displaying changes in Huh-7 multinucleation following consecutive rounds of phagocytosis.** The percentage of multinucleate cells was assessed after each feed for each type of cargo. Nuclei were stained with Hoechst and cell membranes were stained with CellMask™ orange in order to distinguish between individual cells**.** Error bars represent highest and lowest percentage of multinucleate cells. $P<0.05$

3.2 Primary hepatocytes are capable of phagocytosis and cytokine stimulation increases the quantity of internalised cells

Experiments conducted in the early stages of the investigation were done using Huh7 cells. This is an established cell line which is convenient and easy to use as a representative of hepatocytes. However, as such cells are immortalised hepatomas, they do not share the same physiological characteristics. Huh7s do not polarise like hepatocytes and share common features of other immortalised cells. As such, it was not possible to assume that the observed effects would occur *in vivo*. To address this, primary hepatocytes were generously isolated and provided by Dr. Elizabeth Humphries. These cells were stained with CellTracker green CMFDA and then co-cultured for 2 hours with heat-killed Jurkat cells, which had been stained with CellTracker red CMTPX. As cytokine activation is known to increase phagocytosis rates in hepatomas (Nick Weight et al, manuscript in preparation), some cells were treated with TNFα, IFNγ or both prior to incubation with jurkats. Cells were washed, fixed in 1% (w/v) paraformaldehyde, and then imaged using a fluorescent microscope. Merged fluorescent images of 10 fields of view were taken for each cytokine treatment and the total frequency of internalisation, together with number of Jurkats internalised by each hepatocyte was estimated (Figure 5).

Internalised Jurkat cells appeared as black vacuoles within green hepatocyte cytoplasm that corresponded to the positions of red cells (Figure 5A). Hepatocytes conducted phagocytosis of Jurkat cells under all conditions, showing that primary hepatocytes are capable of phagocytosis. Furthermore, prior treatment of hepatocytes with TNFα or IFNγ increased the total level of phagocytosis within these cells and increased the average number of Jurkats internalised per cell (Figure 5B/C). Interestingly, IFNγ induced a greater amplification of phagocytosis. This

suggests that IFNγ may be a more potent activator of phagocytosis and that each cytokine may upregulate phagocytosis through distinct mechanisms. In support of this, treatment with both cytokines elicited a significant increase in phagocytosis than either single treatment ($P<0.05$). This is consistent with our data on cytokine modulation of phagocytosis in Huh-7 cells (32). In total these results show that primary hepatocytes naturally perform phagocytosis of dead cells, a behaviour which is upregulated under inflammatory conditions.

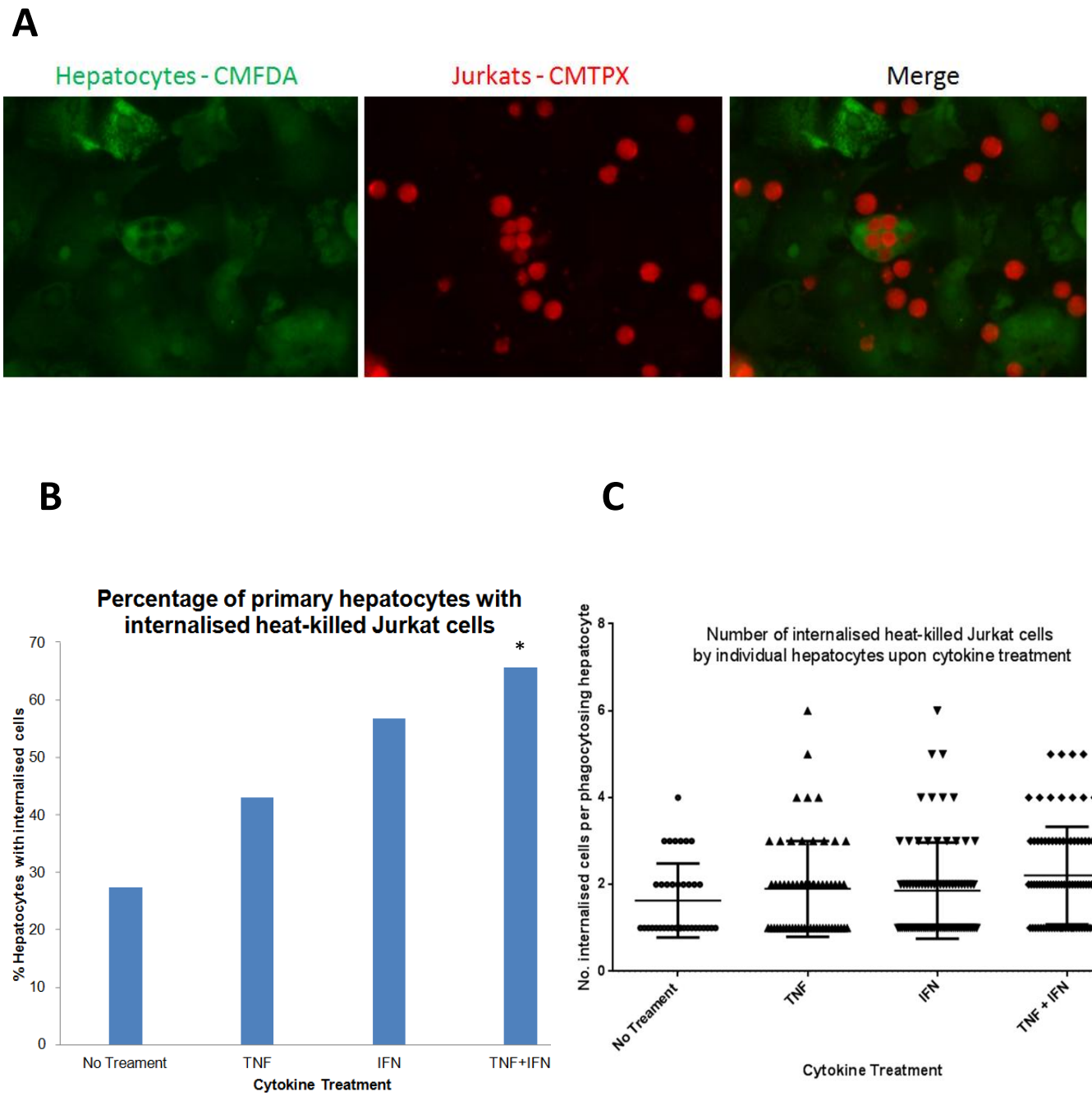

Figure 5: Primary hepatocytes internalise heat-killed Jurkat cells and this is enhanced with inflammatory cytokine treatment: Jurkat cells were dyed red with CellTracker CMPTX prior to heat-killing treatment. Primary hepatocytes were extracted from a donated liver and seeded in 48-well plates at 80% confluence, courtesy of Dr. Elizabeth Humphreys. Hepatocytes were stained green with CellTracker CMFDA and then treated with inflammatory cytokines for 1 hour. Cytokines were washed off and hepatocytes were incubated with heat-killed Jurkat cells for 2 hours. All cells were then fixed with 1% paraformaldehyde in PBS for 5 mins and stored at 4°C in PBS. Ten fluorescent images were then taken of fixed cells for each cytokine treatment. **A: Fluorescent micrographs of phagocytosing primary hepatocytes.** Jurkats were determined as 'internalised' where the appearance of vacuoles within green hepatocytes cytoplasm corresponded to the appearance of red Jurkat cells. **B Bar chart showing the percentage of hepatocytes with internalised cells following cytokine treatment.** $P<0.05$ **C Dot plot showing the number of cells internalised by each phagocytosing hepatocyte following cytokine treatment.**

3.3 Can we measure hepatocyte internalisation of live and dead T-cells in inflammation *in vivo*?

3.3.1 Immunohistochemistry can be used to identify T-cells in diseased livers

To study entosis and phagocytosis of CD4+ T cells in vivo, we made use of the liver tissue bank of formalin-fixed paraffin embedded tissue sections and set out to optimise immunohistochemistry (IHC) staining for CD4. We first conducted anti-CD4 IHC staining of livers from patients with alcoholic liver disease (ALD) and primary biliary cirrhosis (PBC), in order to identify T-cells. These diseases were selected as they are each known to have ample T cell infiltrates during inflammatory responses (39). Antibodies were used at 1:10, 1:20 and 1:40 dilutions in order to optimise the protocol. Staining for these sections was weak or non-specific for all concentrations used, therefore unsuitable for identifying T cells inside hepatocytes (Figure 6). Following this, we tested anti-CD3 staining. For concentrations above and including 1:100, we visualised small cells which were positively stained, scattered throughout each tissue section (Figure 6). Furthermore, aggregates of lymphocytes were seen around portal areas and around fibrotic. As such, these proceedings demonstrated that IHC could be used to identify lymphocytes *in vivo* using an anti-CD3 antibody.

3.3.2 In Situ End-Labelling (ISEL) can be used to detect apoptotic cells *in vivo* without proteolytic treatment

Although we had established a method for visualising lymphocytes within the liver, it was not yet a possibility to determine the viability of these cells. Although it was possible to visualise lymphocytes that had been engulfed by hepatocytes, differentiating between entosis of live cells, or phagocytosis of apoptotic cells remained a challenge. A staining technique for the visualising apoptotic cells had been established called In-Situ End Labelling (ISEL). This technique uses Klenow

fragment to add labelled nucleotides to free 3'OH groups in DNA, created as a result of apoptosis-induced endonuclease activity. This technique had also been optimised for accurate visualisation without the need for enzymatic proteolytic treatment, instead using pressure cooker and citrate buffer solution to unmask epitopes (40). We are now no longer able to use pressure cookers in our laboratories so we had to test treating tissue sections with microwave heat instead. To see if this technique could be used to identify apoptotic cells within paraffin liver sections, ISEL was performed for chronic rejection liver sections. The Klenow fragment was left out for some sections in to ensure that stain was specific to its activity. To optimise the unmasking pretreatment, sections were microwaved for 20, 30 or 40 minutes to identify the time which resulted in a more accurate stain. The technique was also performed on frozen Jurkat cell cytospins, some of which had been treated with FasL to induce apoptosis. Both Jurkats and liver sections which did not receive Klenow fragments only showed haematoxylin counterstaining (Figure 7). This shows that any signal observed from ISEL staining was as a result of the Klenow fragment. Furthermore, all Jurkats that were pre-treated with FasL were positive for ISEL staining, displaying the accuracy of this technique to identify apoptotic cells. Additionally, hepatocytes were ISEL stained successfully for all microwave times for chronic rejection tissues, which are rich in apoptotic cells. Sections undergoing a 20min proteolysis showed prominent nuclear staining, and lower non-specific cytoplasmic staining and blotching in comparison to longer times. This is probably because prolonged microwaving times can damage epitopes. This investigation thus shows that apoptotic cells can be accurately identified within paraffin liver sections using microwave treatment for epitope unmasking.

3.3.3 ISEL and Immunostaining can be conducted together to identify both T-cells and apoptosis

We had so far confirmed that it was possible to identify lymphocytes in liver sections using immunohistochemistry and that it was also possible to identify apoptotic cells with ISEL. The challenge that remained was to develop a protocol which utilised both techniques, which had not been attempted before. To this end, a protocol was devised, whereby tissue sections would initially undergo peroxidase blocking, followed by ISEL and then anti-CD3 IHC staining. We chose a red alkaline phosphatase substrate for ISEL and a green peroxidase substrate for CD3 in order to obtain a greater contrast between the two stains. As lymphocytes have large nuclei encapsulated in a small layer of cytoplasm, we would expect to see large red nuclei, with a “halo” of green representing the cytoplasm. Staining was performed on chronic rejection and alcoholic liver disease sections, as these had proved successful for the previous single stains. Several red cells were seen for both tissue sections, indicating that the ISEL was successful and could be visualised with this red substrate (Figure 8). Unfortunately, the green peroxidase substrate used to visualise anti-CD3 in the combined stained protocol was too bright, non-specifically staining all cell nuclei. Careful titration of the detection reagents is needed to optimise this protocol for the detection of apoptotic T cells in paraffin sections.

3.3.4 Internalised cells and hepatocyte nuclei can be distinguished using anti-HNF4 IHC

We had established that it was possible to identify lymphocytes within paraffin sections and simultaneously determine if they are apoptotic through double staining. Such a technique can be used to identify phagocytosed cells. However, these cells are of a similar size and appearance to hepatocyte nuclei. Furthermore, many hepatocytes are apoptotic within diseased tissues and may provide difficulty when identifying double-stained cells. Finally, as hepatocytes are commonly multinucleate, the appearance of 2 spherical bodies within a hepatocyte does not guarantee that one is the result of heterotypic internalisation. Staining hepatocyte nuclei specifically instead of targeting lymphocytes may overcome this problem. Hepatocyte nuclei exclusively express hepatocyte nuclear factor 4 (HNF4). This could be targeted using IHC to outline hepatocyte nuclei. To this end, primary sclerosing cholangitis (PSC) sections were subjected to anti-HNF4α IHC using a previously described protocol (37). As the unmasking procedures had not been outlined from this study, we tested 3 techniques, using high pH unmasking buffer as previously used, low pH solution of none at all (Figure 9). All stains conducted using low pH buffer or no buffer yield none-specific cytoplasmic staining. However, High-pH unmasked sections showed strong, specific nuclear staining in hepatocytes. Of great importance, biliary epithelial cells were not stained, which emphasises the specificity of this antibody. In total, this technique could be used to highlight hepatocyte nuclei within tissue sections and confirm if cells are multinucleate or contain vacuoles.

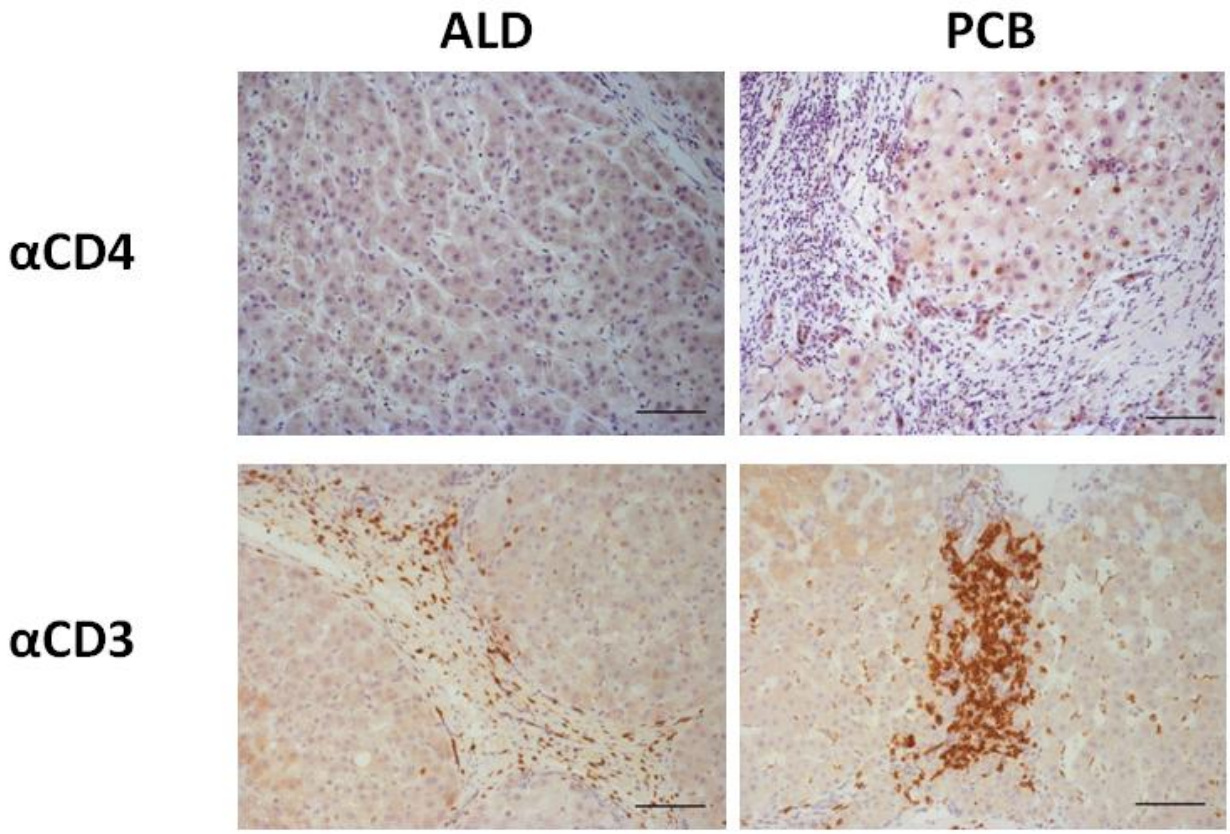

Figure 6: Anti-CD4 and CD3 immunohistochemistry (IHC) of diseased liver sections. Epitopes of paraffin-embedded liver sections were unmasked with high pH citrate buffer and underwent 20min microwave proteolysis prior to staining. Sections were then blocked with peroxidase blocking reagent and 2% casein solution. Sections were incubated with primary antibodies for 1 hour at room temperature. Positive staining was visualised using ImmPRESS HRP universal antibody (Vector) and Diaminobenzidene (DAB) peroxidase substrate. ALD; Alcoholic Liver Disease. PBC; Primary Biliary Cirrhosis. Black lines represent 100µM.

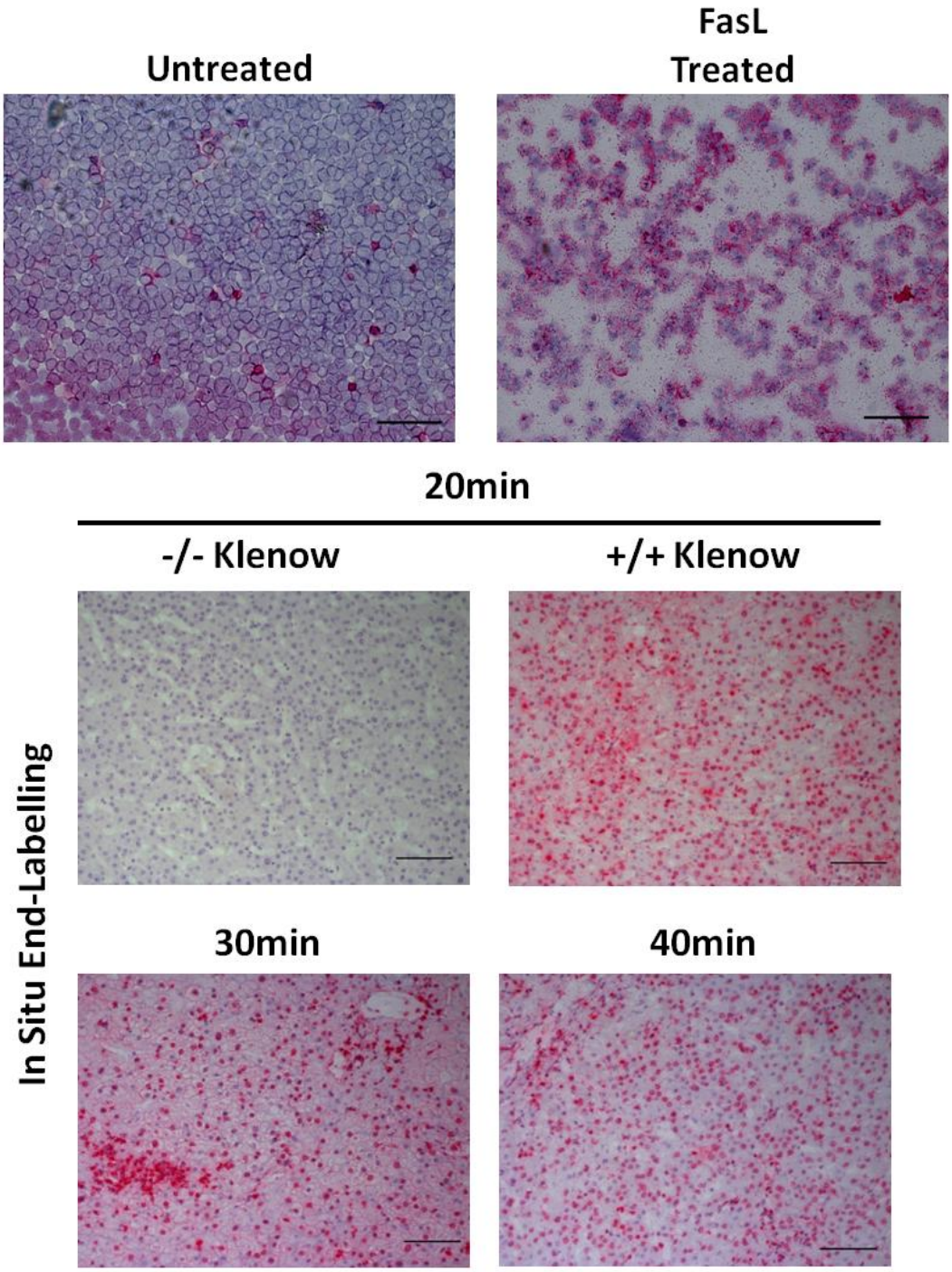

Figure 7: Assessment of In Situ End-Labelling (ISEL) for the detection apoptotic cells in chronic rejection liver sections and frozen Jurkat cell cytospins. Jurkats were cultured in normal media or media containing FasL prior to cytospinning. FasL treated Jurkats were stained as a positive control for the detection of apoptosis. Epitopes on paraffin liver sections were unmasked using high pH citrate buffer and 20, 30 or 40min microwave proteolysis prior to ISEL staining. A control stain was conducted without the Klenow fragment to ensure that the enzyme was actively labeeling free-DNA end. Positive staining was visualised using ImmPRESS HRP universal antibody (Vector) and stayRed/AP substrate (Vector). Black lines represent 100µM.

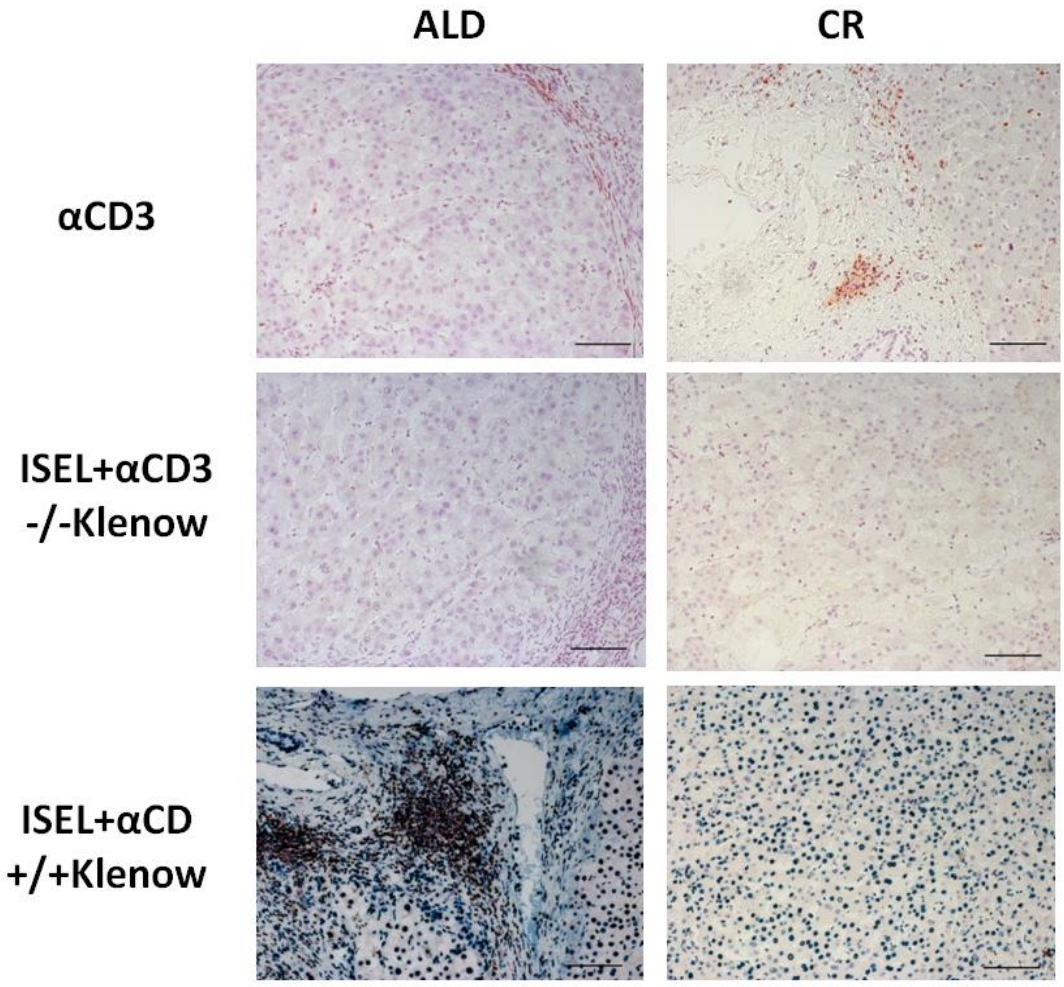

Figure 8: Double staining of diseased liver sections combining αCD3 IHC and ISEL. Epitopes were unmasked with high pH buffer and 20min microwave proteolysis. ISEL stains were performed first, following peroxidase blocking of paraffin sections, and visualised with StayGreen/AP substrate. Following this, liver sections were blocked with 2% casein solution and then inucabated with anti-CD3 monoclonal antibody for 1 hour. using NovaRed™ peroxidase substrate in order to assess the new substrate and observation any effect of ISEL procedures on subsequent IHC. ALD; Alcoholic Liver Disease. CR; Chronic Rejection. Black lines represent 100µM.

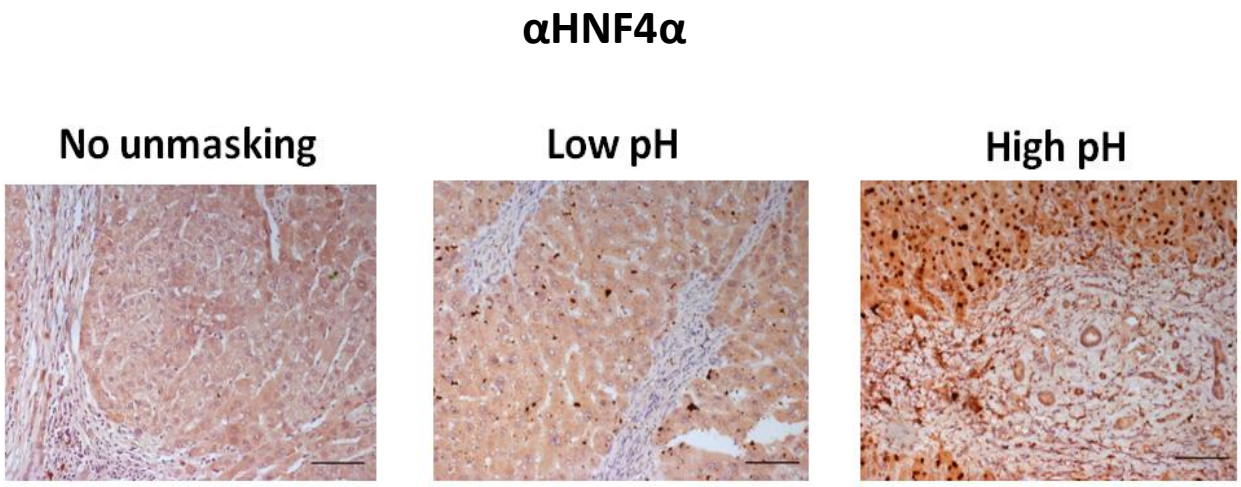

Figure 9: Anti-Hepatocyte nuclear factor 4α (HNF4α) IHC of primary sclerosing cholangitis (PSC) paraffin liver sections. Sections were pre-treated with high pH buffer, low pH buffer or no buffer, and were incubated with αHNFα primary antibody in 1% BSA solution, overnight at 4°C. Positive staining was visualised using ImmPRESS HRP universal and DAB peroxidase substrate. Black lines represent 100µM.

4 DISCUSSION

4.1 Phagocytosis in hepatocytes derivative cells causes accumulation of nuclei and promotes differentiation

It has been shown in recent years that tumours cells can engulf live cells of the same lineage through the process of entosis (2, 3). This generation of cell-in-cell bodies results in polyploidisation, through cytokinetic failure and multinucleation. In addition, specific phagocytotic processes have also been shown to create large intracellular vacuoles which pose physical obstacles for cell division(41, 42). Hepatocytes have been shown to conduct both entosis and phagocytosis, although the outcome of this on hepatocyte ploidy had not been investigated (31, 33). As such, we set out to determine if phagocytosis by hepatocytes results in multinucleation and to establish if such activities could be observed *in vivo*. We found that prolonged, consecutive phases of phagocytosis by Huh7 hepatoma cells induced a cumulative increase in multinucleation amongst these cells. Furthermore, we made the exciting observation that phagocytosis induced these established proliferative cell lines to cease division and differentiate into cells which resemble primary hepatocytes. Of significance we also established that primary hepatocytes were also capable of phagocytosing heat-killed cells, suggesting that prior observations in Huh7 cells were applicable for cells within the liver. Furthermore, immunohistochemistry and ISEL procedures using paraffin liver sections were established for simultaneous visualisation of apoptotic cells and lymphocytes *in vivo*. The observations made throughout these proceedings raise several questions as to the significance of polyploidy within the liver and pave the way for subsequent investigations into the physiological significance of hepatocyte polyploidy.

4.2 The physiological purpose of *in vivo* phagocytosis in the liver

This investigation has shown, together with other evidence from the Stamataki lab that primary hepatocytes phagocytose dead lymphocytes *in vivo*, providing another role conducted by hepatocytes which contribute to homeostasis of the liver. The pro-inflammatory cytokines IFNγ and IFNγ + TNFα enhanced primary hepatocyte phagocytosis (Figure 6C). This was in agreement with data on the regulation of phagocytosis in Huh-7 as shown by Weight et al in our lab (unpublished), The physiological impact of increased ploidy in hepatocytes, as a result of phagocytosis, is uncertain. A mechanism of understanding the significance of these events is to outline the situations where phagocytosis would be considerably enhanced. Although the number of apoptotic cells in the liver is low, acute liver injury or disease amplifies apoptotic-cell death, which induces phagocytic clearing of dead cells by hepatocytes (43). It has been suggested that increases in ploidy provide the regenerative capacity of hepatocytes (18, 24). As such, polyploidisation following liver injury or inflammation may be of benefit, as it may increase the regenerative capacity of the liver and promote healing. A second explanation for liver polyploidisation could be the promotion of genetic resilience. Previous studies conducted in yeast revealed in increasing the number of chromosome sets can mask the acquisition of detrimental mutations (6). In addition, the liver is often exposed to mutagenic substances like alcohol and drug metabolites (24). As such, phagocytosis by hepatocytes could provide protection from harmful mutations through increases in ploidy. Of interest, we observed that treatment of primary hepatocytes with cytokines TNFα and IFNγ induced a significant increase in the number of cells conducting phagocytosis, as well as the number of cells which were internalised by each cell. This suggests that these inflammatory cytokines synergistically up-regulate phagocytic responses in

hepatocytes. Similar interplay between TNFα and IFNγ have been described in macrophage phagocytosis of *Listeria monocytogenes* and *Leishmania major* (44, 45). Hepatocytes may be stimulated through similar mechanisms. As both TNFα and IFNγ are secreted by T-cells and natural killer cells (NK) during inflammation, cytokine stimulation of hepatocytes may be induced to clear dead material from the liver.

Additionally, it had been previously observed that IFNγ impose an inhibitory effect on hepatocyte regeneration (46). Hepatocyte cell division is reduced during phagocytosis, which may explain this result. A further analysis of multinucleation in liver sections utilising anti-HNF4α immunohistochemical staining could be conducted to elucidate whether ploidy is increased in livers during acute injury or inflammation. As spontaneous tumour development is rare in liver, considering that hepatocytes are naturally polyploid, it is unlikely that phagocytosis-induced polyploidisation promotes tumourigenesis (24, 25). In support of this, we observed that phagocytosis did not increase the frequency of cell division in Huh7s (data not shown). This evidence implies that hepatocellular carcinoma may not arise from prolong periods of phagocytosis, although this should be confirmed using aforementioned IHC analysis of cancerous livers. Overall, it is likely that natural increases in liver polyploidy, as a result of phagocytosis, are beneficial to overall liver homeostasis, as well as for the prevention of and recovery from injury or disease.

4.3 Phagocytosis may induce cellular differentiation through aneuploidy

The examination of phagocytosis-induced multinucleation in hepatomas resulted in the surprising differentiation of these established cell lines into two separate lineages. The molecular processes which underlie this event were not apparent. It is

of great interest as to the mechanism of how these differentiated were generated. A possibility may be through the generation of aneuploid cells (Figure 10). Karyotyping in mouse livers has revealed that 70% of hepatocytes in adults had undergone chromosomal loss or gain (13). Further research showed that chromosome from each nucleus within tetraploid, binucleate cells are interspersed following condensation in metaphase (13). Following this, chromosomes are separated along a bipolar or multipolar axis. In this respect, multiple spindle fibres can attach to the same kinetochores. These “lagging chromosomes” to not migrate to a specific pole and are deleted (14). Daughter cells resulting from this division will have chromosomes missing and be genetically distinct to the parent cell. The generation of binucleate cells due to phagocytosis could promote aneuploidy in hepatocytes. As such the generation of the observed differentiated cell lines could have arisen through aneuploidy and the loss of genes which ordinarily would generate the Huh-7 phenotype. In support of this, differentiation as a result of aneuploidy has been observed following long-term culture of mesenchymal stem cells and neuronal cells (15, 16). Procedures that were conducted within this investigation could have been utilised to examine this possibility; Hoechst staining of DNA could be used to identify aneuploidy in Huh-7s throughout cell division once chromosomes have condensed. However, as we were observing nuclear alteration in phagocytosing cells, heat-killed phagocytosing cells were also stained as by Hoechst. As such, the development of aneuploidy within these cells could not be observed. Fluorescence *In Situ* Hybridisation (FISH) analysis of Huh-7s prior to, and following, phagocytosis would be an optimal method for investigating this hypothesis.

Differentiated cells underwent minimal cell divisions, a trait which mimics the behaviour of *ex vivo* primary hepatocytes, which normally die following a short time in culture. This quality of primary cells creates difficulties in obtaining accurate results when regarding the natural activities of hepatocytes, as they are known to regenerate *in vivo.* However, the differentiated cells were still viable despite not undergoing cell division and may represent an accurate and robust model for investigating the behaviour of primary hepatocytes. Studies have aspired to achieve similar results in hepatoma cell lines through culturing in -media containing dimethyl sulfoxide (DMSO), the effects of which have been poorly characterised (17-19). Of interest, DMSO treatment has also been shown to induce multinucleation and cytokinetic failure in *Dictyostelium mucoroides*, leading to the generation of giant cells (3). Phagocytosis of dead cells may induce differentiation through similar mechanisms, although at a lower detriment to cellular physiology and without the requirement of further media supplements in order to prevent apoptosis of these cells. As such, the techniques described in this investigation could provide a more convenient mechanism to obtain data which accurately represents the biology of primary hepatocytes.

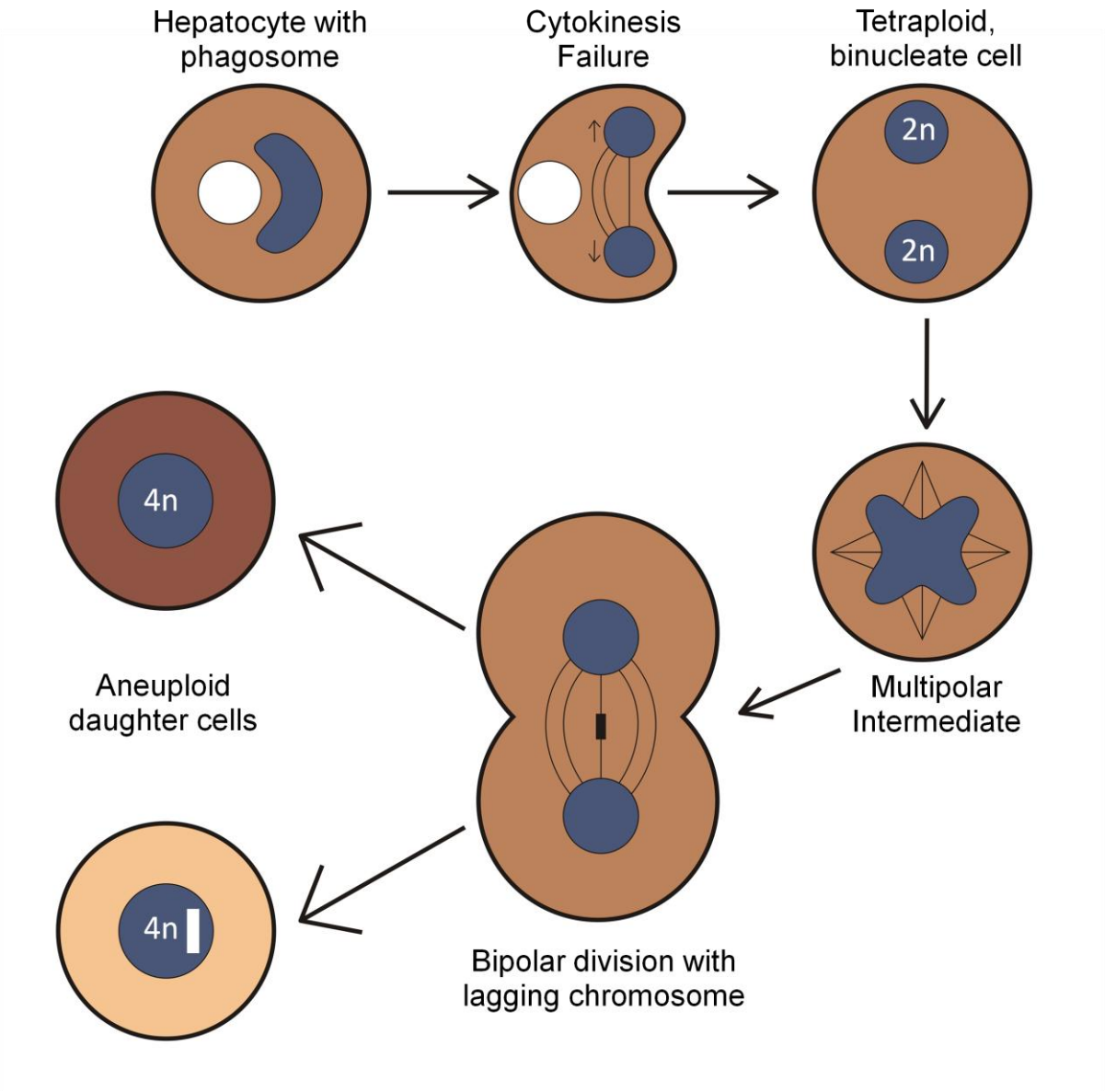

Figure 10: Proposed model for the generation of aneuploid, differentiated cells from Huh7 phagocytosis. The generation of intracellular vacuole within a hepatocyte, resulting from phagocytosis of a dead cell, restricts furrowing during cytokinesis leading to the generation of a tetraploid cell. After the phagosome is processed, the tetraploid cell attempts mitosis. Chromosomes from both nuclei intermingle as the cell attempts to generate multiple mitotic poles. Bipolar segregation generates “lagging chromosomes” which do not migrate to opposites and are subsequently deleted. As such, daughter cells do not receive these chromosomes and become aneuploid. Changes in cytoplasm colour depict genotype alterations.

4.4 Further Investigation

4.4.1 Obtaining a molecular understanding of hepatocyte phagocytosis and the limitations of heat killing

Phagocytosis of apoptotic cells is a well-characterised process; the recognition of cells presenting phosphatidylserine (PS) on the outer leaflet of the cell membrane by phagocytes has been well researched. However, the processes which trigger and regulate phagocytosis in hepatocytes are poorly understood. In this investigation we set out to determine if phagocytosis of apoptotic cells leads to increased multinucleation in hepatomas. We also established the use of ISEL for the specific detection of apoptotic cells *in vivo*. However, we induced phagocytosis in hepatomas using cells which had been killed by heat. This strategy was used, mostly for convenience, but also to ensure that the phagosome retained its shape containing large dead cells (as opposed to the constricting cells that die by apoptosis) and creating an intracellular obstruction. As apoptosis results in cellular condensation, phagosomes generated from these cells may be smaller and less likely to impose an obstacle on cytokinesis. In addition to this, heat-killing is thought to be more representative of necrosis, rather than apoptosis. Although a molecular understanding of necrotic cell phagocytosis lacking, the mechanisms through which it occurs may be distinctly different to that of apoptotic cell engulfment. This brings into question the efficacy of heat-killing for accurately representing the consequences in hepatocyte multinucleation as a consequence of phagocytosis. However, as necrotic death naturally occurs under inflammatory circumstances, it is likely that hepatocytes would naturally engulf necrotic cells to maintain liver homeostasis (20). Furthermore, it has been shown that both processes, although bearing morphological differences, are dependent of PS presentation (21). These

data increase our confidence that heat-killed cells can be used to accurately assess the impact of phagocytosis on Huh-7 hepatomas as a model of primary hepatocytes.

4.4.2 Immunohistochemistry can be used to assess the roles of entosis and phagocytosis in liver homeostasis

We developed a technique which combined the use of immunohistochemical staining ISEL detection of apoptotic cells. Using this method, both apoptotic cells and CD3+ lymphocytes could be visualised within the same liver section. This technique could be utilised to analyse the diversity of internalised lymphocytes and determine their fate. Individual subtypes of lymphocytes can be identified by the expression of exclusive biomarkers. For example, T-reg cells can be isolated based on the expression of the transcription factor Foxp3, T-helper 1 cells exclusive express Tbet, B-cells are identified by CD19 and CD20 expression, etc (22, 23). Antibodies which recognise theses markers can be used to identify individual subsets within tissue sections through the use of IHC. Combining these processes with ISEL can also be used to determine the fate of each individual subset. As such, we can visualise if individual lymphocytes subsets are internalised by hepatocytes. The apoptotic status of these cells can also be deduced by simultaneous ISEL treatment. Furthermore, it can be distinguished as to whether lymphocytes are internalised through phagocytosis or entosis. Benseler *et al*, eluded that autoreactive CD8+ cells actively enter hepatocytes in order to be deleted in a non-apoptotic manner (24). These observations could be confirmed using this double staining technique. The combination of ISEL and IHC can thus be utilised to decipher the complex relationships between hepatocytes and lymphocyte subsets.

4.5 Can phagocytosis be manipulated for therapies targeting cancer?

Hepatocellular carcinoma is the major cancer of human liver cancers and third most frequent cause of cancer in the world (26). The development of hepatocellular carcinoma is closely linked to hepatitis B/C viral infection and is thought to be associated with the dysregulation of genes linked to cell division, growth and migration. Surgical intervention is currently the most efficient treatment method of hepatocellular carcinoma (27). Evidence from this investigation and others suggests that ploidy increases as a result of phagocytosis can minimise the risk of deleterious or oncogenic mutations and increase the regenerative capacity of hepatocytes. As such, encouraging phagocytosis within the liver may be of therapeutic interest. Increased liver generation would improve patients' chance of survival and the effect of recessive oncogenes could be dampened by increasing the number of non-transformative alleles. In addition, as cells undergo reduced cycles of cell division during phagocytosis, encouraging this process could potentially delay the progression of hepatocellular carcinoma. Molecular understanding into how hepatocytes internalise dead cells is required for such therapies, as it is not plausible to increase phagocytosis by promoting cell death within the liver. Understanding how Huh-7 cells differentiated as a result of phagocytosis would be of great interest for anti-cancer therapies, as these ceased to exhibit characteristics of normal hepatomas. As such, increasing the frequency of hepatocyte phagocytosis within the liver may provide of mechanism of modulating the progression of hepatocellular carcinoma, through increased genetic resilience and differentiation of tumour cells into a less aggressive cell type.

5. REFERENCES

1. Krajcovic M, Overholtzer M. Mechanisms of ploidy increase in human cancers: a new role for cell cannibalism. Cancer Res. 2012;72(7):1596-601.

2. Overholtzer M, Mailleux AA, Mouneimne G, Normand G, Schnitt SJ, King RW, et al. A nonapoptotic cell death process, entosis, that occurs by cell-in-cell invasion. Cell. 2007;131(5):966-79.

3. Krajcovic M, Johnson NB, Sun Q, Normand G, Hoover N, Yao E, et al. A non-genetic route to aneuploidy in human cancers. Nat Cell Biol. 2011;13(3):324-30.

4. Comai L. The advantages and disadvantages of being polyploid. Nature reviews Genetics. 2005;6(11):836-46.

5. Abmayr SM, Pavlath GK. Myoblast fusion: lessons from flies and mice. Development (Cambridge, England). 2012;139(4):641-56.

6. Gerstein AC, Chun HJ, Grant A, Otto SP. Genomic convergence toward diploidy in Saccharomyces cerevisiae. PLoS genetics. 2006;2(9):e145.

7. Mable BK, Otto SP. Masking and purging mutations following EMS treatment in haploid, diploid and tetraploid yeast (Saccharomyces cerevisiae). Genetical research. 2001;77(1):9-26.

8. Ganem NJ, Storchova Z, Pellman D. Tetraploidy, aneuploidy and cancer. Current opinion in genetics & development. 2007;17(2):157-62.

9. Andreassen PR, Lohez OD, Lacroix FB, Margolis RL. Tetraploid state induces p53-dependent arrest of nontransformed mammalian cells in G1. Mol Biol Cell. 2001;12(5):1315-28.

10. Srsen V, Gnadt N, Dammermann A, Merdes A. Inhibition of centrosome protein assembly leads to p53-dependent exit from the cell cycle. J Cell Biol. 2006;174(5):625-30.

11. Uetake Y, Sluder G. Cell cycle progression after cleavage failure: mammalian somatic cells do not possess a "tetraploidy checkpoint". J Cell Biol. 2004;165(5):609-15.

12. Wong C, Stearns T. Mammalian cells lack checkpoints for tetraploidy, aberrant centrosome number, and cytokinesis failure. BMC cell biology. 2005;6(1):6.

13. Sotillo R, Hernando E, Diaz-Rodriguez E, Teruya-Feldstein J, Cordon-Cardo C, Lowe SW, et al. Mad2 overexpression promotes aneuploidy and tumorigenesis in mice. Cancer cell. 2007;11(1):9-23.

14. Chen X, Cheung ST, So S, Fan ST, Barry C, Higgins J, et al. Gene expression patterns in human liver cancers. Mol Biol Cell. 2002;13(6):1929-39.

15. Gentric G, Celton-Morizur S, Desdouets C. Polyploidy and liver proliferation. Clinics and research in hepatology and gastroenterology. 2012;36(1):29-34.

16. Fausto N, Campbell JS. The role of hepatocytes and oval cells in liver regeneration and repopulation. Mechanisms of development. 2003;120(1):117-30.

17. Guidotti JE, Bregerie O, Robert A, Debey P, Brechot C, Desdouets C. Liver cell polyploidization: a pivotal role for binuclear hepatocytes. J Biol Chem. 2003;278(21):19095-101.

18. Duncan AW, Hanlon Newell AE, Smith L, Wilson EM, Olson SB, Thayer MJ, et al. Frequent aneuploidy among normal human hepatocytes. Gastroenterology. 2012;142(1):25-8.

19. Celton-Morizur S, Merlen G, Couton D, Margall-Ducos G, Desdouets C. The insulin/Akt pathway controls a specific cell division program that leads to generation of binucleated tetraploid liver cells in rodents. The Journal of clinical investigation. 2009;119(7):1880-7.

20. Sigal SH, Rajvanshi P, Gorla GR, Sokhi RP, Saxena R, Gebhard DR, Jr., et al. Partial hepatectomy-induced polyploidy attenuates hepatocyte replication and activates cell aging events. The American journal of physiology. 1999;276(5 Pt 1):G1260-72.

21. Lu P, Prost S, Caldwell H, Tugwood JD, Betton GR, Harrison DJ. Microarray analysis of gene expression of mouse hepatocytes of different ploidy. Mammalian genome : official journal of the International Mammalian Genome Society. 2007;18(9):617-26.

22. Seitz HK, Stickel F. Molecular mechanisms of alcohol-mediated carcinogenesis. Nature reviews Cancer. 2007;7(8):599-612.

23. Duncan AW, Taylor MH, Hickey RD, Hanlon Newell AE, Lenzi ML, Olson SB, et al. The ploidy conveyor of mature hepatocytes as a source of genetic variation. Nature. 2010;467(7316):707-10.

24. Duncan AW. Aneuploidy, polyploidy and ploidy reversal in the liver. Seminars in cell & developmental biology. 2013;24(4):347-56.

25. Buchmann A, Bauer-Hofmann R, Mahr J, Drinkwater NR, Luz A, Schwarz M. Mutational activation of the c-Ha-ras gene in liver tumors of different rodent strains: correlation with susceptibility to hepatocarcinogenesis. Proceedings of the National Academy of Sciences of the United States of America. 1991;88(3):911-5.

26. Sun HS, Wilde A, Harrison RE. Chlamydia trachomatis inclusions induce asymmetric cleavage furrow formation and ingression failure in host cells. Mol Cell Biol. 2011;31(24):5011-22.

27. Flannagan RS, Cosio G, Grinstein S. Antimicrobial mechanisms of phagocytes and bacterial evasion strategies. Nature reviews Microbiology. 2009;7(5):355-66.

28. Sasaki T, Garant PR. Multinucleated fibroblastic cells in the periodontal ligaments of aged rats. Journal of periodontal research. 1993;28(1):65-71.

29. Moricard R, Canel Y. [Multinucleation of endocervical columnar epithelium in a case of primary papillamatous tuberculosis; problem of the diagnosis of intracervical epithelioma]. Bulletin de la Federation des societes de gynecologie et dobstetrique de langue francaise. 1952;4(3):438-41.

30. Rosin A, Doljanski L. Erythrocytes in the cytoplsm and nuclei of liver cells. Br J Exp Pathol. 1944;25(4):111-5.

31. Dini L, Pagliara P, Carla EC. Phagocytosis of apoptotic cells by liver: a morphological study. Microscopy research and technique. 2002;57(6):530-40.

32. Weight N. Unpublished work.

33. Benseler V, Warren A, Vo M, Holz LE, Tay SS, Le Couteur DG, et al. Hepatocyte entry leads to degradation of autoreactive CD8 T cells. Proceedings of the National Academy of Sciences of the United States of America. 2011;108(40):16735-40.

34. Overholtzer M, Brugge JS. The cell biology of cell-in-cell structures. Nat Rev Mol Cell Biol. 2008;9(10):796-809.

35. Berry MN, Friend DS. High-yield preparation of isolated rat liver parenchymal cells: a biochemical and fine structural study. J Cell Biol. 1969;43(3):506-20.

36. Bhogal RH, Hodson J, Bartlett DC, Weston CJ, Curbishley SM, Haughton E, et al. Isolation of primary human hepatocytes from normal and diseased liver tissue: a one hundred liver experience. PloS one. 2011;6(3):e18222.

37. Tanaka T, Jiang S, Hotta H, Takano K, Iwanari H, Sumi K, et al. Dysregulated expression of P1 and P2 promoter-driven hepatocyte nuclear factor-4alpha in the pathogenesis of human cancer. The Journal of pathology. 2006;208(5):662-72.

38. Normand G, King RW. Understanding cytokinesis failure. Advances in experimental medicine and biology. 2010;676:27-55.

39. Orman ES, Odena G, Bataller R. Alcoholic liver disease: pathogenesis, management, and novel targets for therapy. Journal of gastroenterology and hepatology. 2013;28 Suppl 1:77-84.

40. Panchalingam S, Reynolds GM, Lammas DA, Rowlands DC, Kumararatne DS. Simple method for pretreatment of tissue sections for the detection of apoptosis by in situ end-labelling and in situ nick translation. Clinical molecular pathology. 1996;49(5):M273-7.

41. Fukui Y. Formation of multinuclear cells induced by dimethyl sulfoxide: inhibition of cytokinesis and occurrence of novel nuclear division in Dictyostelium cells. J Cell Biol. 1980;86(1):181-9.

42. Sun Q, Overholtzer M. Methods for the study of entosis. Methods Mol Biol. 2013;1004:59-66.

43. Columbano A, Ledda-Columbano GM, Coni PP, Faa G, Liguori C, Santa Cruz G, et al. Occurrence of cell death (apoptosis) during the involution of liver hyperplasia. Laboratory investigation; a journal of technical methods and pathology. 1985;52(6):670-5.

44. Leenen PJ, Canono BP, Drevets DA, Voerman JS, Campbell PA. TNF-alpha and IFN-gamma stimulate a macrophage precursor cell line to kill Listeria monocytogenes in a nitric oxide-independent manner. Journal of immunology (Baltimore, Md : 1950). 1994;153(11):5141-7.

45. Liew FY, Li Y, Millott S. Tumor necrosis factor-alpha synergizes with IFN-gamma in mediating killing of Leishmania major through the induction of nitric oxide. Journal of immunology (Baltimore, Md : 1950). 1990;145(12):4306-10.

46. Sun R, Gao B. Negative regulation of liver regeneration by innate immunity (natural killer cells/interferon-gamma). Gastroenterology. 2004;127(5):1525-39.

47. Crasta K, Ganem NJ, Dagher R, Lantermann AB, Ivanova EV, Pan Y, et al. DNA breaks and chromosome pulverization from errors in mitosis. Nature. 2012;482(7383):53-8.

48. Nguyen TD, Widera D, Greiner J, Muller J, Martin I, Slotta C, et al. Prolonged cultivation of hippocampal neural precursor cells shifts their differentiation potential and selects for aneuploid cells. Biological chemistry. 2013;394(12):1623-36.

49. Opiela J, Samiec M, Bochenek M, Lipinski D, Romanek J, Wilczek P. DNA aneuploidy in porcine bone marrow-derived mesenchymal stem cells undergoing osteogenic and adipogenic in vitro differentiation. Cellular reprogramming. 2013;15(5):425-34.

50. Sakai Y, Jiang J, Kojima N, Kinoshita T, Miyajima A. Enhanced in vitro maturation of fetal mouse liver cells with oncostatin M, nicotinamide, and dimethyl sulfoxide. Cell transplantation. 2002;11(5):435-41.

51. Sainz B, Jr., Chisari FV. Production of infectious hepatitis C virus by well-differentiated, growth-arrested human hepatoma-derived cells. Journal of virology. 2006;80(20):10253-7.

52. Choi S, Sainz B, Jr., Corcoran P, Uprichard S, Jeong H. Characterization of increased drug metabolism activity in dimethyl sulfoxide (DMSO)-treated Huh7 hepatoma cells. Xenobiotica; the fate of foreign compounds in biological systems. 2009;39(3):205-17.

53. Zong WX, Thompson CB. Necrotic death as a cell fate. Genes & development. 2006;20(1):1-15.

54. Brouckaert G, Kalai M, Krysko DV, Saelens X, Vercammen D, Ndlovu MN, et al. Phagocytosis of necrotic cells by macrophages is phosphatidylserine dependent and does not induce inflammatory cytokine production. Mol Biol Cell. 2004;15(3):1089-100.

55. Palmer MT, Weaver CT. Autoimmunity: increasing suspects in the CD4+ T cell lineup. Nature immunology. 2010;11(1):36-40.

56. Bao Y, Cao X. The immune potential and immunopathology of cytokine-producing B cell subsets: A comprehensive review. Journal of autoimmunity. 2014.

57. Forner A, Llovet JM, Bruix J. Hepatocellular carcinoma. The Lancet. 2012;379(9822):1245-55.

58. Aravalli RN, Steer CJ, Cressman ENK. Molecular mechanisms of hepatocellular carcinoma. Hepatology (Baltimore, Md). 2008;48(6):2047-63.

APPENDIX: LIST OF ABBREVIATIONS

Abbreviation	Meaning
ALD	Alcoholic liver disease
AP	Alkaline Phosphatase
BSA	Bovine Serum Albumin
CD	Cluster of differentiation
cdc20	Cell Division Cycle 20
CMFDA	5-chloromethylfluorescein Diacetate
DAB	Diaminobenzidene
DAPI	4,6'-diaminide-2-phenylindole
DMEM	Dulbecco's Modified Eagle Medium
DNA	Deoxyribonucleic acid
DPX	Di-n-butylPhthalate in Xylene.
ECM	Extracellular matrix
EDTA	Ethylenediaminetetraacetic acid
EMT	Epithelial-Mesenchymal Transition
FBS	Fetal bovine serum
GFP	Green Fluorescent Protein
GTP	Guanosine Triphosphate
H2B	Histone 2B
HCC	Hepatocellular carcinoma
HEPES	4-(2-hydroxyethyl)-1-piperazineethane sulfonic acid
HNF4α	Hepatocyte Nuclear Factor 4α
HRP	Horseraddish peroxidise
Huh-7	Hepatoma cell line
IFN	Interferon
IHC	Immunohistochemistry
IMDM	Iscove's modified Dulbecco's medium
ISEL	In Situ End Labelling
LREC	Local Research Ethics Commitee
Mad2	Mitotic Arrest Deficient
MCF10A Cells	Michigan Cancer Foundation-10A Cells
MHC	Major Histocompatibility Complex
MLC	Myosin Light Chain
NEAA	Non-essential amino acids
PBC	Primary Biliary Cirrohsis
PBS	Phosphate buffer solution
PFA	Paraformaldehyde
PHH	Primary Human Hepatocytes
PI3K	Phosphoinositide 3-kinase
PI3K	Phosphatidylinositol-3-kinase
PSC	Primary Sclerosing Cholangitis

RFP	Red Fluorescent Protein
RPMI	Roswell Park memorial institute medium
SFM	Serum free medium
STAT	Signal transducer and activator of transcription
TBS	Tris Buffered Saline
TBS	Tris Buffered Saline
TBST	Tris Buffered Saline Tween
TGF	Transforming growth factor
TNF	Tumour necrosis factor